1-1-2017

Additive Manufacturing Of Al 4047 And Al 7050 Alloys Using Direct Laser Metal Deposition Process

Amrinder Singh
Wayne State University,

ADDITIVE MANUFACTURING OF AL 4047 AND AL 7050 ALLOYS USING DIRECT LASER METAL DEPOSITION PROCESS

by

AMRINDER SINGH

DISSERTATION

Submitted to the Graduate School

of Wayne State University,

Detroit, Michigan

in partial fulfillment of requirements

for the degree of

DOCTOR OF PHILOSOPHY

2017

MAJOR: MECHANICAL ENGINEERING

Approved By:

_____

Advisor Date

_____

_____

_____

_____

DEDICATION

I would like to dedicate this dissertation to my father Guru Gobind Singh Ji and my family members. Without my father's grace, this could never have been possible. I would also like to dedicate this to my wife Gaganjot Kaur who supported me emotionally and kept my spirits high throughout the degree.

ACKNOWLEDGEMENTS

Firstly, I would like to express my sincere gratitude to my advisor, Dr. Guru P. Dinda who gave me opportunity to work under his precious guidance, for his patience, knowledge and motivation. His guidance helped me all the time of research, publication in journals and writing of this dissertation. I would also like to thank my dissertation committee: Dr. Golam Newaz, Dr. Leela Arava, and Dr. Jeremy Rickli for their insightful suggestions and encouragement. My sincere thanks goes to Dr. Tirlochan Singh who supported and guided in the best possible way.

I am indebted to my lab mates Abhishek Ramakrishna, Venkata Surya Kartik, Karthik Alagarsamy, Rohan Sharma, Arpit Sethi, Harshada Patil, Ajay Sarma, Peter Christian for their valuable input and working together to finish experiments and preparing the final reports.

I am also very thankful to advanced powder solutions inc. who provided us the aluminum powder material for conducting the experiment and encouraged us to explore from various perspectives. I would like to thank Mr Bassam kas-Mikha and Marvin for providing us the necessary machined samples and fixtures.

TABLE OF CONTENTS

LIST OF FIGURES

LIST OF TABLES

CHAPTER 1 INTRODUCTION

1.1 Introduction to Additive Manufacturing (AM)

Additive manufacturing (AM) is a modern technique for building 3D components by layer by layer addition of material. Various AM techniques are capable to produce highly dense and reliable parts similar to quality of parts produced through conventional manufacturing process. Every additive manufacturing (AM) technique has unique applications in way the material is processed. In other words, the process of additive manufacturing (AM) is 3D printing that uses metallic or polymer powder or wire. The basic steps involved in AM is shown in figure 1.1

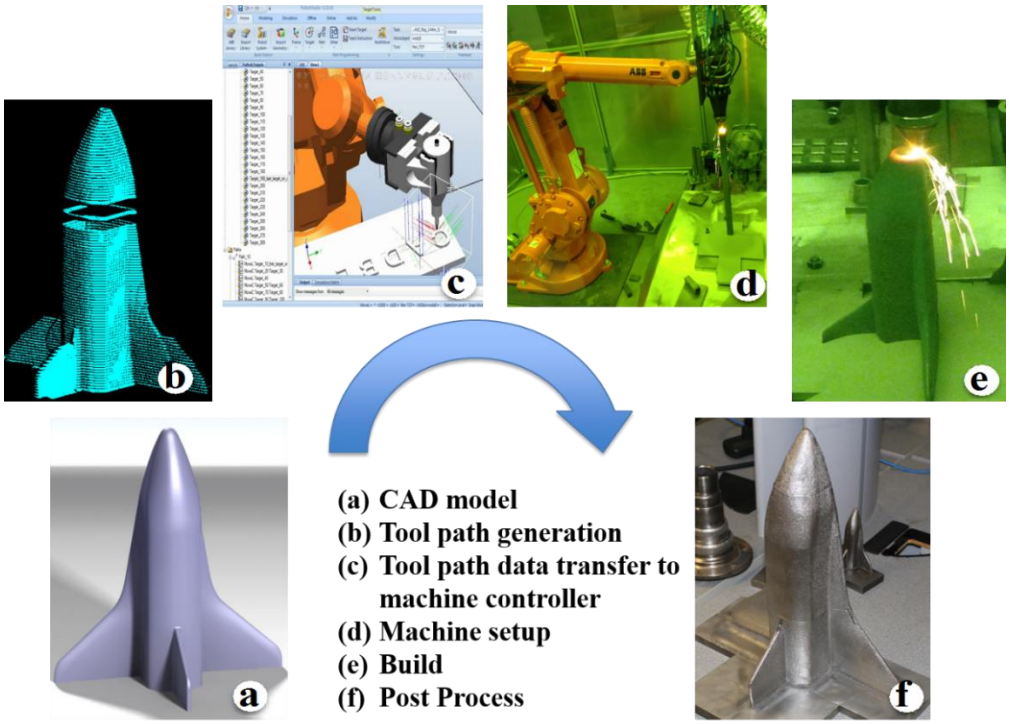

Figure 1.1: Additive manufacturing process.

Additive manufacturing starts with the CAD model designed in any commercial designing software packages such as Catia, ProE, NX etc., convert CAD model into .stl file followed by the slicing of 3D model into layers of specific thickness. Then the actual sliced path is converted into

machine understandable language, G codes or rapid programing .Final step is to build the part and removed from chamber or removed from substrate. Post processing such as machining, heat treatment, hot isostatic pressing etc. of the built part, may require depends on the application. There are various additive manufacturing processes have been developed such as Photopolymerization, Material jetting, Binder jetting, Fuse deposition modeling, Powder bed fusion, Sheet lamination, Directed energy deposition [1]. LMD is directed energy deposition process, which we have used to manufacture different aluminum alloys at Wayne State University. The American Society for Testing and Materials (ASTM) classified the AM processes as follows:

1.1.1 Vat photopolymerisation process

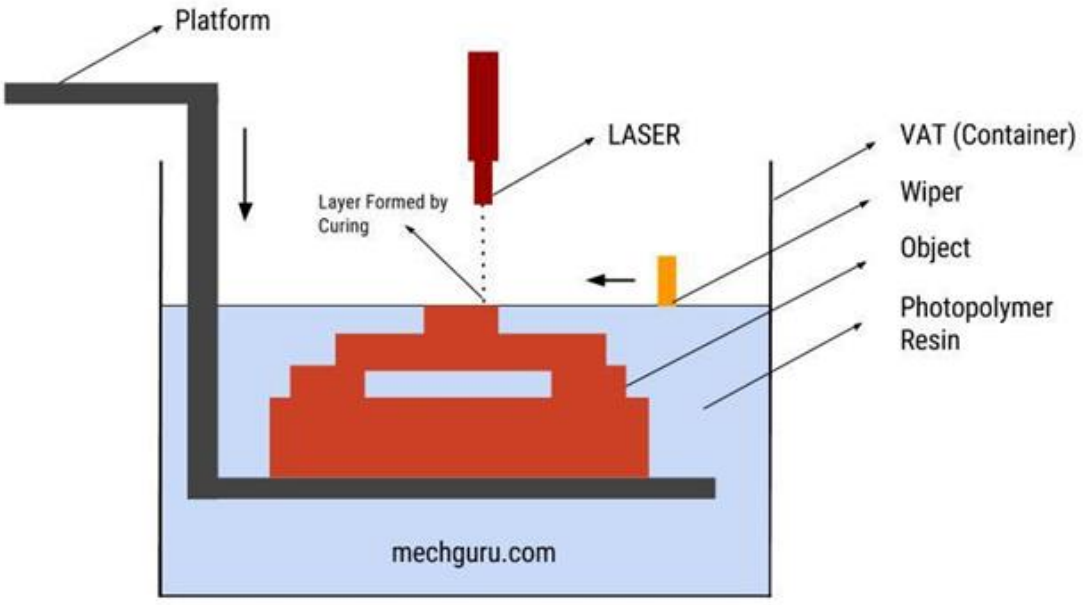

Figure 1.2: Schematics of vat photopolymerisation process [2].

Figure 1.2 schematically exhibits Vat photopolymerization technique in which a vat of liquid (ultraviolet curable photopolymer resin) and UV laser is used for solidifying the polymer. Laser beam follows the tool path at each layer on the liquid resin, which cures and solidifies the pattern traced. After a layer printed, elevator travels down by layer height distance. This layer by layer deposition process continues until the part is completely fabricated.

1.1.2 Material jetting process

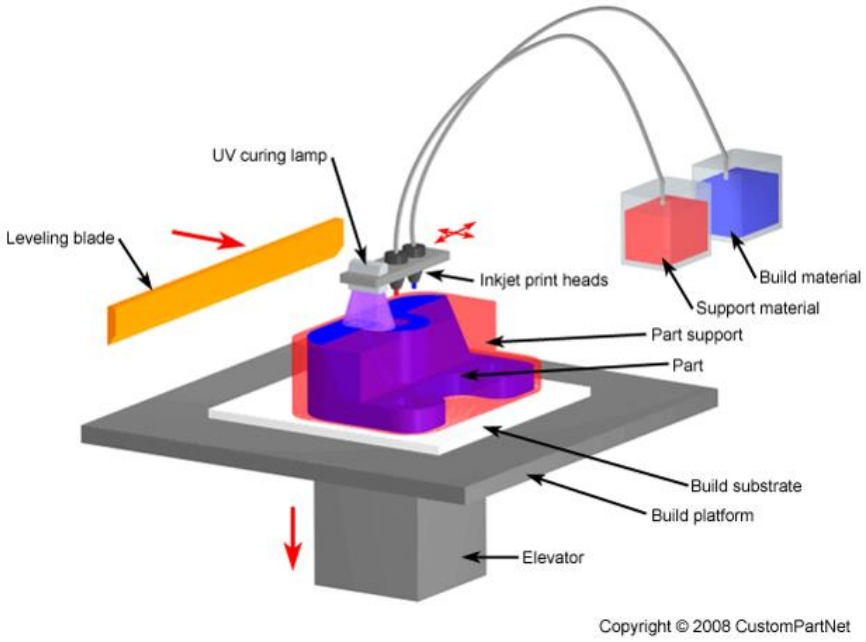

Figure 1.3: Schematics of material jetting process [3].

Figure 1.3 schematically shows the material jetting technique. It uses the print head similar to that of inkjet printer but instead of jetting ink drops, it drops liquid photopolymer on the build platform. Several print heads simultaneously keep dropping material to create single layer. The printed layers are cured via UV laser. A gel like liquid is used as supporting material in case of overhangs or complex designs. Multi-material printing is achievable via this process.

1.1.3 Binder jetting process

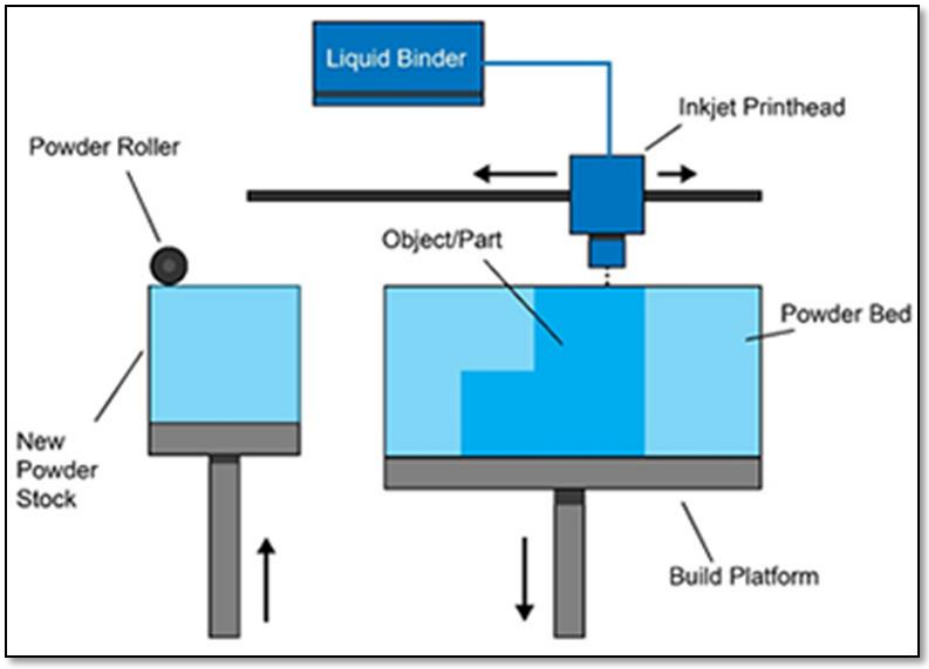

Figure 1.4: Schematics of binder jetting process [4].

Binder jetting is an AM process in which part is built in powder bed platform as shown in figure 1.4 where powder material is spread over the build platform with the help of a roller. It uses the printer head through which the binder adhesive drops on the powder bed and binds the powder. After the first layer is finished, build platform is moved down by layer thickness and roller spreads the powder to build platform for next layer. This process of layer by layer addition is continued until the part is fabricated. Some extra time is required for drying after the fabrication is completed.

1.1.4 Material extrusion process

In this process, the metal or plastic wire is passed through the nozzle as shown in figure 1.5 and heating coil heats up the wire enough to reach plastic stage. This plasticize material is then layer by layer deposited according to tool path profile. Mostly ABS (acrylonitrile butadiene styrene) and PLA (polylactic acid) widely used two plastic filament material. This process is cheapest of all to build plastic customized parts.

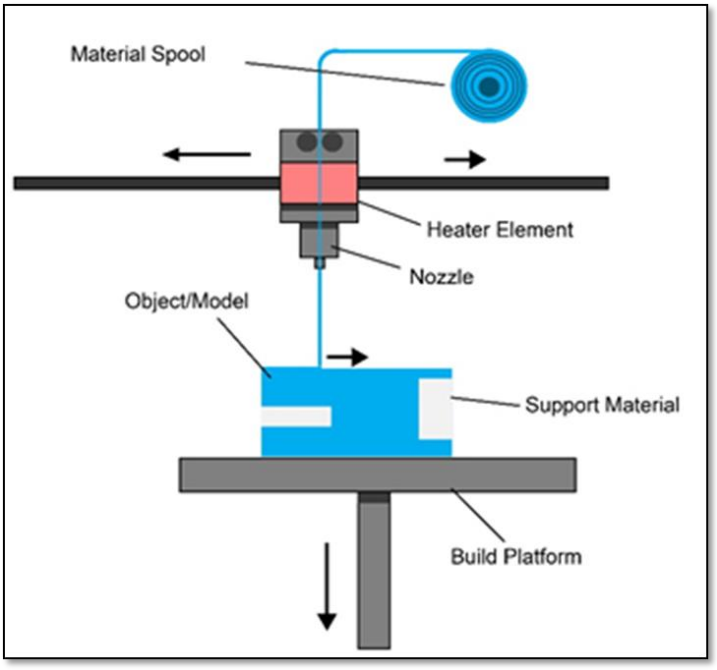

Figure 1.5: Schematics of material extrusion process [4].

1.1.5 Powder bed fusion / Selective laser sintering (SLS)

Selective lase sintering uses laser as heat source to fuse powder particles into a mass with desired 3D shape. The laser scanning speed is very high (about 1 m/s) and fuses the powder layer by layer according to the toolpath generated from a CAD model. After every layer deposited, the powder bed lowers by one layer thickness and roller applies a new layer of powder to build new layer. This process of layer addition continues until the part is fabricated. Unused powder can be reused again.

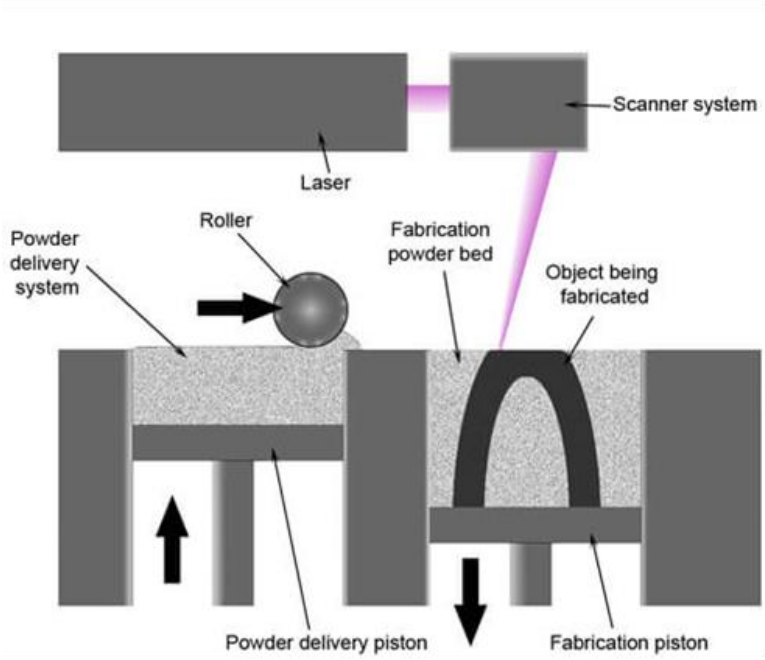

Figure 1.6: Schematics of powder bed fusion process [5].

1.1.6 Sheet lamination process

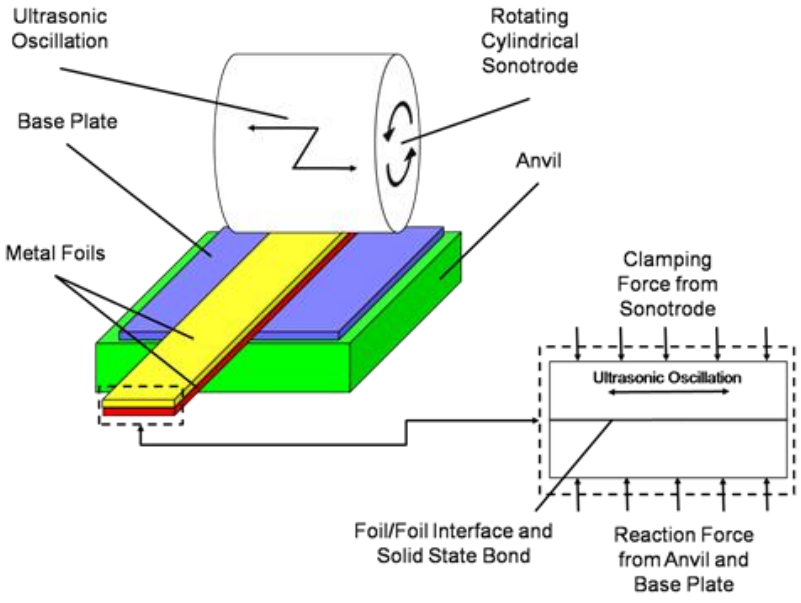

Figure 1.7: Ultrasonic sheet metal 3D printing process [5].

Sheet lamination processes uses thin sheets as starting material. Sheet material can be paper, metal or any kind of polymer. These sheets or ribbons of metal are bonded together using

ultrasonic welding in layers. CNC machine is then used for milling the bonded sheets to desired shape. Sheets of materials can also be used which are joined using some kind of glue and then precisely cut into desired shape.

1.1.7 Directed energy deposition

In directed energy deposition (DED) process, the material powder is focused through a nozzle on the substrate along with the laser as heating source typically electron beam or laser. The heating source is focused onto a substrate to create a melt pool and simultaneously melting the injected material into melt pool. Each DED pass in specified tool path direction creates a solidified layer of material. After printing of first layer, DED head moves up or platform moves down by a layer thickness and continue with the consecutive layer. Figure 4.2 shows the setup for directed energy deposition process.

1.2 Potential applications

Additive manufacturing (AM) has many advantages over the conventional manufacturing process driving industrial interest to implement it at commercial level. AM grants ample design freedom, which in case conventional manufacturing is limited, due to limited machining processes (subtractive manufacturing) available for sophisticated design. AM has potential to provides custom-made parts, as tooling remain same in this process and only CAD design is changed to make different parts. This CAD model can be sent from anywhere in the world from headquarter to the manufacturing location. Currently in manufacturing industry, additive manufacturing is being mostly used on large scale for remanufacturing and repairing of high value parts. Die remanufacturing process also profits with this technique. Die usually is expected to have two special properties, one it has to be good conductor of heat and second it has to be strong to bear the continuous impact. This can be achieved by joining two different materials. AM is a perfect candidate to fabricate a component with multiple material. US federal aviation had cleared a AM

component (Housing for the sensor knows as T25) made by General Electric to be used inside jet engines. The above-mentioned benefits corroborate that continuous research in AM is essential, as it has potential to play a pivotal role in the much awaited next industrial revolution, and hence can help provide solutions for technological needs more efficiently and in a better way. Figure 1.8 shows that the customization gets expensive with traditional manufacturing as compared with the AM.

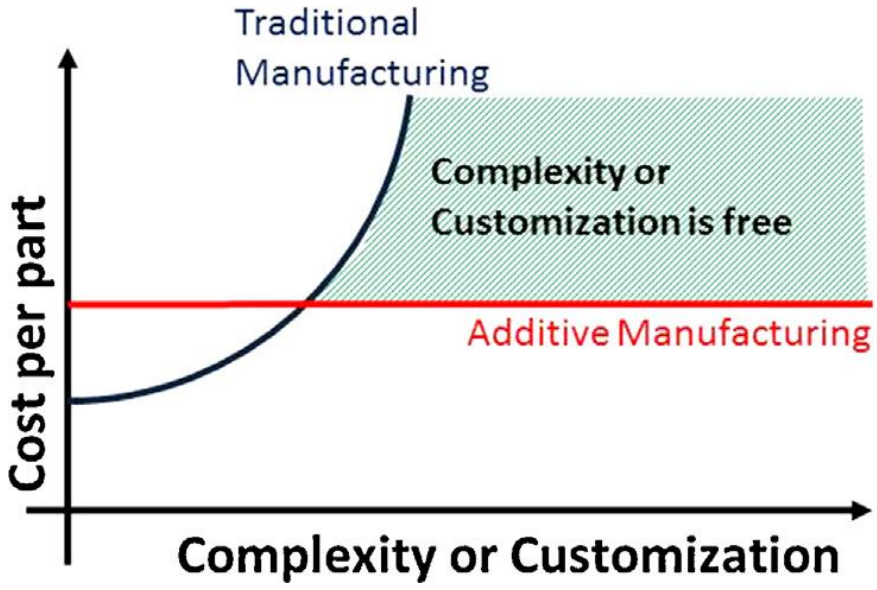

Figure 1.8: With AM, customization becomes free [6].

CHAPTER 2 STATE OF THE ART OF ADDITIVE MANUFACTURING OF ALUMINUM ALLOYS

2.1 Various aluminum alloys and their applications

Aluminum is a silvery white metal which is very lightweight, ductile and malleable in nature, usable in daily life it has to be alloyed to achieve required mechanical properties. Aluminum alloys contains aluminum in significant proportion along with small amounts of different alloying elements e.g silicon, zinc, magnesium, copper, tin and manganese, that are added to enhance the mechanical, physical and structural properties. Aluminum is a non ferrous metal which is used extensively all over the world with the annual worldwide consumption rate of about 24 million tons [7]. The paramount reason for such an extensive use of aluminium from making frying pans to ultrasonic air crafts is its high strength to weight ratio. The major ore for aluminum is Bauxite. The aluminum alloys exist in two forms commercially: cast and wrought alloy. In general, wrought alloys have better mechanical properties than cast alloys, which is partially due to the defects that appear during casting [7]. Presence of large amounts of silicon and copper in cast alloy causes a heterogeneous structure resulting in brittle faces. The aluminum alloy designation is a standard method followed to distinguish between various aluminum alloys, first digit e.g. 1, 2, 3 etc. represents principal alloying constituent. Second digit represents the variations of initial alloy. Third and fourth digit are unique e for each alloy depicting its alloy variation. Casting alloys follow similar designation with a small difference of a dot after third digit e.g. 1xx.x, 2xx.x etc. In case of aluminum alloys, fourth digit after dot can be 0, 1 or 2. Casting is designated by 0 whereas 1 and 2 represents ingot alloys. Aluminum alloys are usually tempered after manufacturing to improve the mechanical properties. Various temper designation are shown in table 2.1.

Table 2.1: Temper designation symbol

Temper Designation symbol	Explanation
F	As Fabricated
O	Annealed
H	Strain Hardening
W	Solution Heat Treated
T	Series of heat treatments, Generally solution heat treatment followed by quenching and precipitation hardening.

2.1.1 1xxx (Pure Aluminum)

Pure aluminum is highly corrosion resistance and electrical conductivity makes it perfect candidate for electrical applications. Aluminum being highly formable is extensively used in making foil and strip for packaging chemical equipment, car bodies and sheet metal work. This series is strain hardenable and is non-heat treatable.

2.1.2 2xxx (Al-Cu)

2xxx series is a heat treatable Al alloys and known for high strength especially at high temperature. General 2xxx series is used in manufacturing truck and aircraft body parts. Several other 2xxx series alloys also used in making fasteners and rivets. This series is realtively less corrosion resistant so it has to be painted or cladded.

2.1.3 3xxx (Al-Mn)

3xxx series is strain hardenable and highly corrosion resistant. This series aluminum alloys is used for manufacturing cooking utensils, roofing for heat exchangers. Almost all beverage cans are made of Al 3004 and Al 3104. It can be easily welded, brazed and soldered.

2.1.4 4xxx (Al-Si)

High silicon composition makes this alloy highly flowable, hence it has been used in making casted products for automotive and other sectors. Pistons, shock tower hoods, engine

blocks are the most widely used products made from this alloy. It is also used as filler material in welding of most of the aluminum alloys.

2.1.5 5xxx (AL-Mg)

5xxx series are strain hardenable, highly resistant to corrosion even in saltwater and maintains high toughness at cryogenic temperatures. Owing to these properties, it is appropriately used in manufacturing cryogenic tank and systems reaching near absolute temperatures. It has moderate strength which makes it useful for marine applications. Radiant automotive trims are usually made Al 5657. This alloy can be easily affected by stress corrosion cracking if Mg is present more than 3 percent by weight.

2.1.6 6xxx (AL-Mg-Si)

6xxx series is heat treatable, and high extrudability of this series makes it usable in the structural and architectural applications. Corrosion resistance and moderately high strength renders good application of this series in making rail cars, bridges and other marine products. Big arena structures are made of 6xxx series aluminum alloy.

Table 2.2: Ultimate tensile strength of various alumiun alloys [8]

	UltimateTensile Strength Range (KSI)	
Alloy Sereis	**Wrought Alloy**	**Cast Alloy**
1xxx	10-27	-
2xxx	27-62	19-65
3xxx	16-41	19-40
4xxx	25-55	17-25
5xxx	18-51	17-25
6xxx	18-58	-
7xxx	32- 88	30-55
8xxx	17 - 35	15-30

2.1.7 7xxx (Al-Zn)

7xxx series is heat treatable, and possess best combination of resistance to stress corrosion cracking and immense toughness. It is best suited for application for the parts having 3 to 6 inches thickness. Above mentioned properties make it profoundly useful in aerospace products: fuselage frames, bulk heads and wing skins are generally made of Al 7050 alloy. Automotive bumpers are made from this alloy reduce the overall weight of transportation vehicles.

2.1.8 8xxx (Alloys with other elements)

8xxx series is primariliy alloyed with Fe, Li and Ni. This is a heat treatable series and has good electrical conductivity. Li additions gives this alloy very high strength and makes it useful in aerospace application, heat-sink device, aluminum foil and lid stock.

2.2 Conventional aluminum manufacturing practices

One might wonder why do we need to understand casting process while applying AM of aluminum alloys. This is because AM is undoubtedly casting at micro level, thus known as micro casting process. Conventional way of manufacturing aluminum parts is by casting. Castability is the general term used to determine ease of forming defect free casting. There are three factors that play vital role in estimating castability of an alloy; (a) major alloying elements (control castability), (b) minor alloying elements that control solidification and refine grain size, and (c) impurity elements that might limit or enhance the properties.

Figure 2.1: Al alloys components produced by vacuum risers casting [9].

2.3 Cast microstructure of aluminum alloys

Microstructural evolution is influenced by solidification rates, thermal gradient and alloying elements. Each alloying element results in a unique microstructure of different pattern depending on the cooling rates. All conventional cast and AM aluminum alloy microstructure involves formation of columnar and equiaxed dendrites (coarse as well as fine). Current study involves additive manufacturing (AM) of 4xxx and 7xxx series aluminum alloy. Hence it becomes important to study microstructural evolution of these series and develop a correlation between microstructure and resulting mechanical properties. This section focuses discussion on 7xxx and 4xxx series cast microstructure. During solidification of molten metal in a mould, rapid nucleation take place at the cold mould walls which results in very finer grain size, known as chill zone as shown in figure 2.2. As solidification process contonues, this solid grows towards the center of mould forming columnar dendrtire.

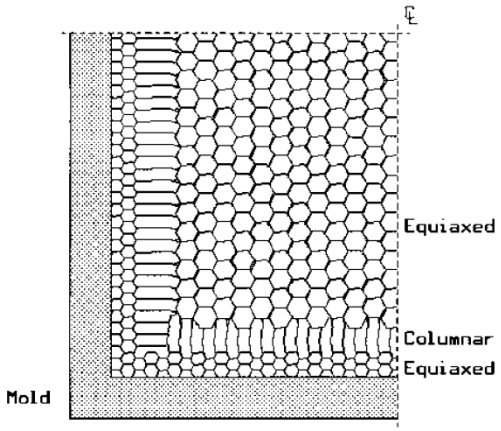

Figure 2.2: Grain pattern of metal in Casting [7].

After some time thermal gradient changes again and at this point temperature become uniform throughout, leading to nucleation of equiaxed grains as shown in figure 2.2. In case of AM of aluminum alloys microstructure is dynamic in nature, which implies that in the same manufactured part we would develop different kinds of grain structure because solidification velocity and thermal gradient are different at different location of the melt pool. As shown in figure 2.3 microstructure of Al-Si alloy manufactured through AM has all kind of microstructure from coarse to fine microstructure and equiaxed to columnar dendrites.

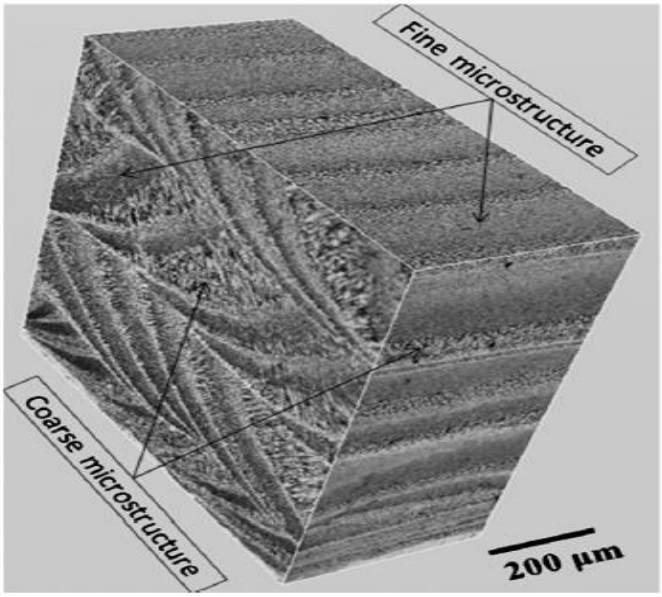

Figure 2.3: 3D Microstructure of laser deposited Al 4047 alloy [10].

In case of casting, drastic changes in microstructure have not been observed as it is not a rapid solidification process. As shown in figure 2.4, the as-cast aluminum 4xxx series microstructure is uniform throughout the casted part with bright phase as aluminum and dark needles represents silicon particles. Figure 2.4 b shows as-cast microstructure of modified 4xxx series alloy.

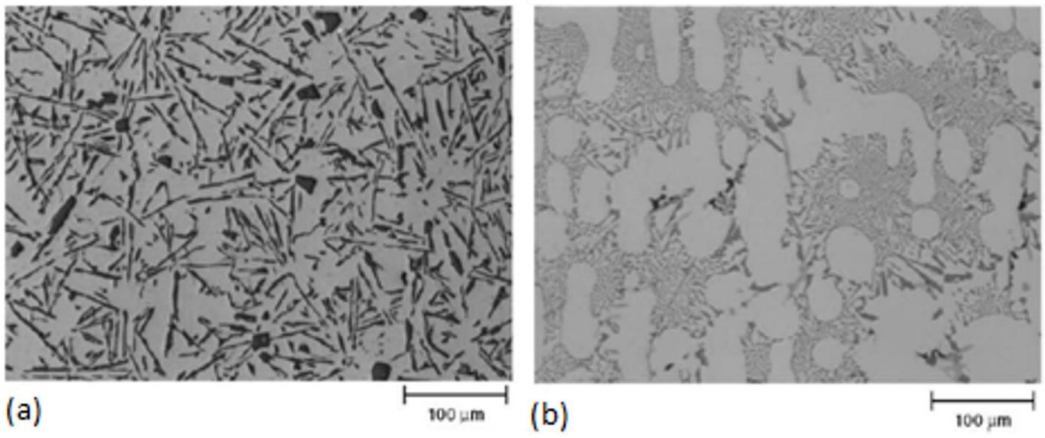

Figure 2.4: As cast microstructure of Al 413.0: (a) 150x not modified, and (b) 150x modified [11].

2.4 Limitation of conventional method of manufacturing of Al 7xxx alloys

It has been challenging task to manufacture near net shaped cast components from Al 7050 alloys because of several reasons. One of the biggest challenge is hot tearing, which is a very common in casting of 7xxx series aluminum alloys as shown in figure 2.5. Numerous studies have been conducted on hot tearing effect and a solution was proposed by Ghiaasiaan et al. [12] using controlled diffusion solidification (CDS) process to avoid hot tearing. Detailed investigation in hot tearing susceptibility was conducted by Bai et al. [13]. In susceptibility study, investigation was carried out on five-7xxx series aluminum alloy by Bai et al.as shown in figure 2.6.

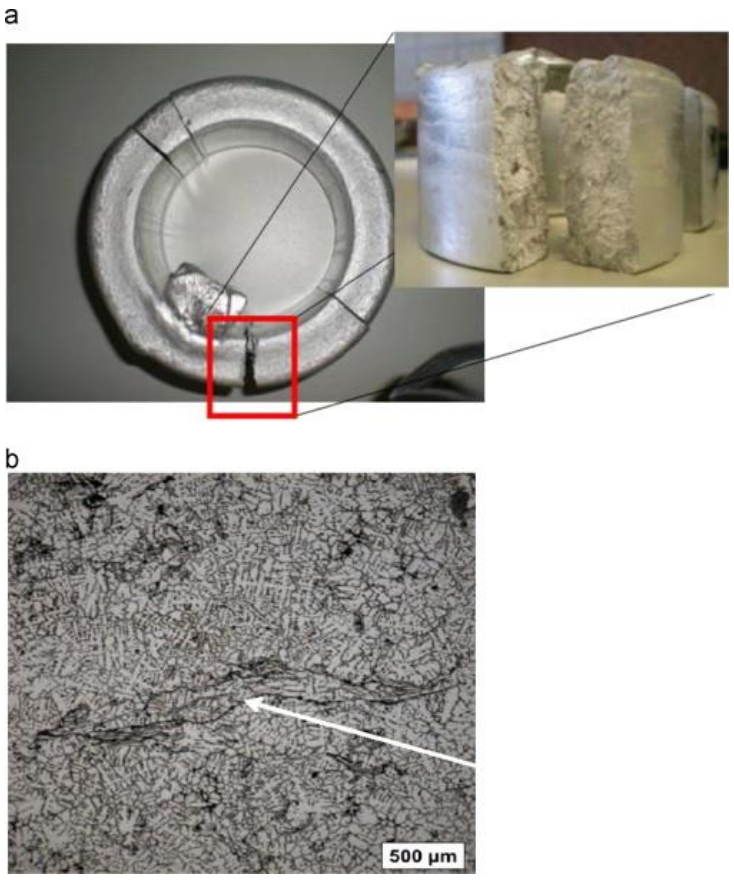

Figure 2.5: Hot tearing effect in as-cast sample (a) macro crack in 2014 aluminum alloy, and (b) micro crack in 7050 aluminum alloy [12].

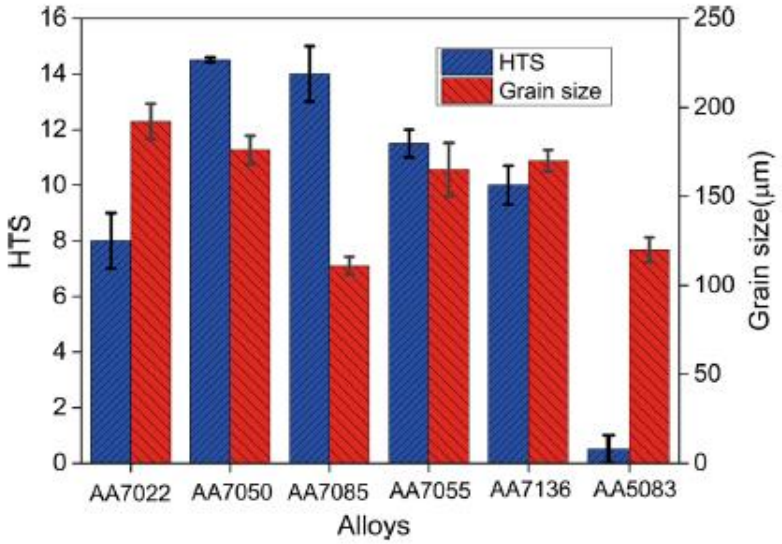

Figure 2.6: Hot tearing susceptibility for various 7xxx series aluminum alloy [12].

figure 2.6 exhibited the high susceptibility for Al 7xxx series alloys towards hot tearing. The hot tearing susceptibility for an alloy increases with the increase in Zn content. Zn/Mg ratio also plays vital role in hot tearing susceptibility according to Bai et al. [13].

2.5 Additively manufactured 4xxx series aluminum alloys

In 21st century, aluminum is second to steel in automotive sector, because of its superior strength to weight ratio, good formability, oxidation and corrosion resistance etc. Hence, developing AM for aluminum alloys is imperative to make sure industry gains maximum benefit from AM. So far, no literature is available for direct laser metal deposition of 7xxx series aluminum alloy to best of our knowledge till date. Various powder bed additive manufacturing techniques not including direct laser metal deposition have been applied to deposit 4xxx and 7xxx aluminum alloys [10, 14-20].

2.5.1 Directed energy depositon of 4xxx aluminum alloys

Directed energy deposition technique using CO_2 laser has been applied for depositing aluminum 4047 alloy in a study conducted by Dinda et al. [10]. In this study, a single wall 4 mm

high and 50 mm long was fabricated by successive deposition of sixteen layers using two deposition pattern shown in figure 2.7.

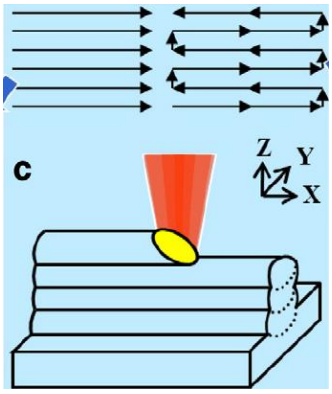

Figure 2.7:Tool path pattern for depositing single wall of Al 4047 alloy [10].

Microstructural investigation was reported by Dinda et al. which revealed that the AM of this alloy may be implemented in any industrial sector via laser metal deposition. These reported results encouraged our team to go ahead and test some more pattern. We have studied the effect of different deposition pattern on the resulting mechanical properties of laser deposited Al 4047 samples. Current research could be useful and directing commercial manufacturer to adopt this technology. The microhardness results reported by Dr Dinda et al. were around 107.8 ± 2.5 HV and 105.6 ± 2.9 HV which is comparable to our current study with hardness values around 98 HV. The study [10] mostly reports microstructural evolution using two different tool patterns and suggests that DED technique can control microstructure evolution by controlling process parameters discussed in section 1. Dinda et al. used a 6 KW CO_2 which is relatively expensive as compared to diode laser used in present investigation. Hence, diode laser based LMD systems can serve as a relatively cheaper option as compared to CO_2 laser based LMD systems.

2.5.2 Manufacturing of 4xxx series aluminum alloy using powder bed technique

Electron beam and laser sintering technique [14-16] has been used for manufacturing 4xxx series aluminum alloys. Eyitayo et al. [16] reported the deposition of various composition of 4xxx

series using laser sintering technique. Modified version of laser sintering named as Laser Pulse AM (P-SLM) technique has been applied to Al-12Si [14] to achieve 95% dense parts and vickers hardness value around 135 HV. Eyitayo et al. [16] used starting material as mixture of prealloyed Al-12Si and pure aluminum of varying sizes as shown in table 2.3 to fabricate samples via laser sintering. Eyitayo et al. used 200 W CO_2 laser at scanning speed of 50 -160 mm/s with a layer thickness of 0.25 mm/s and spacing of 0.1 mm. Instead in P-SLM [14] 0.5-4.5 KW pulsed Nd:YAG laser was used at scanning speed of 90-180 mm/min and spacing of 0.1 mm. Detailed deposition parameters are given in table 2.4. Powder used in P-SLM was provided by valimet inc (Stockton, CA) namely S20 and S10. Powder morphology is shown in figure 2.8.

Table 2.3: Various alloying compositions for AlSi alloy deposited using laser sintering. [16]

Designation	Powder Samples	Al	Si
I	90 wt% Al-12Si + 10 wt% AL-3	86.3	11.6
II	75 wt% Al-12Si + 25 wt% AL-3	89.3	8.7
III	50 wt% Al-12Si + 50 wt% AL-3	91.5	6.0
IV	75 wt% Al-12Si + 25 wt% AL-1	88.9	8.7
V	75 wt% Al-12Si + 25 wt% AL-2	89.3	8.7
VI	75 wt% Al-12Si + 25 wt% AL-4	89.5	8.6
VII	75 wt% Al-12Si + 20 wt% AL-3 + 5% Al-4	89.7	8.9
VIII	75 wt% Al-12Si + 15 wt% AL-3 + 10% Al-4	89.0	9.0
IX	75 wt% Al-12Si + 10 wt% AL-3 + 15% Al-4	89.8	8.6
X	75 wt% Al-12Si + 5 wt% AL-3 + 20% Al-4	90.2	8.5

The energy density required to melt the S10 and S20 Al-12Si has been reported as 1220J/mm3 and 1620 J/mm3 and was calculated using energy equation reported by Wang et al. [17].

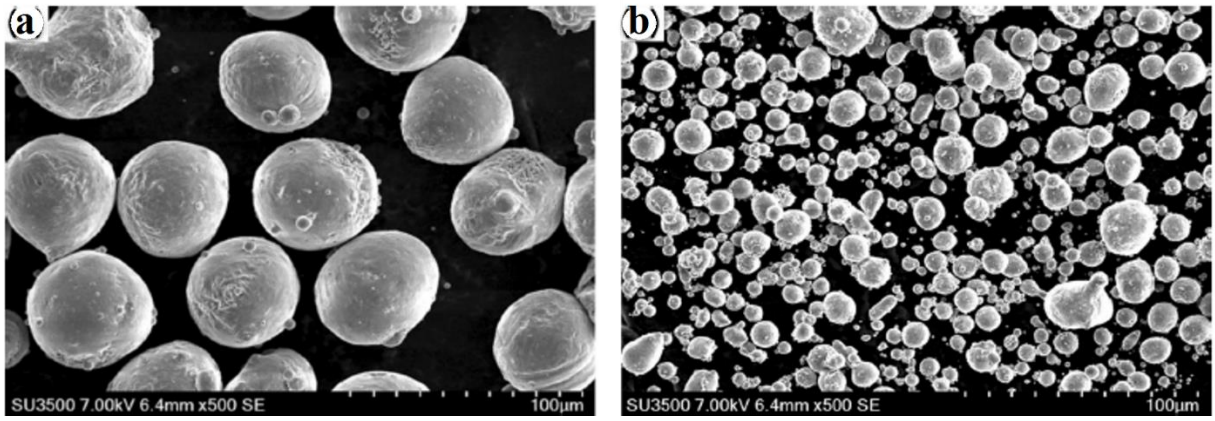

Figure 2.8: Powder morphology of Al-11.28Si alloy (a) S20, and (b) S10 [14].

Density reported by Wang et al. [17] was to the maximum of 97.8 percent. Also tensile test has been reported by Wang et al. as shown in figure 2.10, was performed using tensile test samples deposited in dog bone shape as shown in figure 2.9 under different enviorment of inert gasses to see difference in properties of the deposited sample. Helium gas enviroment when used seems to have significantly reduced tensile properties of the deposited samples. In case of laser sintering or laser melting process, fine powder is recommended as reported by Chou et al. [14] that fine Al-Si powder (S10 from Valimet Inc) needs less energy density to achieve peak density as shown in figure 2.9. The reason behind this phenomena is that the finer powder has more surface area for the interaction with laser, which improves the melting reaction [17, 21].

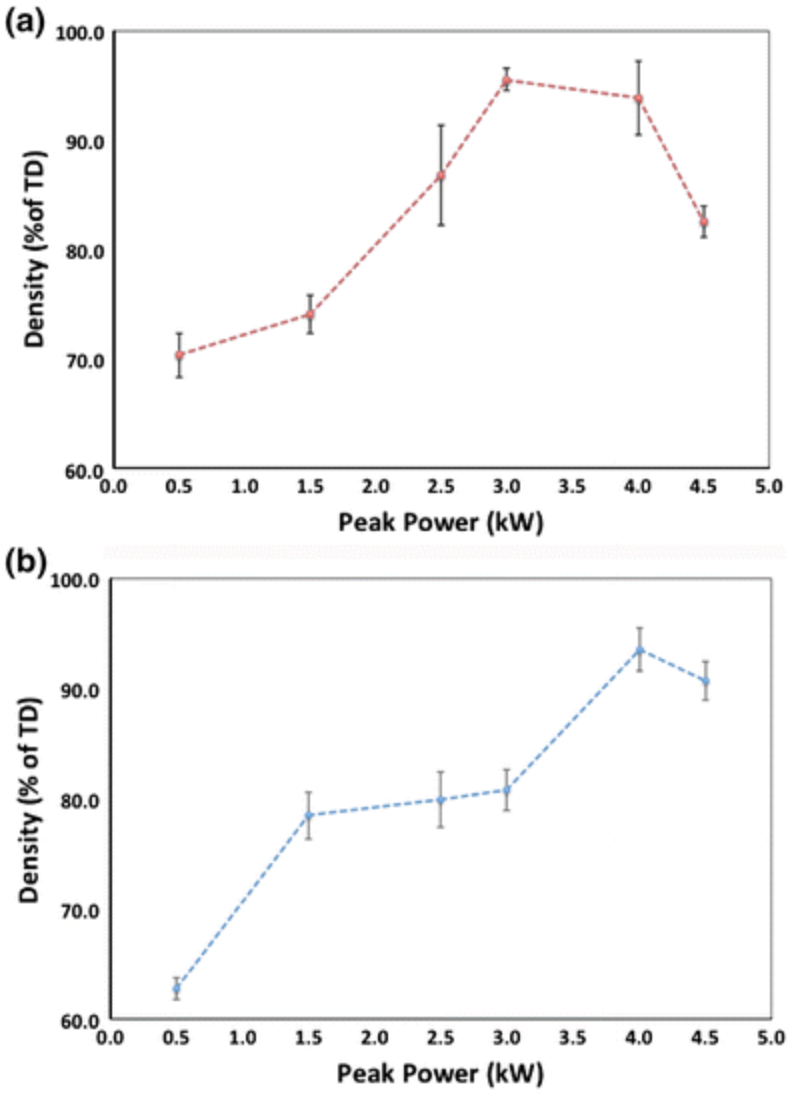

Figure 2.9: Variation in density of deposited sample using different laser power for two different mesh sized Al-Si alloy powder (a) S10, and (b) S20 [14].

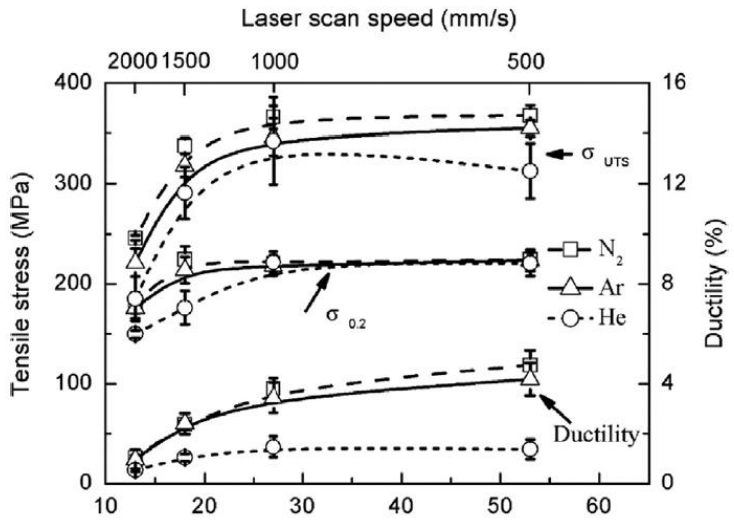

Figure 2.10: Tensile properties of SLM produced Al-Si samples under N2, Ar and He enviroment [17].

2.5.3 4xxx series Al alloy deposition parameters and deposit density found in literature

Table 2.4: Al 4xxx series depositions parameters from published literature

Technique	**Laser Power (W)**	**Scaning Speed (mm/s)**	**Layer thickness (mm)**	**Hatch spacing (mm)**	**Height (mm)**	**Ref.**
Laser Sintering	200	50-160	0.25	0.1		[16]
P-SLM	500-4500	1.5-3	0.1	0.1	5	[14]
Laser Sintering	200 W	375-2000	0.05	0.15	10	[17]
Direct Energy Deposition	600	6	1.0	-	4	[10]

The deposition parameters shown in table 2.4 served as good starting parameters for the current direct laser metal depsoition . Especially, the values in the last row from energy deposition technique have been immensely useful. The max height so far for Al-Si alloy that has been achieved is only 10mm in form of a cylindrical rod as seen from the table 2.4. No practical application has been accomplished so far using this technology. Laser sintering scanning speed

shown in the table 2.4 , seems to be very fast and is best suited for small sophisticated parts only. The biggest constraint here is the bed size. The max density achieved via sintering technique as shown in table 2.5 reported by Rchou et al. via sintering technique.

Table 2.5: Density of deposited Al-Si samples via laser sintering technique.[14].

Alloy	Condition	Density (%)	Hardness (HV)
Al-12Si (S20)	P-SLM	93.8 ± 1.9	135 ± 5
Al-12Si (S10)	P-SLM	95.6 ± 1.0	135 ± 5
Al-12Si	SLM—CW	60–80	55–107
Al-12Si	SLM—CW	97	115
Al-12Si	SLM—CW	99.5	130

2.5.4 Microsctrutural evolution of Al-12 Si during AM

Microstructural evolution of Al-Si manufacturing during AM is very interesting and immensely important to study as it aids in prediction of mechanical properties. The microstructure features are very different for every technique. Overlapping circular melted pools are observed in the direction of scanning laser in case of pulsed laser melting [14] as shown in figure 2.11; whereas tear drop shaped melted pool is observed in continuous-wave laser beam as shown in figure 2.11 a.

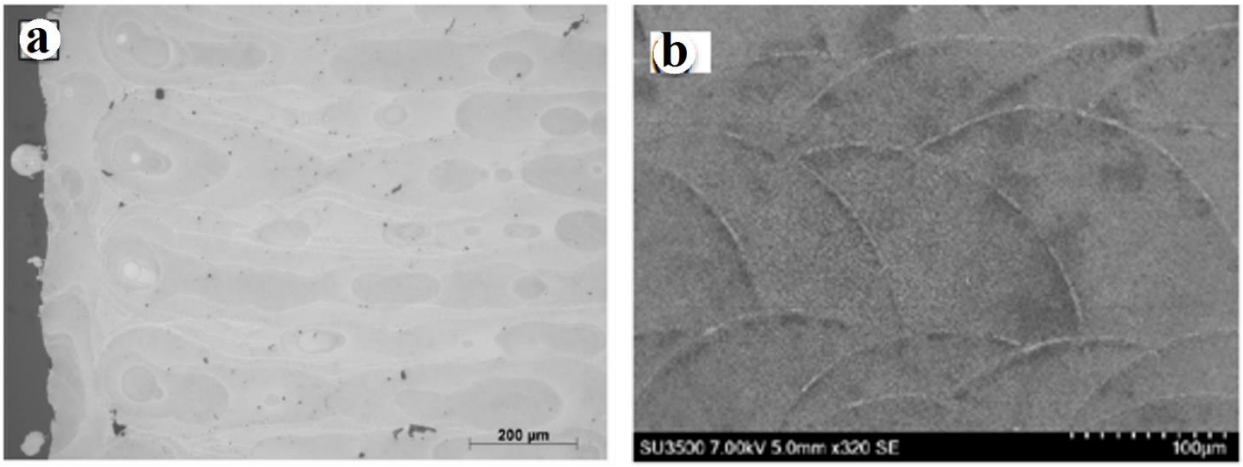

Figure 2.11: SEM micrographs for Al-Si alloy additvely manufactured via (a) C-SLM, and (b) P-SLM [14, 22].

Continuous circular bands were also observed in the direct energy deposition reported by Dinda et al.as shown in figure 2.13 which shows that P-SLM exhibits similar microstructure to that of direct energy deposition of Al-Si alloy . Since Si is insoluble in the molten aluminum solution, Si fibres can be easily observed after solidification. Fine and coarse microstructure has been reported in both direct energy and powder bed deposition of Al-Si alloy.

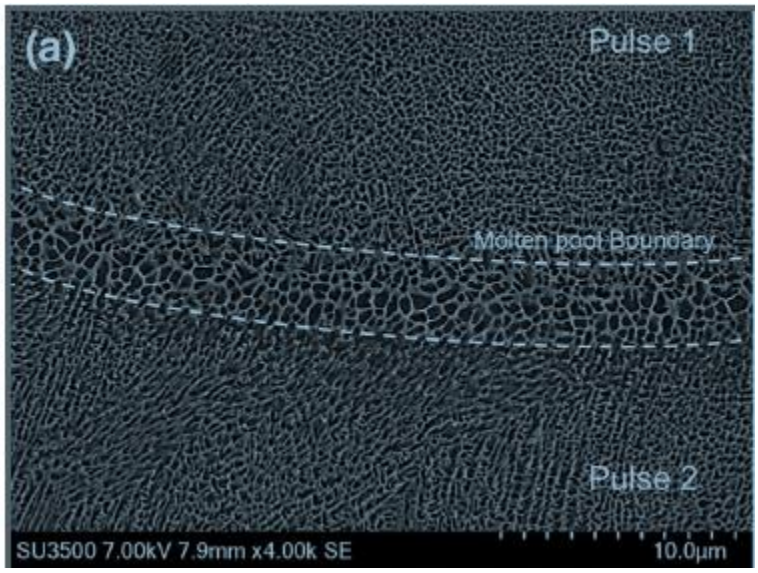

Figure 2.12: SEM micrograph of Al-Si alloy prcoessed via P-SLM [14].

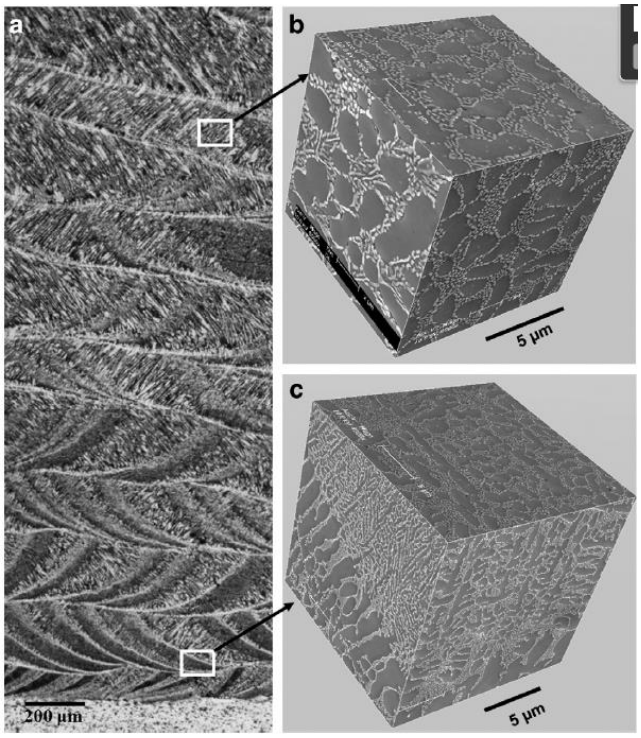

Figure 2.13: SEM micrographs of Al-11.28Si alloy at different locations [10].

2.6 Additively manufactured 7xxx series aluminum alloys

This is still an unexplored area and a great deal of research and development need in to go into manufacturing defect free 7xxx series aluminum alloy. Laser sintering of 7075 Aluminum alloy was attempted in the previous year (2016) by Reschtnik et al. [19] The deposition developed some initial cracks and work is still under progress according to the published article. Laser deposition has not been published to best of our knowledge, though laser cladding was attempted in 2011 by Cottam et al. [18] to devolp reapiring techniques.

2.6.1 Additive manufacturing of 7075 aluminum alloy using powder bed technique

The manufacturing of 7075 aluminum alloy using Selective Laser Melting (SLM) was attempted only recently by Reschetnik et al. [19] and Wang et al.[23] . There has not been any literature published regarding use of the powder bed technique, except for above mentioned work to best of my knowldege till date. In SLM high laser scanning beam interacts with the thin powder

layer in well defined tool path as shown in figure 2.14. EN AW-7075 powder with mean size of 42.1 µm was used.

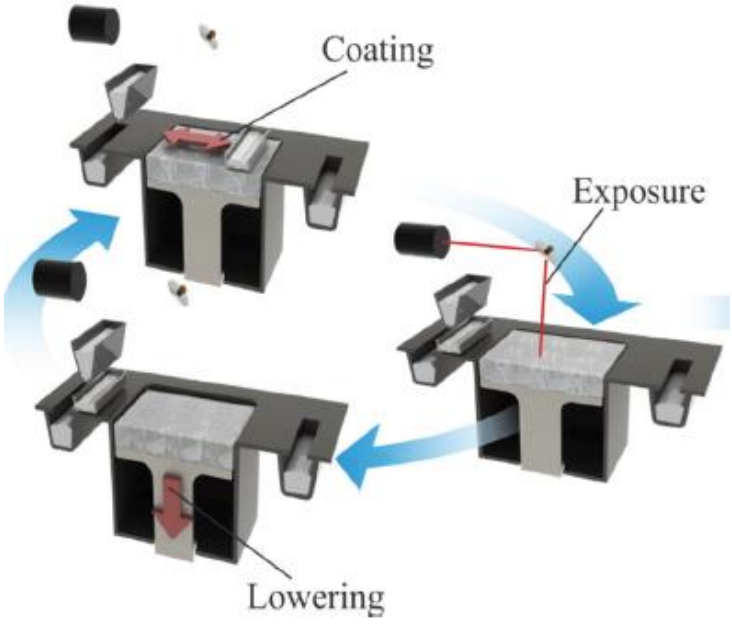

Figure 2.14: Selective laser melting process [19].

The composition was determined by the author using EDX as shown in table 2.6. Two types of specimens were made using SLM to conduct the tensile and fracture tests. Results are shown in table 2.7 shows that the ultimate tensile strength values are much lower than conventional values for both as-deposited and heat-treated sample.

Table 2.6: Composition of Al-7075 [19].

Element	Si	Fe	Cu	Mn	Mg	Cr	Zn	Ti	Al
Norm value	0.4	0.5	1.2-2.0	0.3	2.1-2.9	0.18-0.28	5.1-6.1	0.2	Balance
Casting / melting	0.2	0.2	1.6	0.05	2.5	0.2	5.8	0.01	Balance
Powder particels	0.4	0.32	2.13	-	1.95	0.26	5.1	-	Balance

Table 2.7: Tensile test results for Al 7075 alloy manufactured via laser sintering [19].

Condition	Load direction	UTS (MPa)	Elongation (%)
As-built	Parallel to building direction	203±12	0.5±0.2
As-built	Perpendicular to building direction	42±7.5	0.51±0.25
Heat treated	Parallel to building direction	206±25.7	0.56±0.11
Heat treated	Perpendicular to building direction	45±0.5	0.2±0.05

2.6.2 Manufacturing 7xxx series aluminum alloy using direct metal deposition technique

There is no literature available to best of my knowledge in laser metal deposition of 7xxx series Aluminum alloy. There have been attempts to laser clad single layer of 7075 aluminum alloy onto substrate of 7075 with the objective of developing a repair technique for high strength aluminum alloys [18]. In this attempt of cladding, Nd:YAG laser (2.4KW) was used with powder coming from side nozzle at 30 degree and forms a clad layer as shown in figure 2.15.

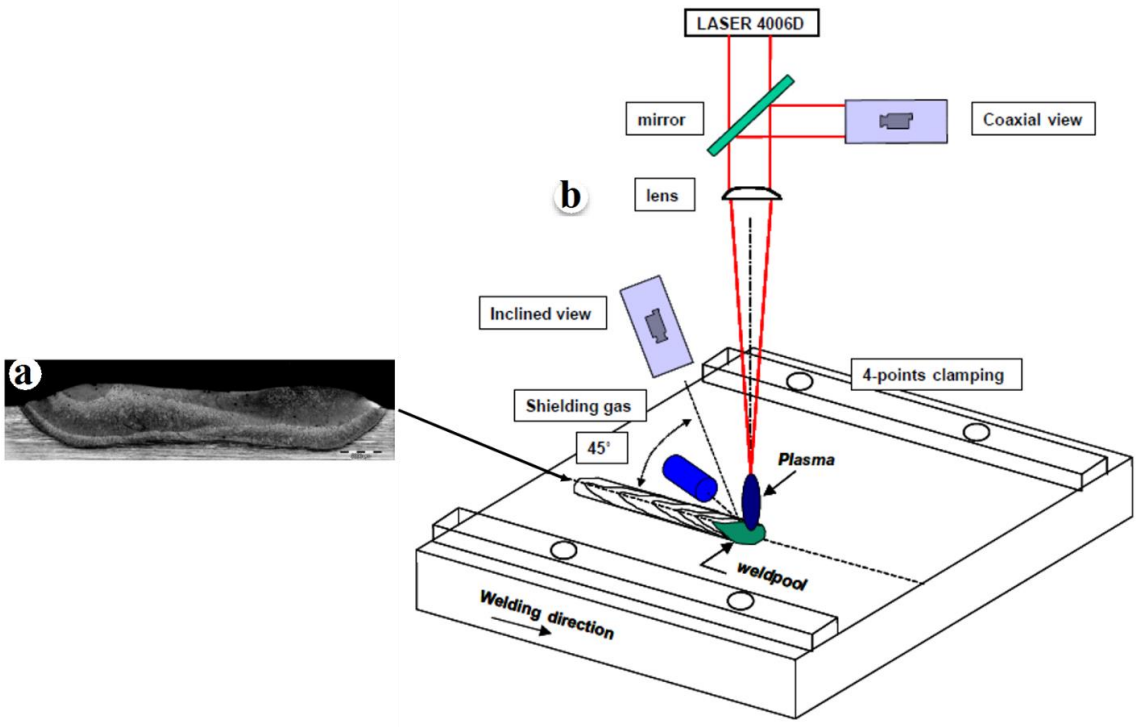

Figure 2.15: (a) As-deposited Al 7075, and (b) Experimental setup of laser caldding process [18, 24].

Direct metal laser metal deposition is continuous laser cladding, making it a suitable choice for the current research work. Very high intensity laser was required to melt the 7075 aluminum alloy resulting in high thermal diffusivity because of which even small changes in laser power result in significant variations in depth of melt pool [18]. Micro Metal Deposition (MMD) technique is the only method that has been tried so far to deposit 7075 aluminum alloy [20]. MMD is a novel technique in which miniaturized parts e.g. poros micro thin walls [25] can be manufactured. The experimental set up is shown in figure 2.15. Deposition is done in a chamber filled with inert gas and substrate is fixed on 3d platform controlled by Program Multiple Axis Controller (PMAC). Heating furnace melts the metal and droplets are controlled by droplet generator.

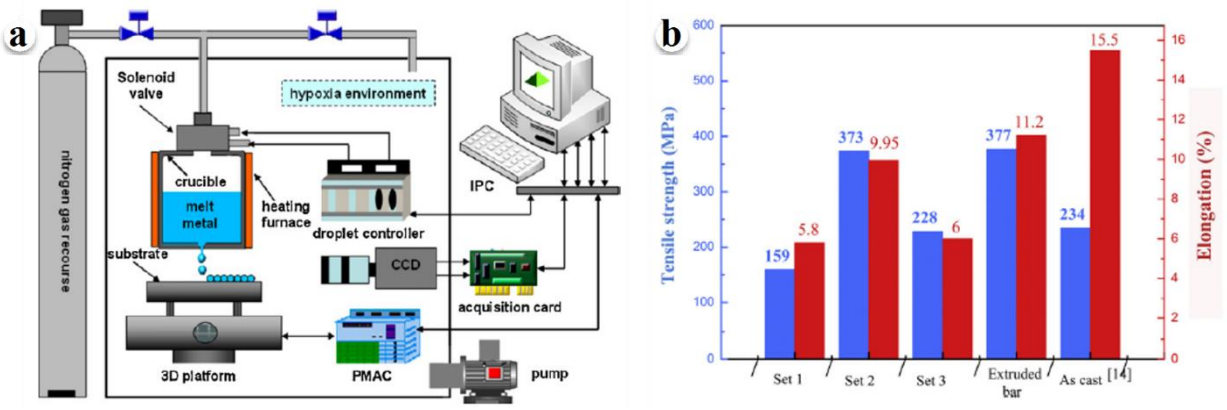

Figure 2.16: (a) Micro droplet deposition experimental setup (b) Tensile test results of micro droplet deposited samples [20, 25].

In case of MMD, key parameter is the deposition distance between nozzle to substrate. Hanzong Zou and colleagues used MMD technique to deposit 7075 aluminium alloy. They used 7075 aluminum bar as raw material on copper substrate. A tensile test sample from deposited block using MMD with best optimised parameter was found to be 377 MPa along with 11.2 percent

elongation as shown in figure 2.16 b. MMD deposition study was focused on the interfacial bonding between the metal droplets.

2.6.3 7xxx series aluminum alloy deposition parameters for deposition found in literature

There is very limited information available in open published literature as far as the deposition of 7xxx series aluminum alloy is concerned. Table 2.8 shows date available data till date in form of deposition parameters. The closest technique is Laser cladding which is suitable for coating surfaces, but there remains a dire need for developing deposition parameters to be used with 7xxx series alloy to enable additive manufacturing of 7xxx series aluminum alloys In laser sintering process [19], researchers observed cracks while depositing the 7075 aluminum alloy. MMD technique does not involve any laser, and metal is instead melted in a furnace followed by formation of molten metal droplets.

Table 2.8: Deposition parameters reported in literature for 7xxx series aluminum alloy

Technique	**Laser Power (W)**	**Scanning Speed (mm/s)**	**Layer thickness (mm)**	**Height (mm)**	**Ref.**
Laser Cladding	2378 W	31.67	-	-	[18]
Micro Droplet Deposition	Furnance Melting	-			[20]
Laser Sintering	350 W	930	0.05	10	[19]

2.7 Effect of heat treatment on additively manufactured 7xxx aluminum alloys

The heat treatment cycle data is extensively available for the cast and wrought 7xxx series aluminum alloy. However, limited studies are available with heat treatment cycle data for additively manufactured 7xxx aluminum alloys; available data is shown in table 2.9. As Al 7xxx series alloy is responsive to precipitation hardening, solution heat treatments were performed for different time periods followed by two stage aging to enhance the microstructure-property combination of the as deposited Al 7075 alloy by various authors [18, 19]. Heat treatment had

minimal effect on additively manufactured parts generated using laser sintering of Al 7075 alloy as shown in table in 2.9. The tensile strength was reported to have increased from 203 MPa to 206 MPa when built direction was parallel and from 42 MPa to 45 MPa when built direction was perpendicular. The HT on the Laser cladded [18] region found to be responsive, as deposited clad of 7075 was around 100 HV and it was increased to 150 HV after heat-treatment.

Table 2.9: Heat Treatment for additively processed 7xxx series aluminum alloys

AM Technique	**Solution Heat Treatment**	**Aging**	**Ref**
Laser Sintering	1.5 hours at 480 ^{o}C	170 ^{o}C for 6 hours	[19]
Laser Clading	1.5 hours at 490 ^{o}C	121 ^{o}C for 24 hours	[18]

2.7.1 Low tensile properties of additively manufactured 7xxx series aluminum alloys

It is very clear from section 2.6.1 that additively processed 7075 aluminum alloy has low tensile properties when compared to as-casted. The max value of additively manufactured parts to be 203 MPa and literature suggests that casted 7075 has maximum value of 540 MPa in T7[19]. This suggests that successful processing of 7xxx series aluminum alloys yet have to achieved via additive manufacturing process. Development of initial cracks in case of laser sintering of Al 7075 was the reason behind low tensile properties reported by author. In case of laser cladding, Zn and Mg vaporize due to high heat generated by the laser. The reduction in amounts of Zn and Mg was reported as shown table 2.10. Vaporization of Zn and Mg shown in table 2.10 results in less formation of strengthening precipitates (Mg_2Zn and Al_2CuMg) and hence poor mechanical properties.

Table 2.10: Composition of 7075 Alumiun alloy in wieght percent [18].

Sample	**Al**	**Si**	**Cu**	**Fe**	**Mg**	**Zn**	**Cr**
Substrate	Bal	0.06	1.41	0.19	2.43	5.52	0.24
Powder	Bal	0.16	1.55	0.27	2.56	2.56	0.21
Clad	Bal	0.1	1.44	0.24	2.15	4.53	0.24

2.7.2 Microstructure of Laser Cladded 7075 aluminum alloy

Laser cladding shows the closest microstructure achieved through LMD technique. Figure 2.17 shows the coarse second phase particles. These second phase particles were rich in Zn, Al and Cu and were indentified using EDS [18]. After heat treatment (table 2-10), these particles shrinked to a very small size according to Cottam et al. [18].

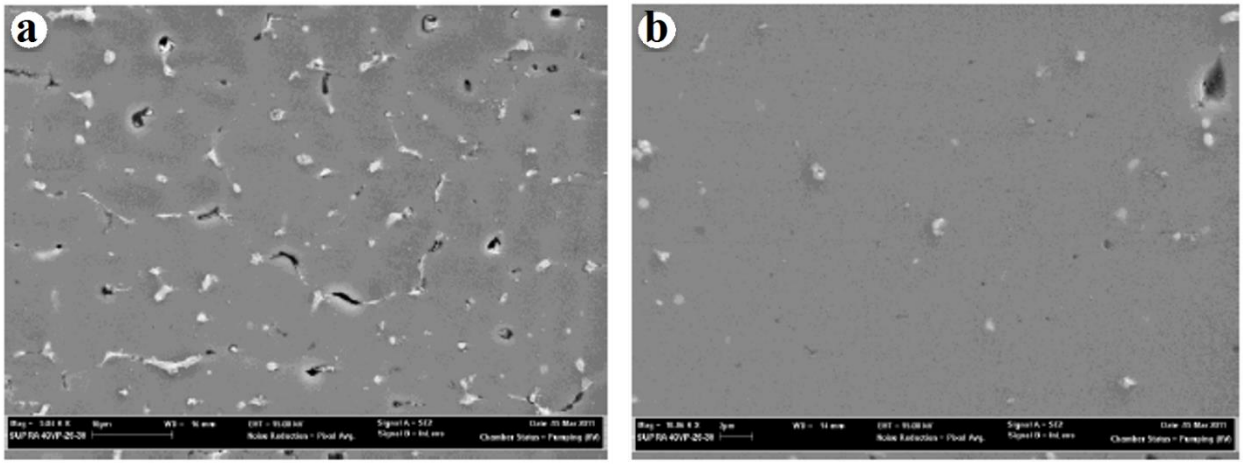

Figure 2.17: (a) SEM micrograph of Al 7075 as-deposited clad region , and (b) Zoomed view[18].

2.8 Strengthening mechanisms of 7xxx series aluminum alloys

The 7xxx series aluminum alloys consist of alloying elements such as Zn, Mg, Cu, and Zr. These alloying elements form precipitates after conducting the solution heat treatment followed by age hardening. This process enhances the microstructure-properties. The effect of above mentioned particles depends on their size, spacing and distribution. Broadly, these alloying elements are classified into three types of second phase particles [26].

- ***Constituents***: The coarse constituent particles result because of impurities e.g. Fe and Si. The size range of constituents varies from 5 to 30 µm.
- ***Disperoids***: These are intermetallic particles, which have low solubility in aluminum matrix at all temperatures. Mainly elements like Cr, Mn and Zr are the disperoids and

vary in size between 20-500 nm. They helps to pin grain boundaries and avoid grain growth during solution heat treatment. Finally, it results in fine recrystallized grain size to achieve high strength and better corrosion resistance.

- ***Strengthening precipitates***: strengthening precipitates are formed from super saturated solid solution (SSSS). SSSS is a solution, which has more solute than solvent can dissolve in itself.

SSSS ⟶ GP Zones ⟶ ή ⟶ η (Nominally $MgZn_2$) [26]

Table 2.11: Equilibrium Phases [27].

Phase	**Notation**	**Crystal Structure**
Al	α	FCC
$MgZn_2$, CuMgAl	η	HCP
$(Al,ZN)_{49}Mg_{32}$,$CuMg_4Al_6$, Al_2Mg_3Zn	T	cubic
$FeAl_3$	X	Monoclinic
Al_2CuMg	S	

Clusters of particles are formed after quenching known as guiner presto (GP) zones which are spherical in shape. As heat of solution for Zn and Mg is negative, they form cluster together on quenching [27]. The composition of GP zones depends on the Mg to Zn ratio. η phase is incoherent where as GP zones are coherent and ή is semicoherent. If the aging temperature is held for long time, fine strengthening precipitates are formed which are incoherent with aluminum lattice. $MgZn_2$ found to hexagonal plate like structure preferably on (111) plane [26]. Precipitation hardening mechanism found to be the most contributing factor for rise in strength of around 100 Mpa reported by the Dixit et al. [26]. There are various mechansim through which the strength of 7xxx alloy increases, such as solid solution strengthening (SSS), grain boundary strengthening, dislocation strengthening. In SSS mechanism, one atom of second phase prticle added to the cystalline lattice of aluminum and

forms solid solution. Mg is most soluble among all other particels present in 7xxx series aluminum and hence can provide SSS to the alloy. Recrystalization in smaller grains due to heat treatment increses yield strength of alloy. Enormous study has been conducted on the heat tretment of 7xxx series aluminum alloy [28-32]. As casted 712 aluminum alloy have tensile stregth value of 241 MPa. Han et al. [28] conducted various solution heat treatments on aluminum alloy 7050 to find the effect on tensile strength, fracture toughness, and yield strength. The maximum strength found to be after conducting solution heat treatment at 470 ^{o}C as shown in figure 2.18. This clearly shows significance of heat treatment on aluminum 7050 alloy.

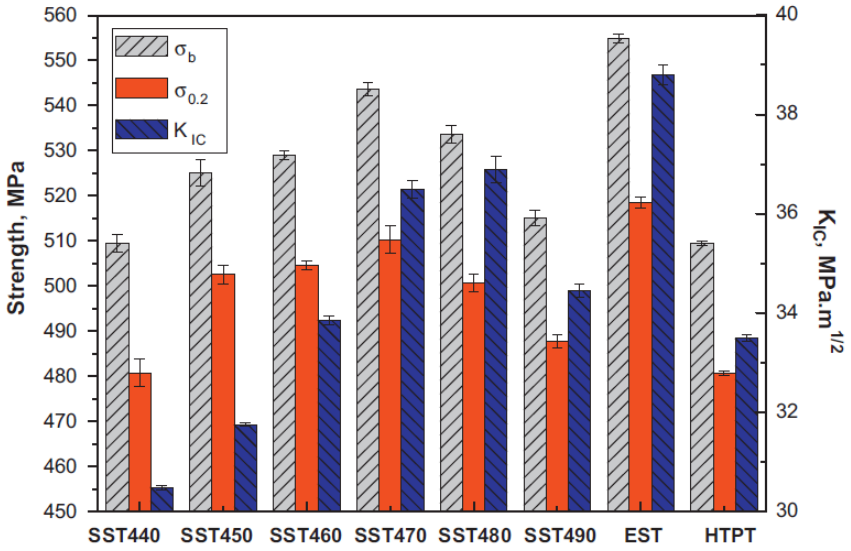

Figure 2.18: Tensile properties of wrought Al 7050 alloy after solution treatment [28].

2.9 Strengthening of 7xxx series aluminum using friction stir processing (FSP)

The welding institute (TWI) invented the Friction Stir Welding (FSW) process in 1991 at United Kingdom. It is a solid state joining process in which the tool keep rotating while plunging in the metal which in turn makes the material to move front to back around the tool pin itself resultng in filling the hole. Fine microstructure is produced during severe plastic deformation of

material. There is no open literature available on friction stir processing of additively manufactured Al 7050 alloy to best of my knowledge however FSW on wrought Al 7050 rolled plate was studied by Mishra et al. [33]. This study was conducted on 7050-T7451 aluminum alloy to establish relationship between FSW parameters and weld nugget and HAZ zones hardness values. Two different welds were made at 0.85 and 3.8 mm/s translational speed along with tool roational speed of 120 and 540 rpm respectively. The hardness value of weld nugget is maximum at the center and minimum at the heat affected zone (HAZ). It shows that faster the rotation speed in weld, higher is the hardness.

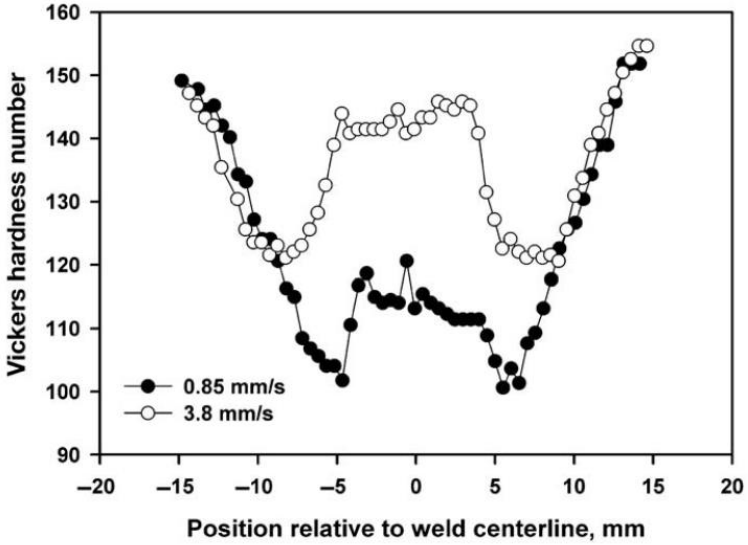

Figure 2.19: Hardness value of FSW Al 7050-T7541 at two different rotational speeds [33].

There is very close relation between the harndess variation shown in figure 2.19 and temperature distribution shown in figure 2.20. Slower is the translatioanl speed and high is pin rotational speed, more is the temperature at center line as shown in figure 2.20.

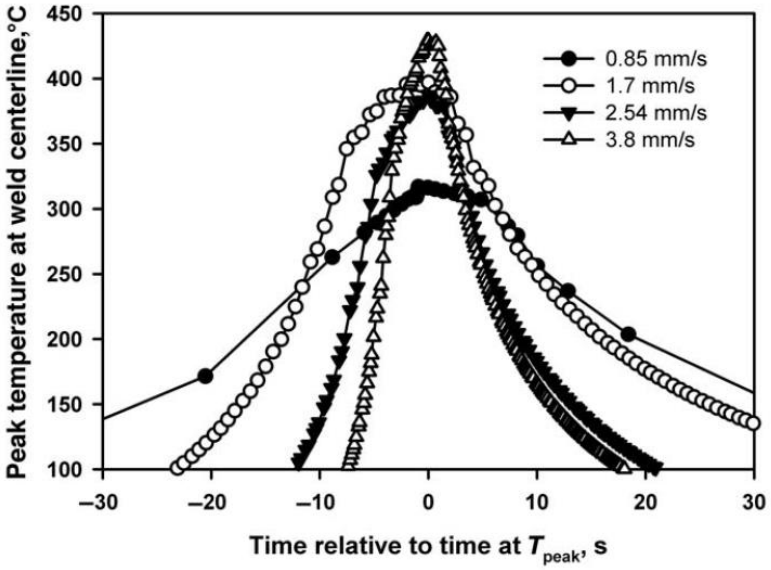

Figure 2.20: Temperature plots for FSW Al 7050-T7541 at various translation speeds [33].

There is highest temperature at the centerline and highest is the hardness which suggest that temperature reached at that speed results in solution heat treatment. Temperature at the HAZ was around 300 ^{o}C at which M phase is formed, this M phase is non strenghtening and in coherent. Hence the harndess value decreases at the HAZ area. The effect on grain evolution was studied by Rhodes et al. [34] on 7050-T76 aluminum alloy showed that when the sample is plunged at higher rpm, finer is the grain size. The recystalized grain size at 300 rpm was 25-40 nm and 100 nm at 500 rpm, respectively. After FSP, Rhodes et al. heat treated the FSP samples and observed increase in size of grains as shown in figure 2.21.

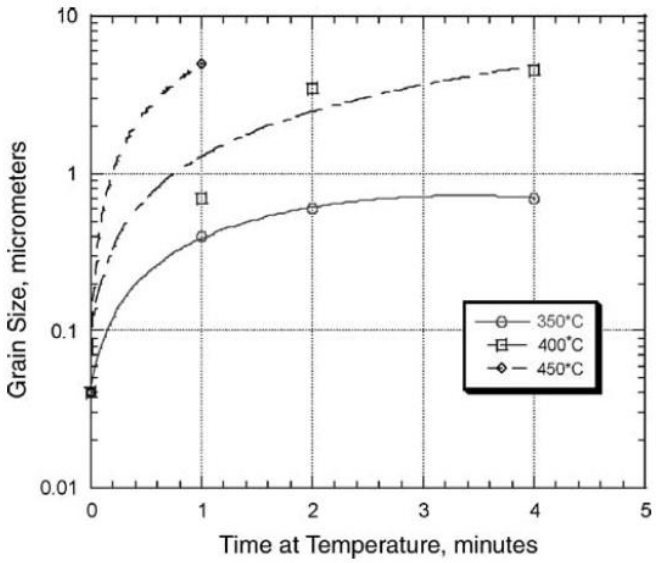

Figure 2.21: Grain growth behavior of FSP 7050-T76 [34].

CHAPTER 3 RESEARCH OBJECTIVES

Additive manufacturing (AM) gives a lot of flexibility in terms of customization and repair technology especially for automotive, aerospace and biomedical industries. Lightweight design combined with the high strength is the one of the first priority in the current era of automotive and aerospace industry. The combination of low density (2.7 g/cm^3) with high strength makes 7xxx series aluminum alloys a potential candidate for light weight applications [35]. The ultimate tensile strength of 7050 aluminum alloy after heat treatment is 543 MPa [28] which is approximately twice of 4xxx series aluminum alloys. AM of aluminum alloys always remained a challenge and specifically for 7xxx series aluminum alloys. Recently Reschntnik et al. [19] and Hansong et al. [20] additively manufactured 7075 aluminum alloy using powder sintering and micro metal deposition technique, respectively. Process induced cracks were found by Reschtnik et al. during AM of 7075 aluminum alloys using selective laser melting. Micro droplet deposition manufacturing (MMDM) technique involves melting of Al 70705 billets using induction furnace. Hence, at present, no directed energy deposition technique-using laser as heat source attempted so far for processing 7xxx series Al alloys. There is a dire need of AM of 7xxx series aluminum alloys because of its endless applications in automotive and aviation industry. The objective of this study is to optimize the laser deposition parameters for manufacturing defect free 7050 aluminum alloy and to investigate the microstructure properties relationship in laser deposited samples. Ultimate tensile strength of additively manufactured and heat treated Al 7075 alloy using selective laser melting [19] found to be 203 MPa with elongation of 0.5 percent. Precipitation mechanism have been widely studied in spray forming, equal channel angular processing, controlled diffusion solidification etc. [12, 26, 30, 31, 36-41]. Precipitation was also observed during laser metal deposition of Al 7050 alloy. However, there is limited literature available on precipitation kinetics

during laser additive manufacturing of Al 7050. This study opens door for direct energy deposition process for any kind of 7xxx series aluminum alloys. The 4xxx series aluminum alloy is important as 7xxx series because of its vast application from engine to structural components in automotive industry. Most of the castings used in automotive industry uses Al-Si alloys, putting necessary emphasis on implementation of deposition of Al-Si alloy using AM. Numerous studies show additive manufacturing techniques been used to successfully deposit Al-12Si however no open literature is available on deposition of Al-Si alloy on existing automobile parts and none of them discussed challenges if AM is applied at commercial level [10, 14-17]. This study also deals with challenges involved using Direct Laser Metal Deposition technique (LMD) to deposit Al-12Si on the existing cast parts. LMD combines both laser cladding along with the rapid prototyping, which gives full freedom to manufacture any sophisticated shape. LMD has an advantage over laser sintering technique, it can print on existing parts without requiring the extra process of combining the additively manufacture part to existing part. This study has proven the reliability and consistency of the LMD to achieve the deposition of Al-12Si on existing Al-Si casting. LMD has an upper hand as it deposits highly dense (99.9 percent) eutectic Al-Si alloy as compared to the maximum density achieved in sintering which is 99.5 percent via Pulsed Selective Laser Melting (P-SLM) [22]. The practice of casting all components first and then joining them using various welding techniques has long been followed in the automotive industry. The best solution is LMD, which brings us the possibility to print other components on the existing cast part. This provides the designer with a lot of freedom to change design as per customer requirements. This study could be used as a guide for implementation of direct metal deposition of 4xxx series alloy using LMD technique in automotive sector. LMD has vast application other than manufacturing parts including surface coating, repair, remanufacturing etc. [42-46]. Laser sintering has been used for depositing

hyper and hypo eutectic alloys [10, 14-17, 21, 22, 47] but so far mechanical test results has been only provided by X.J Wang [17] using Powder bed technique (Laser Sintering). However, tensile test result for the direct metal deposition sample has never been reported so far in literature till date to best of my knowledge. Hence, It becomes necessary to study mechanical properties so that industry can take advantage of this revolutionary technique and could implement on commercial scale. The specific research objectives of this research are directed towards:

1. Systematically investigate the effect of laser deposition parameters on the resulting microstructural evolution and mechanical properties to deposit the defect free Al 4047 and Al 7050 alloys.
2. Establish the correlation between chemical composition of the powder feed with the composition of the deposited material.
3. Study the effect of post deposition heat treatment and friction stir processing on the resulting mechanical properties of laser deposited sample.
4. Design an appropriate 7xxx series aluminum alloy for additive manufacturing applications.

CHAPTER 4 EXPERIMENTAL PROCEEDURE

4.1 Fundamentals of laser metal deposition technology

Robotic direct Laser Metal Deposition (LMD) technology was developed at Wayne State University having four main components 1.2KW Diode Laser, ABB IRB-1410 six axis Robot, Coaxial nozzle, 1200SP-1 Powder feeder. LMD technology combines the rapid prototyping with laser cladding into solid freeform fabricating process. Various other processes similar to LMD were developed with distinct names such as Direct Metal Deposition (DMD) [45] at University of Michigan, Laser Engineered Net Shaping (LENS) [48] at Sandia National Laboratories, Direct Light Fabrication (DLF) [49] at Los Alamos Laboratories.

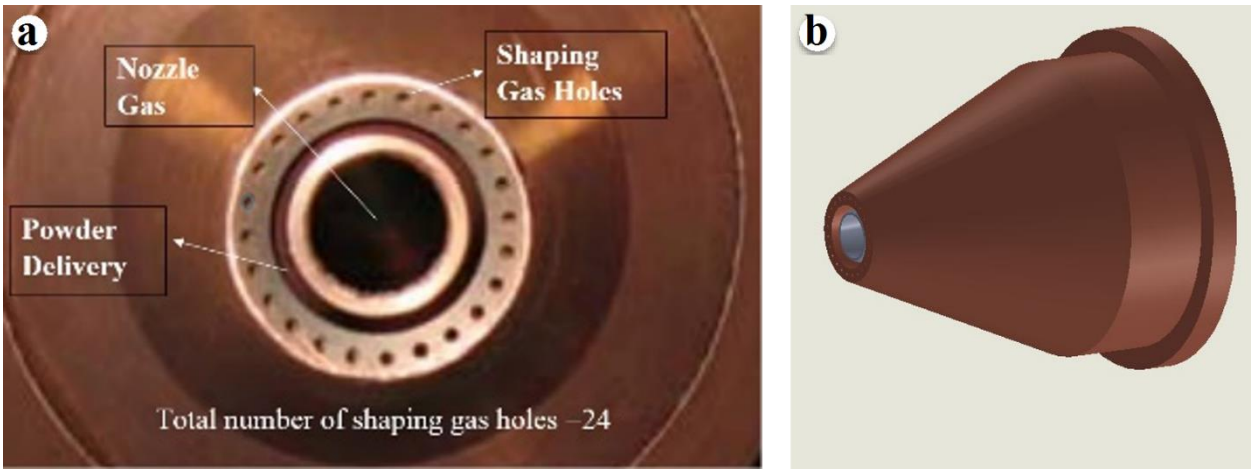

Figure 4.1: Coaxial copper nozzle, (a) Bottom view, and (b) Side view.

Copper Nozzle shown in figure 4.1 shows all the different openings for powder delivery, Nozzle gas, and shaping gas holes. The coolant from chiller is circulated inside the nozzle to avoid damage to the nozzle due to immense heat produced by laser. Nozzle is made from copper to dissipate the heat at faster rates. Powder hopper delivers the powder to the nozzle powder delivery openings and then the powder is concentrated on the substrate with the help of shaping gas coming from shaping gas holes. The nozzle gas is used to protect the laser lens from powder dust and vapors.

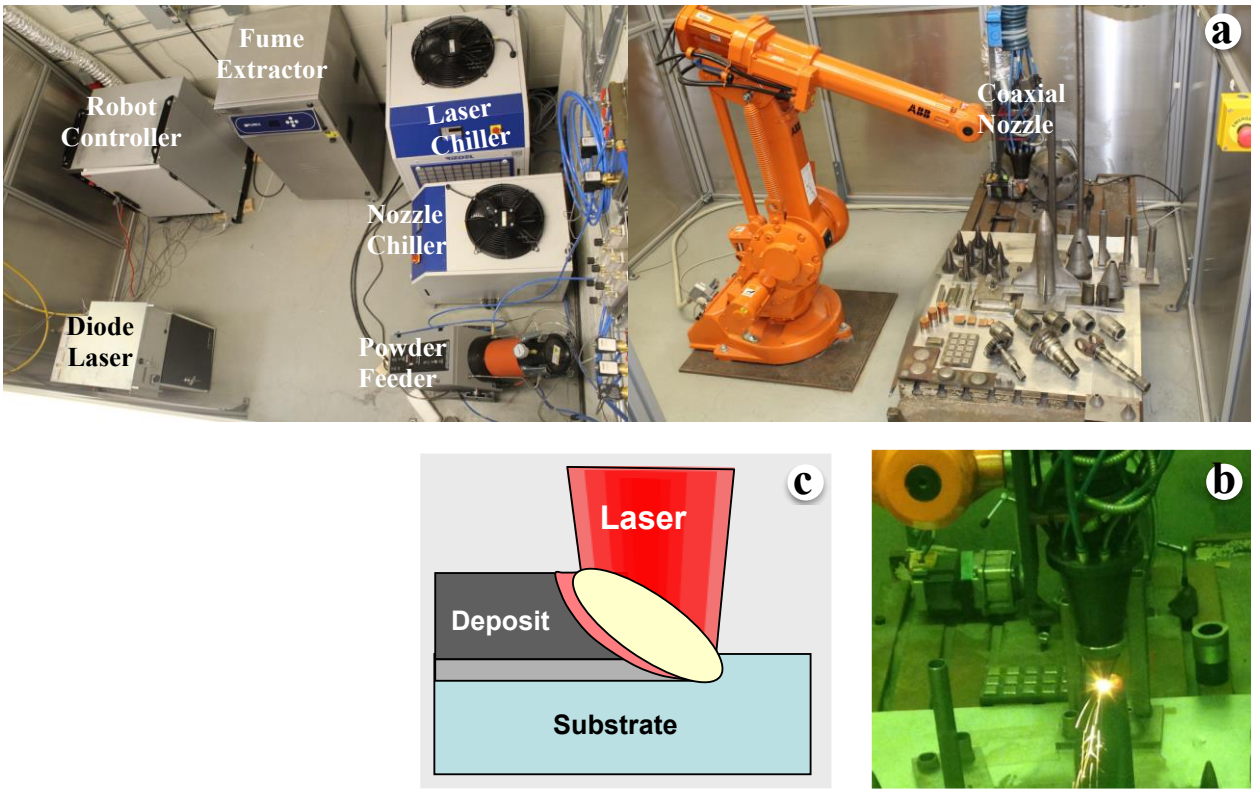

Figure 4.2: Robotic laser metal deposition (LMD) equipment developed at Wayne State University. (a) Individual components of LMD system as shown in figure, (b) image of the LMD process in action, and (c) the schematics of LMD process.

Through optical fiber, laser is focused from the center of the nozzle on to the substrate or previously deposited layer and creates a melt pool. The concentrated powder gets melted as soon as it falls in the melt pool and when the nozzle moves linearly, the melted powder solidify (Shown in figure 4.2 c). Moving nozzle leaves behind continuous solid metal bead, for this reason AM is also knows as continuous welding process. The nozzle moves in the definite pattern known as tool path. The schematics of the manufacturing process is shown in figure 4.3 b.

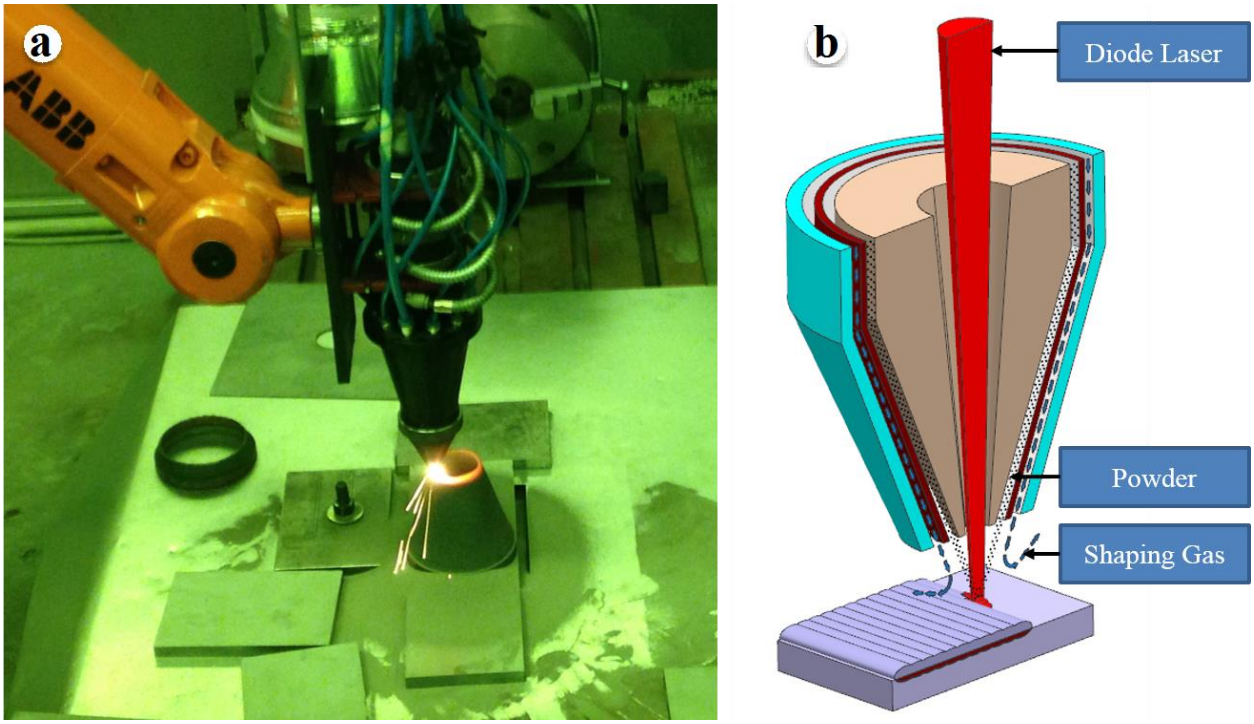

Figure 4.3: (a) Coaxial nozzle connected at the end of robotic arm, and (b) Schematic of LMD process.

4.2 Laser metal deposition process paramters optimization strategy

As already elaborated in detail in introduction the basic functioning of Direct Laser Metal deposition, there are three LMD parameters involved in manufcturing of any alloy.

- Laser Power
- Powder Feed Rate
- Linear Velocity
- Gasses flow Rate (Powder feeder gas, Nozzle gas, Shaping Gas)

4.2.1 Strategy followed to devolp to find defect free LMD parameters

DOE is good tool to optimise the process paramters with less number of experiments, as the experiments were performed it was realized that one DOE is not good enough to predict the defect free optimisation paramters. Hence various experiments were performed using L9 array of

taguchi method. Coupons of 20x20 mm were made of 3 mm height and then inspected visually to check quality of deposit. Once the eye inspection is passed, coupon is cut exactly in half and mounting is done for further inspection under optical microscope to check the porosity. In this way samples are processed with various LMD paramters and inspected untill we get the optimised paramters to achieve defect free sample. The detailed strategy for optimising the LMD parameters 7xxx series aluminum alloy is shown in figure 4.4, Firstly an estimated parameters window was chosen from the literature survey and then parameters were varied between +50% from the center of parameter window. The processing parameters of the second design of experiments (DOE-2) were conducted within ± 25% from the best parameters found from DOE-1. Subsequently, DOE-3 narrowed down the processing parameters, which varied within ± 10% from the optimized parameters of DOE-2.

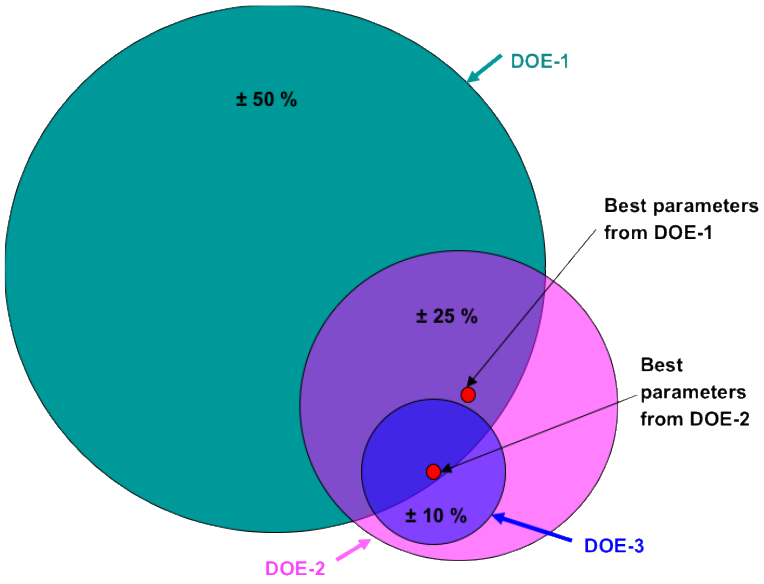

Figure 4.4: DOE strategy applied to optmize process parameters for defect free deposition.

4.2.2 Effect of LMD Parameters on deposition quality

All LMD parameters plays significant role in the quality of deposit. The ultimate objective of variation of all parameters is to maintain continous melt pool and to achieve the defect free deposit. Following are the four main LMD paramters.

- **Laser**: The primary objective of the laser is to create a melt pool so the inomcing powder feed can be melted. Theroetically laser power should be enough to melt the powder. Theoretically laser power should produce temperature more than 600 ^{0}C to create the aluminum alloy melt pool however due to the high thermal conductivity of aluminum alloys, higher temperature is required to maintain conitnous melt pool. Especially first layer should have highest laser power , Intial high laser power serves two purpose, one is it heats up the susbstrate which in turn reduce the defects at the interface and secondly it helps in good bonding at the ineterface. At the same time the estimation of laser power also depends on the powder flow rate, if the powder flow rate is too high then high energy density is needed to create melt pool of aluminum powder but low energy desity is required for low powder flow rate.
- **Powder Flow Rate**: Powder flow rate has to be optimized for mainly two reasons, to maintain desired height and secondly to achieve high density of deposition . If powder flow rate goes too high, it may come too close to nozzle which might hit the bottom part of nozzle and may damage the nozzle by welding itself with the bottom part of nozzle. On the other hand if powder flow rate is too slow then deposition height will be less and at some point of time powder might not even hit the target substrate and layer building will be stopped eventually.

- **Linear speed**: Linear speed of robot is crtical in terms of quality. With constant laser and powder flow rate, if linear speed is too high, energy density will be less and powder will not be able to melt which in turn results in less height deposition and debonding. Melt pool might not be continous resulting in no deposition at all. On the other hand if the linear speed is too slow which results in higher energy density, hence build rate increases and deposit might hit the nozzle.
- **Gasses flow rate**: Gasses flow rate generally not varied too much. The primary objective of the gas is to transport the powder from powder hopper to the nozzle, to protect the nozzle from dust or vapurs, and create a shield to avoid the oxidation of melted powder. In case of aluminum for single wall creation it has to be kept high for avoiding certain kind of defects. If powder particle size is small or powder is too heavy, more powder gas is required to move the powder from powder hopper to nozzle.

4.2.3 Tool Path

In laser metal deposition of 4xxx and 7xxx series alloy, two kind of tool path strategies have been used. Single wall tool path, in which the nozzle translates in one direction only. Second strategy was implemented to make tensile test samples and square coupons for microstrucural study, in which the subsequent layers were deposited perpendicular to each other as shown in figure 4.5. In case of hatch pattern as discussed above to make coupons of 20x20mm, there is overlap of the bead to previous bead by at leat 0.5 mm to achieve the highly dense deposit.

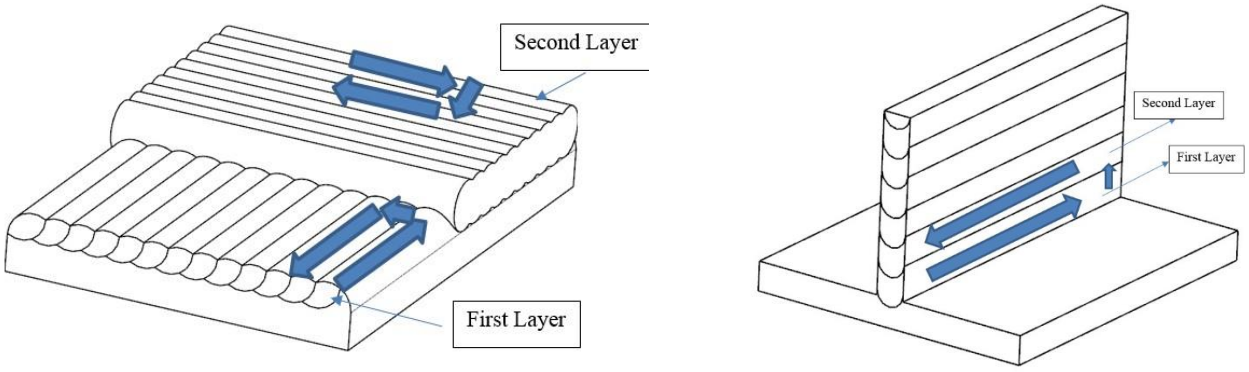

Figure 4.5: Tool Path strategy for (a) Block deposition, and (b) Single wall deposition.

4.3 Challenges of processing of aluminum alloys by LMD

So far in this research of deposting 4xxx and 7xxx series Al alloys, following challenges have been faced so far.

4.3.1 Sintering issue

This issue occurs while doing single wall deposition of 4xxx Al alloys. The reason behind this sintering issue is that as explained ealier that laser power has to be high while doing deposition but also powder flow rate has to high in case of single wall depostion. Powder catchup is less in case of single wall due to less space avaialble on the top surface of single wall 2.5 mm thickness. Laser has to hit that at the top of thin wall which increases the chances of loosing the powder on either sides of the wall. While doing experiments it has been observed that this loose powder falling either side of the wall sticks to the hot surface of wall and get sintered with the wall. This loose powder then start making double walls on both sides of actual single wall as shown in figure 4.6. This issue has limit the hight the component to about 15 mm.

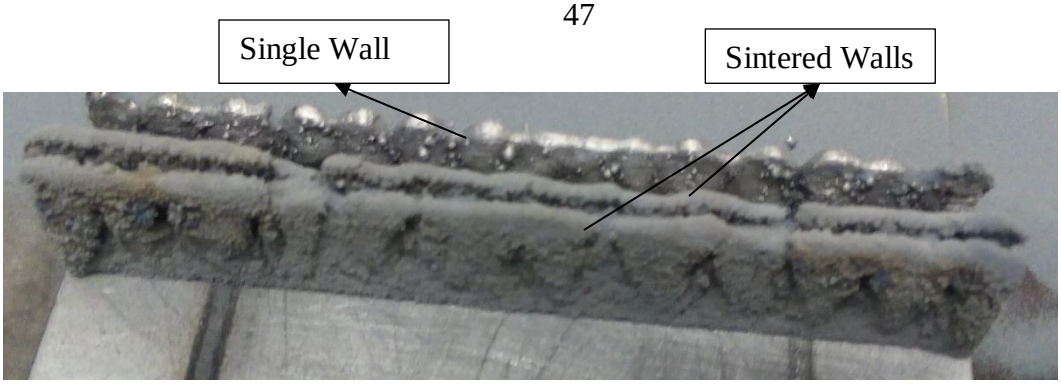

Figure 4.6: Single wall depostion of 4xxx Aluminum alloy with sintered wall on both sides .

4.3.2 Wavy Pattern at top

After finishing the depostion of single wall, it was observed a waviness at the top of the single wall deposit as shown figure 4.6. There is couple of solutions proposed for this issue is that to stop at certain hieght wherever it becomes too wavy and mill the wavy part using milling machine. Then start from height unitll we see again waviness. Reason for this wavy pattern seems to be unstable melt pool due to high thermal conductivity of aluminum alloys. Keeping nozzle close during the depostion reduces the waviness issue.

4.4 Sample preparation for mechanical testing and microstructural study

Mechanical properties of laser deposited aluminum 4xxx and 7xxx series include tensile testing and microhardness testing.

4.4.1 Micro hardness investigation

Study of microhardness of deposited 4xxx and 7xxx gives good idea about variation of hardness from substrate to last layer of depostion. Hardness was measured throughout the deposit area to see if any hardness gradient exist along the height of deposit or remains constant. Interface area that is the very first layer bonding with the substrate is of great interest where hardness might vary from the rest of the deposit. In the same way top layers of the depositied material is expected to exhibit higher microhardness values. Coupon of 20x20 mm was depositied for both 4xxx and

7xxx series aluminum alloy and then cut the sample into two equal halves. Then one of these halves is mounted using buehler hot compression mounting machine as shown in figure 4.7.

Figure 4.7:Buehler hot mounting machine.

Vickers hardness test is by applying 100g of force for 10 seconds with diamond indentor of square based pyramid. Using manual tool in software, resulting indentation diagonal was measured. Then this mesured diagonal and test load is substituted in specific formula to calculate the vickers harndess value. This is an autoamted process in software.

4.4.2 Tensile testing

Tensile testing was proposed to find three basic mechanical properties that is Ultimate Tensile stress, Yield Strength and Modulus of Elasticity so it can be compared to conventional manufactured material mechanical properties.

Tensile Sample Preparation:

- A block (100 mm x17 mm x15 mm) was deposited using LMD of Aluminum alloy 4xxx and 7xxx series.
- The block was then given dog bone shape in machine shop using below given dimensions as per ASTM E-8 standard shown in figure 4-6. Milled dog bone block shown in Figure 4-7.

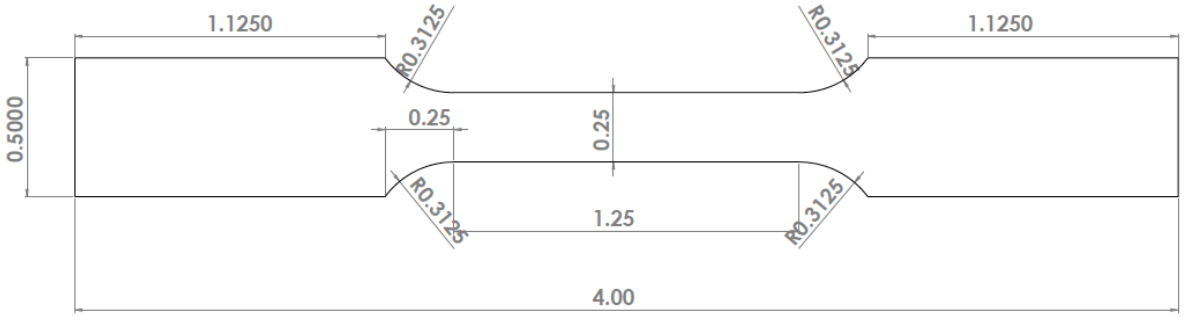

Figure 4.8: Tensile test sample (All dimension in inches)

Figure 4.9: Al-11.2Si Block milled to Dog Bone Shape.

- Tensile test samples of 2 mm thickness is EDM cut from above dog bone shaped block as shown in figure 4.

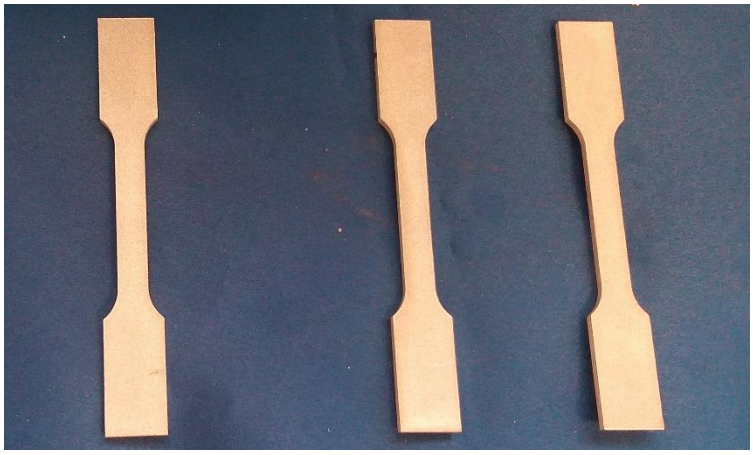

Figure 4.10: EDM cut samples of Al-11.2Si Alloy.

Tensile testing Machine:

Universal tensile testing machine (MTS 810) as shown in figure 4.11 was used for tensile testing of final samples as shown in figure 4.10. Significant clutching pressure was set so that sample do not slip while under tension. Tensile testing was done at ramp up speed of 0.05 mm/s.

Figure 4.11 (a): Tensile testing machine.

4.4.3 Microsctural studies and crystallography

Scanning electron microscope was used to study the microstructural evolution of the Al 4047 and Al 7050 alloy deposit. LMD is layer by layer and rapid solidification process and each layer might have different thermal history which results in variety of microstructure pattern. The Deposited 4xxx and 7xxx series aluminum alloys, lattice parameters has to be known to find the type crystal planes and atomic distances. For this puprose Xray Diffraction analysis was conducted. For xrd sample preparation, deposited material is cut out from substrate and topmost layer of the deposited material is flatten and polished. Then X ray scanning is done with two theta angle being varied from 20 till 100 degree at scanning speed of one degree per minute.

4.5 Practical implementation of 4xxx series aluminum alloys

To achieve the goal of implementation of the 4series aluminum aloys in manufacturing an automotive part, laser metal depostion was conducted on shock tower hood.There are several components that is currently being spot welded on the shock tower hood. So instead of spot welding, LMD can be implemented to print various parts on the shock tower hood itself. Bracket is one of the component that is spot welded on the shock tower hood. Before the replicating bracket, a series of feasibility study was done on substrate to optimise the parameters for single wall and find achievable maximum height. A series of tensile test was done before printing on shock tower hood. Thickness test study was conducted on thinest substrate for deposition, so while implementing in industry, sustrate thickness could be standardised for optimised paramters.

4.6 Mechanical properties enhancement techniques

In this LMD study of aluminum, two techniques was followed to enhance the mechanical properties of Al 4047 and Al 7050 deposit: heat treatment and friction stir processing.

4.6.1 Heat treatment

The 7xxx series aluminum alloy is precipitation hardening alloy. There are precipitataes in the Al 7050 deposit which are intially coarse and decorated around the interdendritic region. Fine precipitates provide high strength if spread uniformly and dissolved in aluminum matrix which can be achieved through heat treatment as suggested in open literature [30, 31, 36-41, 50-55], heat treatment was carried out in furnance as shown in figure 4.12.

Figure 4.12: Tube furnace used for heat treatement.

Solution heat treatment was conducted from one hours to eight hours and then perform two step aging for 24 hours followed by air cooling. Conduct Metallography and hardness test on each heat treated sample to study post heat treatement mechanical properties and mocrostructural properties.

4.6.2 Friction stir processing

This is a unique way for the enhancement of mechanical properties, it is a solid state welding process, as already explained, also sometimes known as friction stir processing. The LMD of aluminum 7xxx series was friction stir processed at various rotational and translational speeds with special frictional stir welding machine as shown in figure 4.13 to fine down the coarser precipitates and recrystallize to finer grain structure.

Figure 4.13: (a) Friction stir processing (FSP) machine, (b) Schematics FSP strategy, and (c) SFP tool used in this study.

4.6.3 Friction stir processeing and heat treatment

Study of combination of both heat treatment and Friction Stir Processing would be worth a look to see how much difference it can make.

CHAPTER 5 LASER METAL DEPOSITION OF AL 4047 (AL-11.2SI) ALLOY

Direct laser metal deposition can be used to manufacture either a solid or a hollow part. Hollow part can be considered as thin wall structure with particular shape. So given these two scenarios, block and single wall deposition was carried out to investigate microstructure and mechanical properties before implementing the technique to shock tower hood (automotive part). Gas atomized Al-Si alloy powder was supplied by Valimet Inc within the mesh size of -100/+325 was used for the deposition purposes. The morphology of powder is shown in figure 5.1. The powder particles were rather spherical, some having satellite powder particles as shown in magnified view in figure 5.1 b. The composition of the as-received powder is shown in table 5.1.

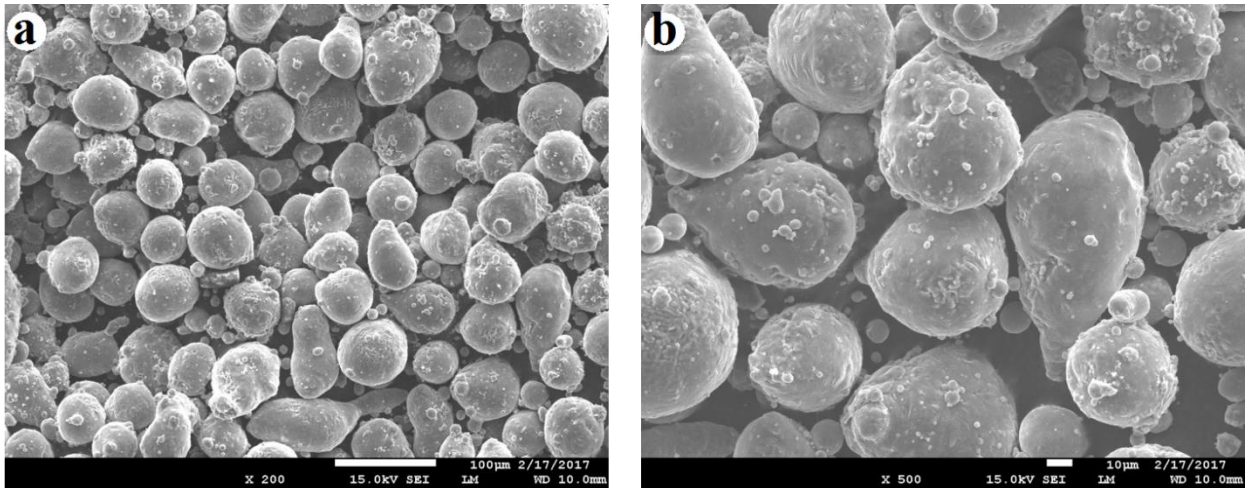

Figure 5.1: (a) SEM image of as-received Al-11.2Si powder, and (b) Zoomed view of alloy powder.

The Al 6061 rolled plate was used as substrate material on which initial coupons were deposited to optimize the process parameters before replicating the bracket on shock tower hood. Various parameters (laser power, powder feed rate, and linear velocity) were optimized, as each parameter has significant effect on the build quality of deposit, to achieve the high density and defect free Al-Si deposition. The required laser power to melt Al-Si alloy is higher than other

alloys such as Ni-, Fe- and Co-alloys, although the melting point of Al alloys is substantially lower than Ni-, Fe- and Co-alloys, because of high thermal conductivity of Al alloys. The scanning velocity and powder feed rate has to be coupled to achieve a stable melt pool. Due to high thermal conductivity of Al alloys, the melt pool can be unstable if above mentioned process parameters are not optimized. As a result, the process window for Al alloy processing is rather narrow compared to the conventional alloys. Similar observation was made by R Cottam et al. in cladding process [18].

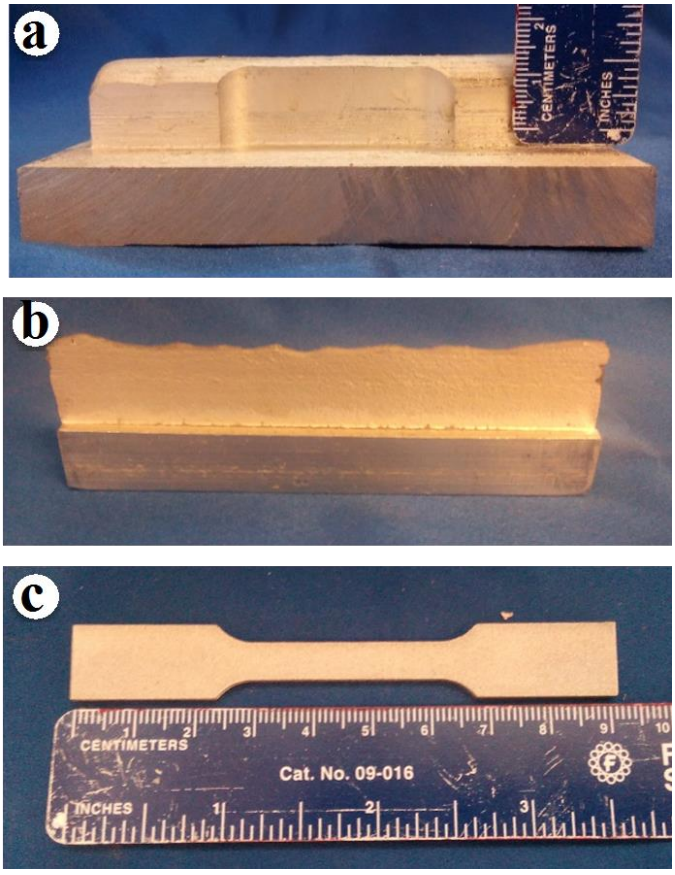

Figure 5.2: (a) Block deposit milled to dog bone shape as per ASTM E8 standard, (b) Single wall deposit milled on both sides, and (c) Final tensile test sample.

The primary objective of this study is to deposit Al-Si alloy on any existing automotive cast parts using direct metal laser deposition to prove its utility. Not only these parameters but also

working height from nozzle to build height has to be constant all the time to get the defect free deposition, which is trickier in case of Al-Si alloys. The primary objective of this study is to deposit Al-Si alloy on any existing automotive cast parts using direct metal laser deposition to prove its utility. A shock tower hood was chosen for demonstrating the deposition of Al-Si alloy. The tensile test sample prepared from a Al-Si block (100 mm × 17 mm × 15 mm) as shown in figure 5.2 a and single wall deposition as shown in figure 5.2 b, deposited using optimized laser deposition parameters. These tensile test samples were machined as per ASTM E8 standard dimensions. Resulting milled dog bone block is shown in figure 5.2 c. Three tensile test samples of 2 mm thickness were cut using wire EDM from above dog bone shaped block. Three single wall deposits were made to mill three more tensile test samples. The primary objective of preparing samples from single wall and block was to investigate the effect of scanning pattern on mechanical properties. Moreover, the bracket on the shock tower is a single wall structure, so it was necessary to study the mechanical and microstructural properties of single wall deposition. . Metallographic etching was done by dipping samples in solution of 100 ml H_2O, 25 ml HNO_3, 15 ml HCL, and 10 ml HF for 10 -12 seconds.

Table 5.1: Composition of Al-11.2Si

Si	Fe	Al
11.2	0.15	88.65

5.1 Block deposition of Al-11.2Si alloy

Block deposition was carried out using hatch pattern as shown in figure 5.3 a. Two blocks with dimensions, 20 mm × 20 mm × 3 mm and 100 mm × 17 mm × 15 mm were deposited on a rolled Al-6061 substrate. The smaller block (20 mm × 20 mm × 3 mm) was cut into two equal halves and used for microscopy analysis.

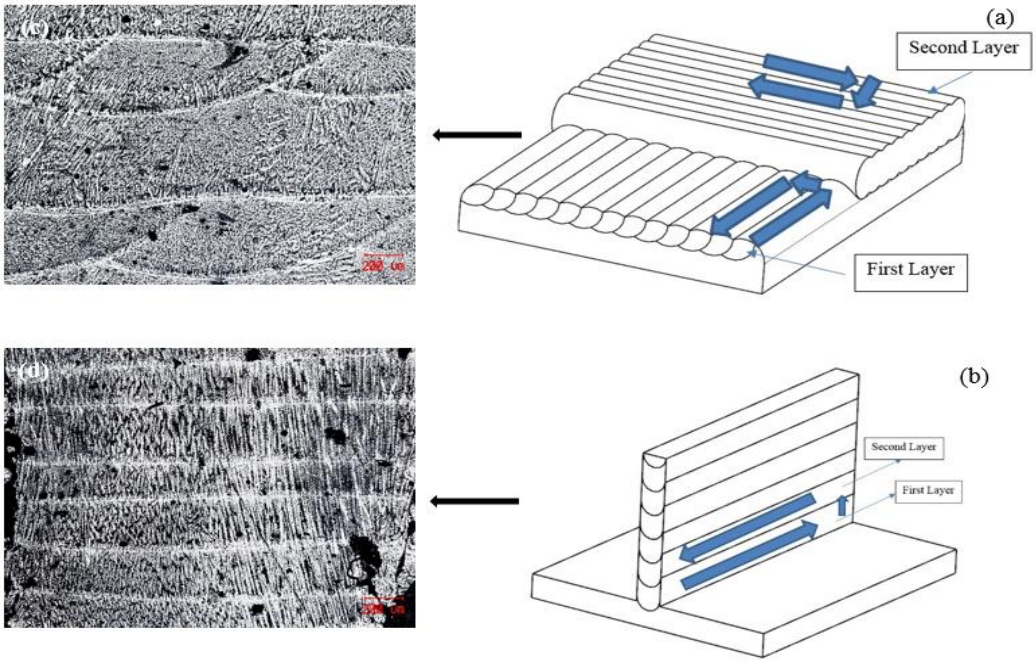

Figure 5.3: **:** (a) Block hatch deposition pattern, (b) Single wall deposition pattern, (c) Optical micrograph of the as- deposited block sample, and (d) Optical micrograph of the as-deposited single wall deposit.

Optical micrographs confirmed the density of block deposition was greater than 99.9 %. The bigger block was used to make tensile sample. Tensile test exhibited excellent combination of elongation (9%) and ultimate tensile strength (225.7 MPa) as shown in figure 5, which is comparable with conventional cast component. Mechanical properties achieved through direct laser metal deposition process is comparable with the combination (Elongation & UTS) achieved through selective laser sintered samples as per reported in available literature [56, 57]. Present results indicate that deposition is of good quality and hence practical implementation is feasible. Optimized laser deposition parameters are given in table 2. In the very first layer of deposition the powder flow rate was kept low (2.6 g/min) to achieve good bonding with the substrate. It was observed that the laser power particularly has to be kept high (900 Watt) for the aluminum alloys to achieve the continuous melt pool because of high thermal conductivity of aluminum. Block

deposition samples showed very consistent stress strain results as shown in figure 5.4, which points towards the isotropic properties. Hence, the hatch pattern provides the uniform properties of Al-Si alloy deposit across the height of block.

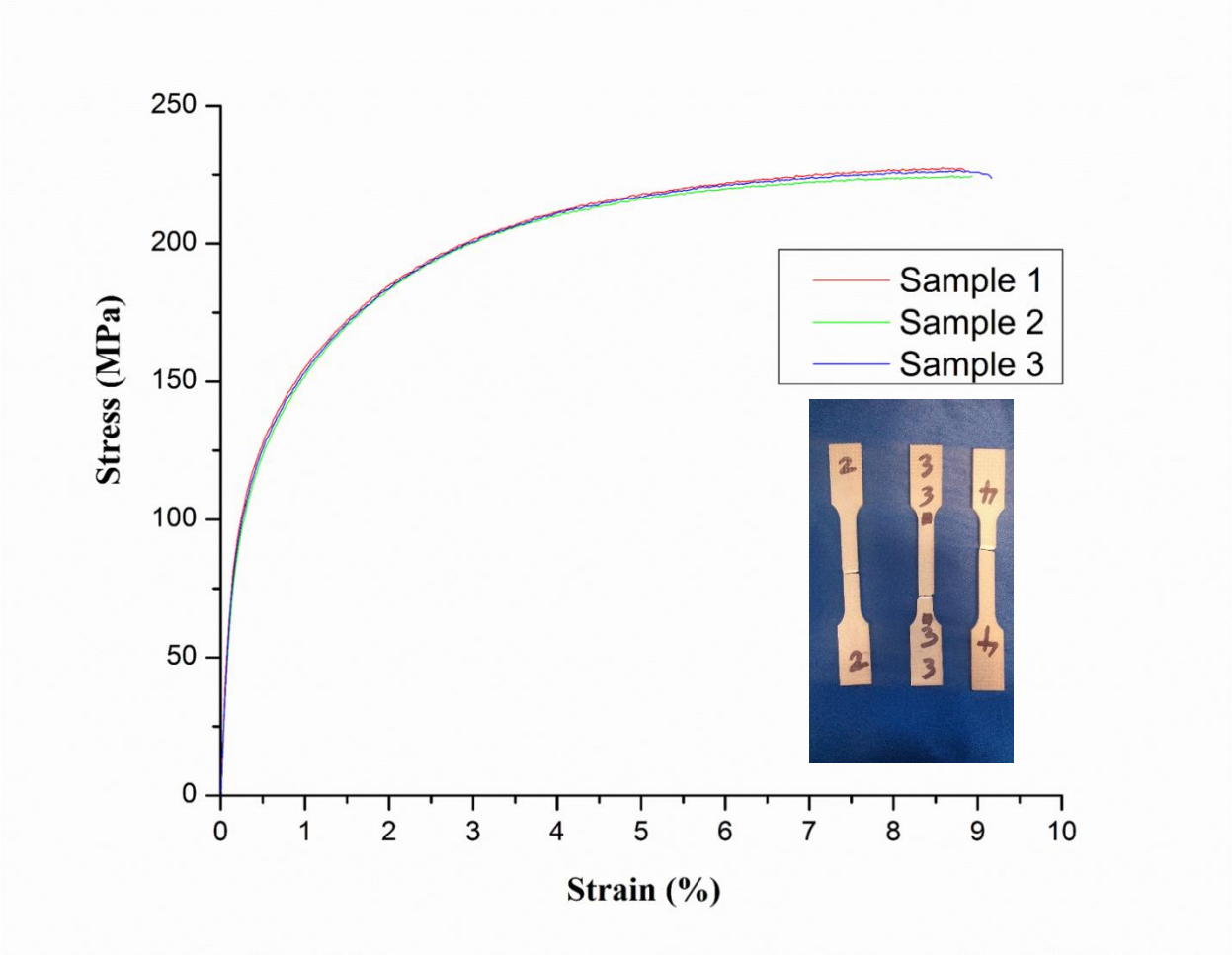

Figure 5.4: Stress strain curves of the as-deposited Al-11.2Si block tensile samples.

In case of block deposition, there is continuous pattern of alternate layer of overlapping bead like structure as shown in figure 4c. This unique microstructure pattern was a result of hatch scanning. In hatch scanning pattern, circular overlapping beads was observed in the first layer as shown in 4c, second layer was deposited perpendicular to previous deposited layer and hence the transverse layer shows no overlapping beads. The microstructure of transverse section of deposited block shows that coarse columnar dendrites gradually transformed to fine equiaxed dendrites

around middle of each layer. Silicon particles is the brighter phase and darker phase is the α-aluminum dendrites. Since the bead boundary area is the liquid/solid interface and due to high thermal gradient and low solidification velocity at the lower part of the melt pool, columnar dendrites are formed above the bead boundary opposite to the direction of heat flows. In figure 6b, it was found that the secondary inter-dendritic arms spacing on an average was about 2.4 μm. No major defects like cracks, de-bonding at interface or between layers observed. In figure 6c, the observed voids are the result of fallout of the Si particles while polishing the samples. Low thermal gradient and high solidification velocity at upper part of the melt pool resulted in equiaxed microstructure as shown in figure 6d. Low hardness value of 70 HV was observed just above the bead boundary due to the presence of coarse dendrites. Present results indicate a high value of hardness of 90 HV at the upper part of each deposited layer due to the presence of fine equiaxed microstructure. This increase in hardness value is about 28 percent from the soft circular pattern area to the upper part of each layer of deposit. Dinda et al. has reported 10 percent change in hardness while depositing Aluminum 4047 alloy using CO_2 laser [58].

Table 5.2: Optimized laser deposition parameters for Al-11.2Si.

	Block Deposition	**Single Wall**
Laser Power (Watt)	900	900[1]
Powder Flow rate (g/min)	3.5	6.3
Scanning Speed (mm/min)	720	576

[1]Laser power was reduced by 50 watt after every 5 mm layer deposition until final laser power reached to 800 watt.

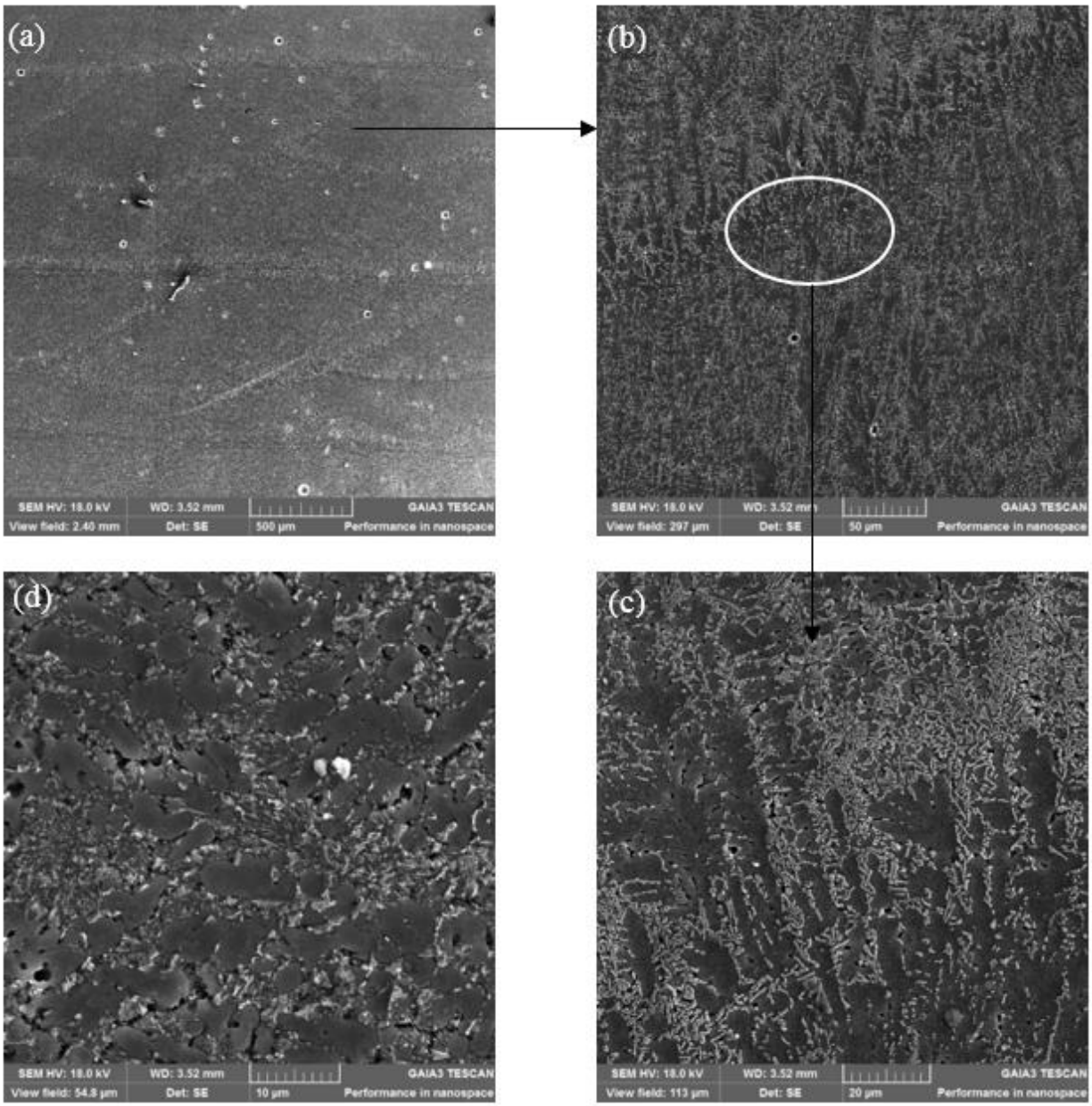

Figure 5.5: (a, b, c) SEM micrographs of Al-11.2Si block sample showing dendrites around circular pattern, and (d) Equiaxed microstructure at top part of sample.

5.2 Single wall deposition of Al-11.2Si alloy

Laser deposition parameters was optimized for single wall deposit, as the parameters are dependent on material type and design requirements. Optimized parameters for single wall deposit as shown in table 5.2. Single wall was deposited using scanning pattern as shown in figure 5.3.

The first objective was to deposit defect free single wall sample with high deposition rate. This objective is crucial because as we are trying to replace the welded bracket with deposited bracket. To accomplish the bracket deposition on shock tower hood, we had to demonstrate that LMD can build tall enough deposit to replace welded bracket design. Before printing on the shock tower hood, single wall sample was deposited on the Al-6061 rolled substrate. Building single wall structure was a challenging process with aluminum alloys, because of high thermal conductivity of Al alloy. High laser power makes the single wall sample hot enough so that loose powder falling on the sides gets sintered and hinders the further deposition process. To overcome this challenge, laser power had to be reduced after every 5mm while maintaining continuous melt pool. This sintering issue was hurdle to achieve height more than 15 mm. The top surface of the wall at the end of the deposition was found to be wavy in nature and not flat. Waviness might be due to unstable melt pool and high thermal conductivity of aluminum alloy. Substrate thickness test was conducted in which single wall was deposited on three different substrate having thickness of 1.5 mm, 2.0 mm, and 3.0 mm. This test revealed that minimum 2 mm thick substrate was required to avoid distortion in the substrate. Note that the shock tower hood thickness was about 3 mm, hence, same process parameters was used to build single wall bracket on the shock tower hood. Before printing on the shock tower, last step was to analyze the mechanical properties to test the feasibility for practical implementation. The tensile test of single wall sample exhibited average ultimate tensile strength of 225 MPa with average elongation of 9.4%. Though the average UTS and elongation was found to be same as of block deposited sample but in case of single wall tensile test sample, there is maximum variation of 50% in elongation and 9% variation in UTS. Tensile test results shows that mechanical properties are at par with the conventional cast counterparts. After conclusive tests, single wall was printed on shock tower hood as shown in figure 5.10 with

optimized parameters. No deformity was observed after printing on shock tower hood, only minor impression was located right at bottom of deposition.

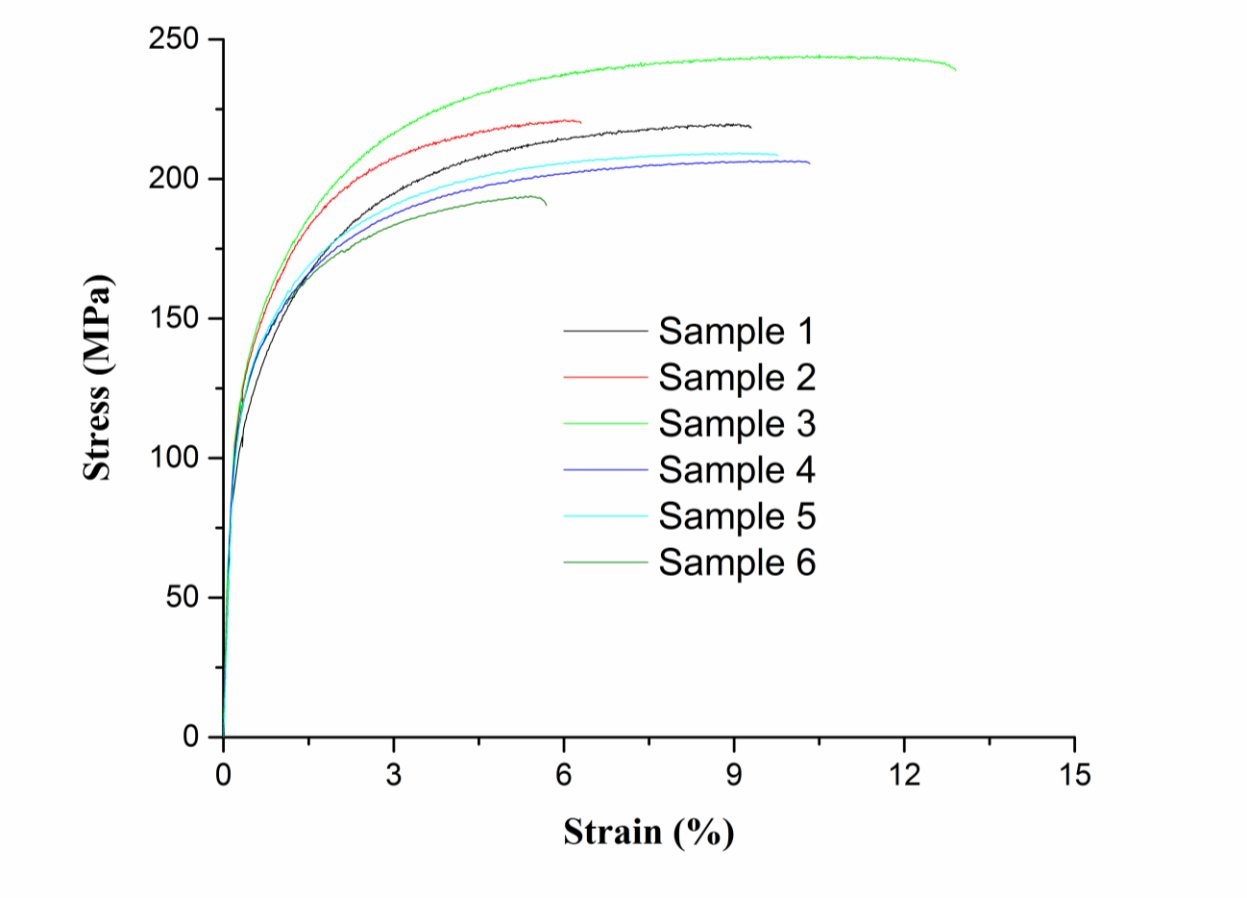

Figure 5.6: Stress strain curves of the as-deposited Al-11.2Si single wall tensile samples.

Table 5.3: Mechanical properties of as-deposited Al-12Si alloy.

	Block Deposition	Single Wall Deposition
Yield Strength (MPa)	122.43	105.43
Ultimate Tensile Strength (MPa)	225.7	225.6
Elongation (%)	9.0	9.4

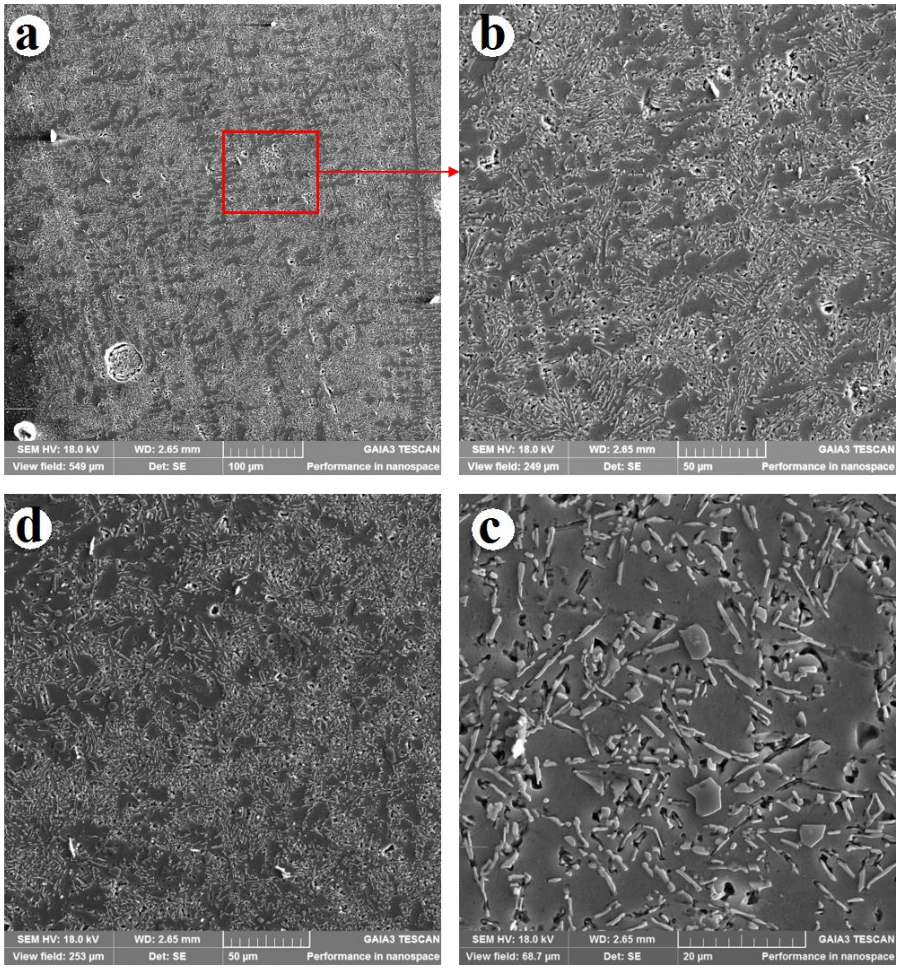

Figure 5.7: Micrographs of single wall deposit: (a) Overview of dendritic structure, (b) Zoomed view around columnar dendrite, (c) Zoomed view at height of 15 mm, and (d) Top of single wall.

The continuous columnar dendrites were observed as shown in figure 8a and no circular bead boundary was spotted because the sample for the microscopy of single wall was cut perpendicular to scanning direction. figure 5.3 exhibited the epitaxial growth of α-Al dendrites over successive layers due to directional heat flow towards the substrate. The gray primary dendrites is the α-aluminum and bright constituents represents the silicon particles. Inter dendritic region has eutectic structure as shown in figure 5.7 b. Polygonal shaped silicon particles were observed just below the solid/liquid interface due to coarsening of fibrous eutectic Si particles because of secondary heating during subsequent layer deposition as shown in figure 5.7 c. Since

the top part of top layer was not re-melted, therefore top part of single wall deposit exhibited equiaxed structure as shown in figure 5.7 d due to low thermal gradient and high solidification velocity.

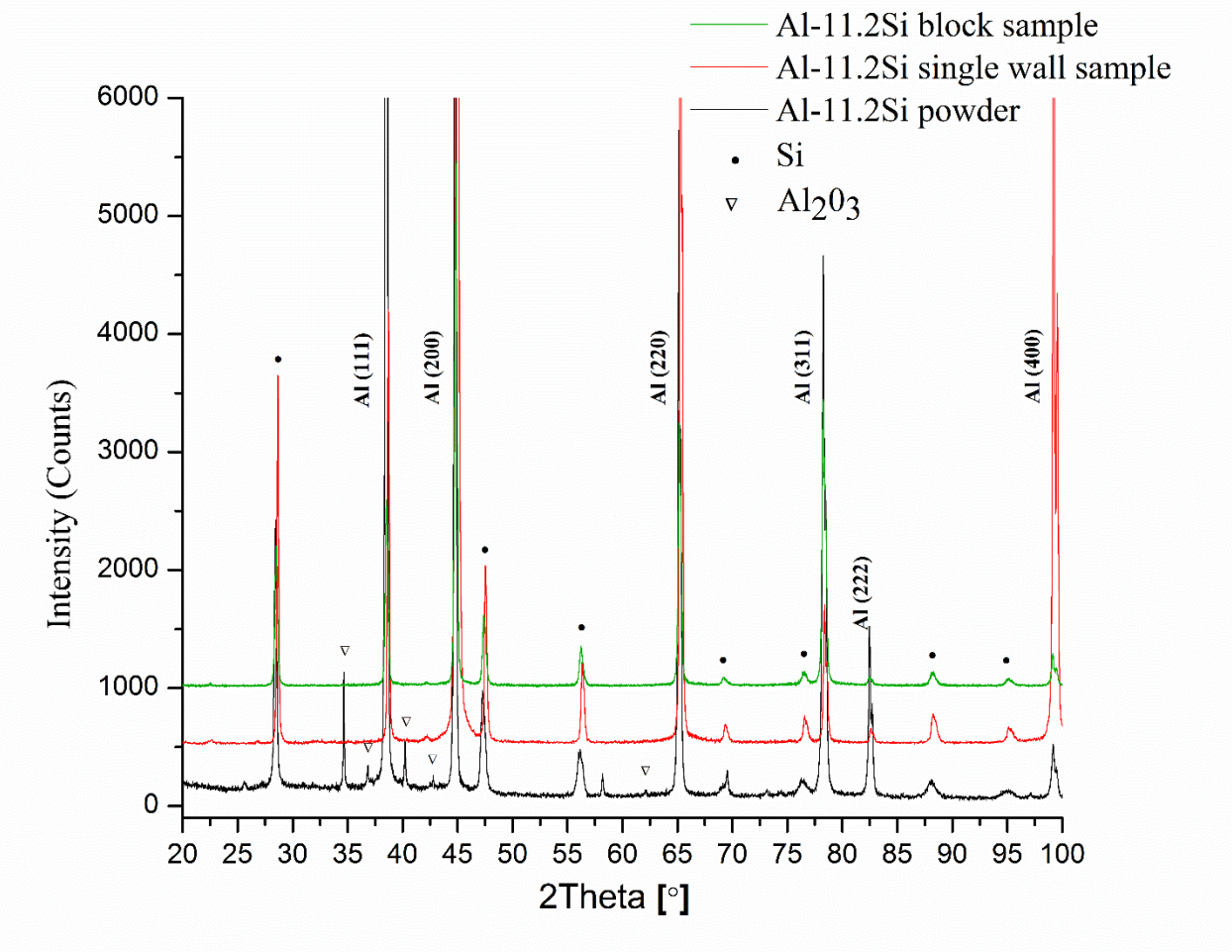

Figure 5.8: XRD plots of Al-11.2 powder, single wall sample, and block sample.

The microhardness test of single wall sample revealed average microhardness of about 76.71 HV. Top part with equiaxed microstructure had the highest microhardness value of 82.13 HV and rest of the deposit exhibited about 74 HV. XRD investigation revealed that α-Al and Si phase exist in powder, single wall and block deposition. Oxidized Al was observed in as-received Al-11.2Si alloy powder as shown in figure 5.8. The lattice parameter for α-Al calculated using

braggs law found to be 0.404 nm for both single wall and block deposition. Si peaks were higher in case of single wall sample depicting the presence of coarser Si particles than in block deposit.

5.3 Fabrication of Al 4047 automotive components via laser metal deposition

On this particular cast automotive component, there is lot of small components (e.g. bracket) that are casted separately and then joined back on the shock tower hood using spot welding. If we can directly deposit on the shock tower hood cast, joining time and cost would be a big saving. The elaborative study explained in section 5.1 and 5.2 shows that deposition on the shock hood can be performed and strength of printed parts are at par with conventional properties. The electronic box was manufactured using the optimized parameters as shown in figure 5.9. . Final deposition on shock tower hood shown in figure 5.10.

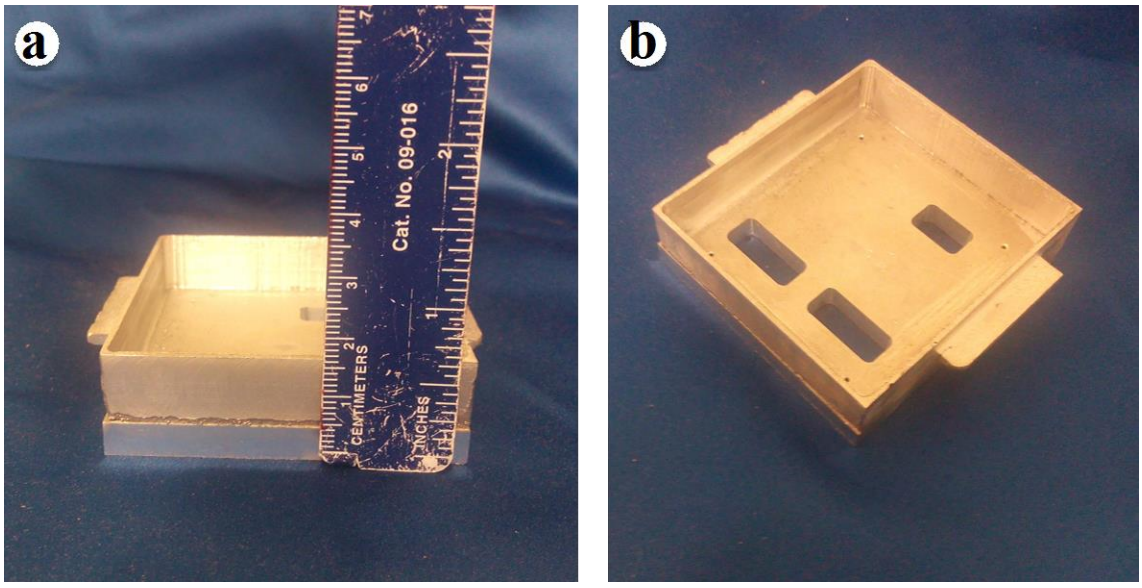

Figure 5.9: Additively manufactured electronics box from Al-11.2Si alloy

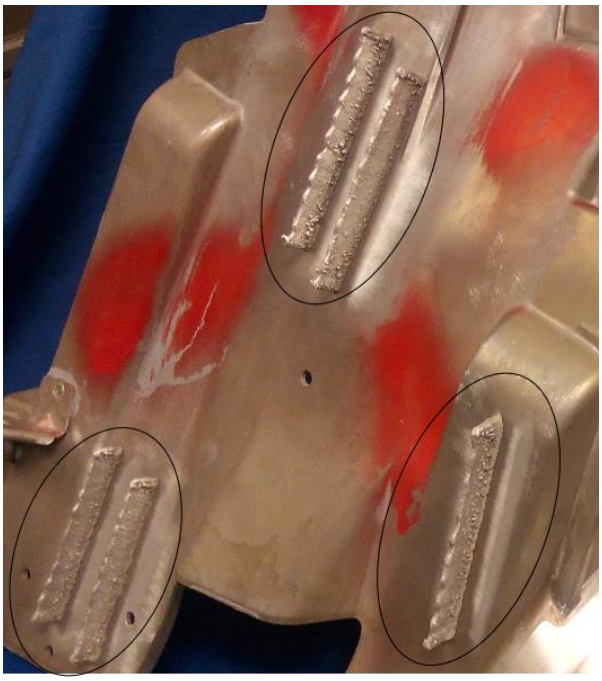

Figure 5.10: Shock tower hood with Al-11.2Si deposition single wall deposits.

CHAPTER 6 LASER METAL DEPOSITION OF AL 7050 ALLOY

6.1 Block deposition of Al 7050 alloy

Advanced Powder Solutions Inc. supplied the Gas atomized 7050 aluminum alloy powder. The range of powder particle size found to be from 5 to 50 µm and powder particles found to be elongated. Table 6.2 shows the composition of supplied powder which has been determined using EDAX as shown in figure 6.1 a. The deposition was conducted on the 6061 rolled aluminum plate. The first challenge was to achieve defect free deposition of 7050 aluminum alloy powder.

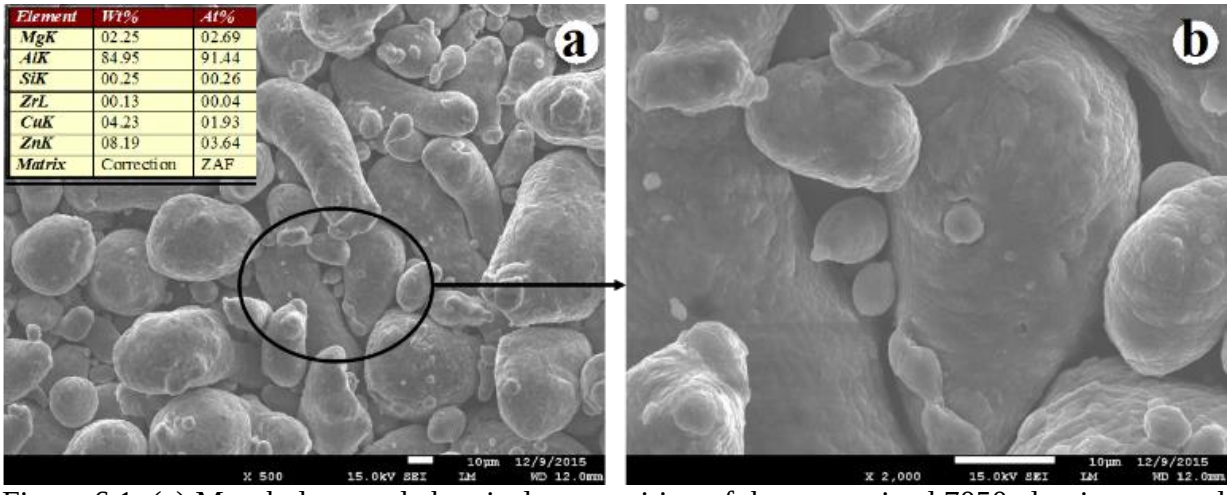

Figure 6.1: (a) Morphology and chemical composition of the as-received 7050 aluminum powder , and (b) Zoomed morphological view.

Various parameters (Laser Power, Powder Feed Rate, and Scanning Speed) was optimized to achieve high density of 7050 aluminum alloy deposition, as each parameter has significant effect on the build quality of deposit. Parameter optimizing window found to be small as all parameters are dependent on each other and could not be varied much. After various initial attempts as shown in figure 6.2 (a), final optimized parameters were achieved as shown in table 6.1. Coupons of 20 mm x 20 mm was made as shown in figure 6.2 (b) of 3.2 mm high for microstructural evolution and micro hardness study. The hatched tool path pattern as shown in figure 6.3 a followed for both coupon and block sample with bead overlap of 0.5 mm. Layer thickness was kept at 0.4 mm.

Optical microscopy of as-deposited 7050 aluminum alloy revealed greater than 99.5 % dense deposition. No major defects like cracks, de-bonding at layer interface was observed.

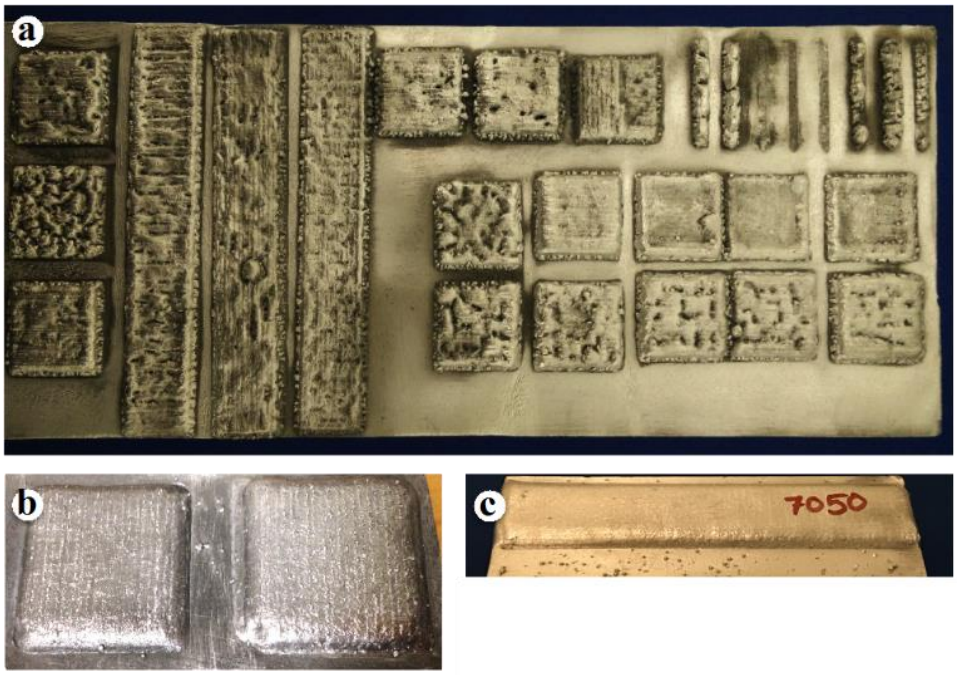

Figure 6.2 (a) Initial attempts for 7050 aluminum alloy deposition, (b) Optimized defect free 7050 aluminum alloy (20 mm x20 mm coupon), and (c) Optimized defect free 7050 aluminum alloy (100 mm x 16 mm) block sample.

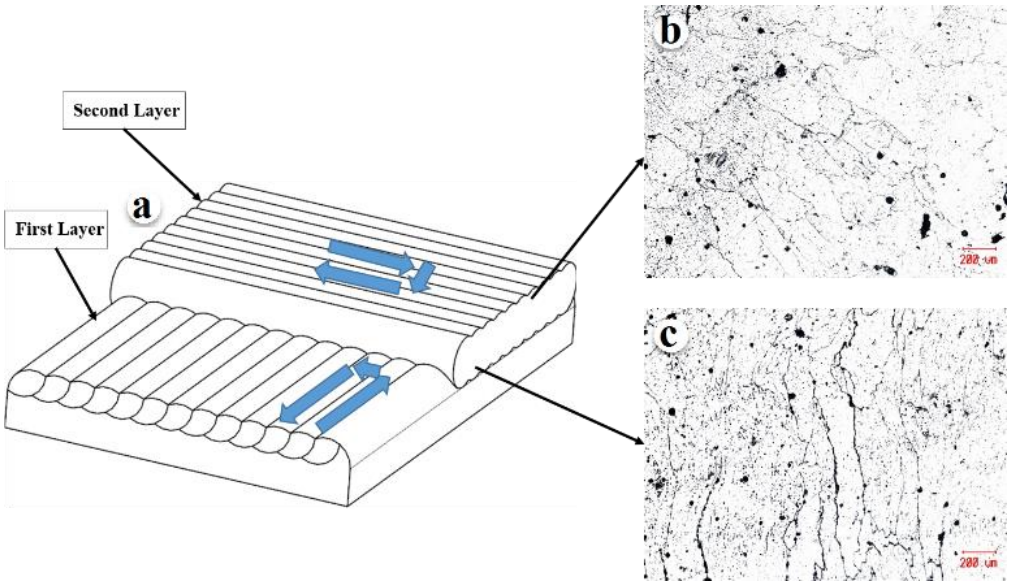

Figure 6.3: (a) Hatch deposition pattern, (b) Optical micrograph of top of as-deposited 7050, aluminum alloy coupon, and (c) Optical micrograph of bottom of as-deposited 7050 aluminum alloy.

The top part of deposition was polished and made flat for xrd analysis (Bruker D8) to identify various phases in the as deposited and heat-treated samples. Samples for SEM investigation were prepared by cutting half of as-deposited and heat treated coupon. These half cut samples were mounted, polished and etched in solution of 100 ml H_2O, 25 ml HNO_3, 15 ml HCl, and 10 ml HF for microstructural investigation. Samples were submersed for 5–10 s followed by rinsing with water and then dried. It is well known fact some elements get segregated during rapid solidification in the interdendritic region, so EDS investigation was carried out to study the elemental distribution from center of the dendrite to the interdendritic region.

Table 6.1: Optimized LMD parameters

Laser Power (Watt)	Powder Flow Rate (gm/min)	Scan Speed (mm/min)
1050	3.5	500

Tensile test samples were prepared as already explained in research section as shown in figure 6.4. Tensile testing was done on the milled sample, as EDM cut samples developed some defects because of heat produced during the cutting process.

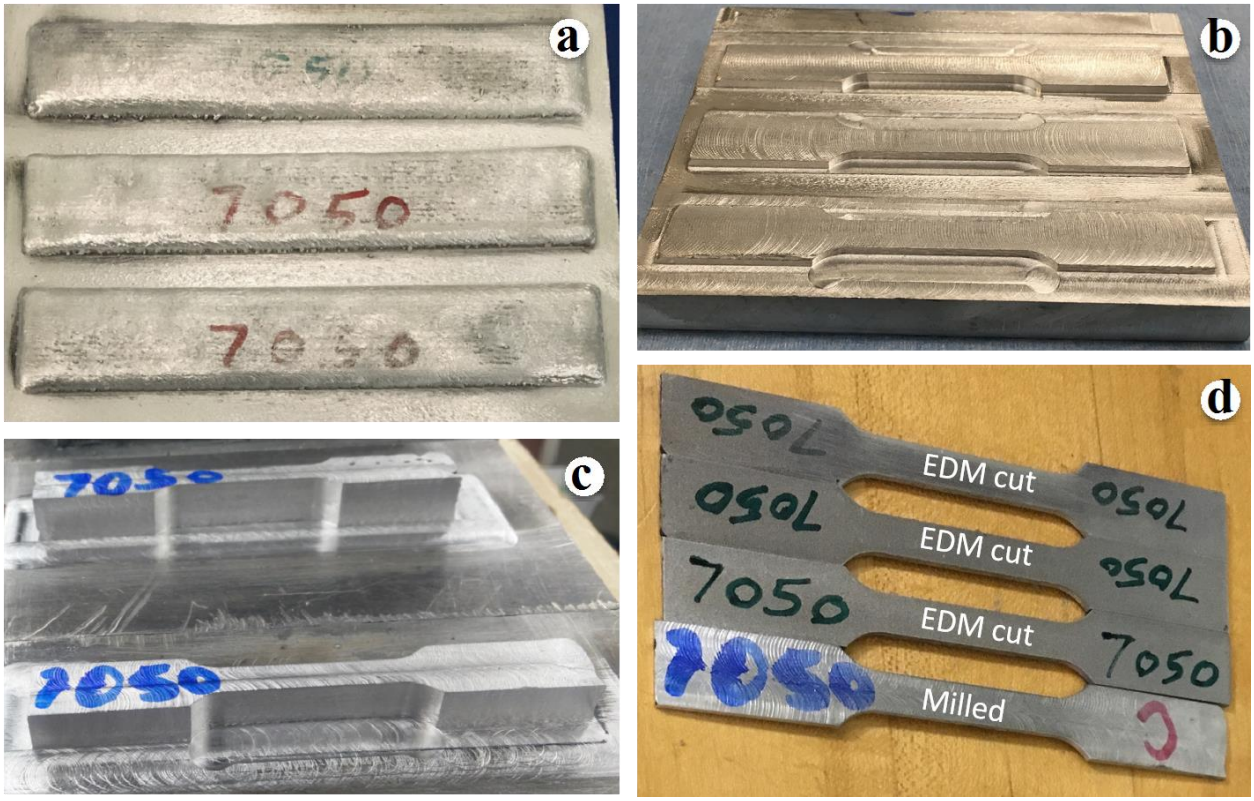

Figure 6.4: Tensile test samples preparation steps, (a) As-deposited blocks (100 mm × 16 mm × 3 mm), (b) Dog bone shaped samples made by CNC milling, (c) Slicing and reducing the thickness to 2 mm thick, and (d) EDM cut and milled samples.

Heat treatment was carried out to enhance the mechanical properties of tensile samples and study microstructural evolution during heat treatment. Segregation of second phase particles in the interdendritic region due to rapid solidification during LMD process makes the deposition brittle and results in low tensile strength. Hence, the heat treatment become necessary after depositing the samples. Both tensile test samples and the samples for microscopy were heat treated in tube furnace OTF-1200X . T6 heat treatment was followed in which solution heat treatment was carried

at 475 ^{o}C followed by water quenching. Three as-deposited (coupons and block) samples were solution heat treated (SHT) for 1, 2, 3 hours (HT-1, HT-2, HT- 3) respectively and all samples then artificially aged at two different temperature as follows: heating at 135 ^{o}C for 5 hours and followed by heating at 163 ^{o}C for 24 hours, then air cooled. At first, the deposition quality visually checked to see any voids, cracks or any major defects. No major defects found during visual inspection. Optical microscopy and using image J measurement revealed that deposition was greater than 99.5 % dense. The grains are equiaxed at the top of coupon sample and columnar in nature at bottom of deposition as shown in figure 6.3 (b) and figure 6.3 (c) respectively. High thermal gradient and low solidification velocity at the bottom of melt pool results in columnar dendrites at the bottom of each layer. In contrast low thermal gradient and high solidification velocity results in equiaxed dendrites.

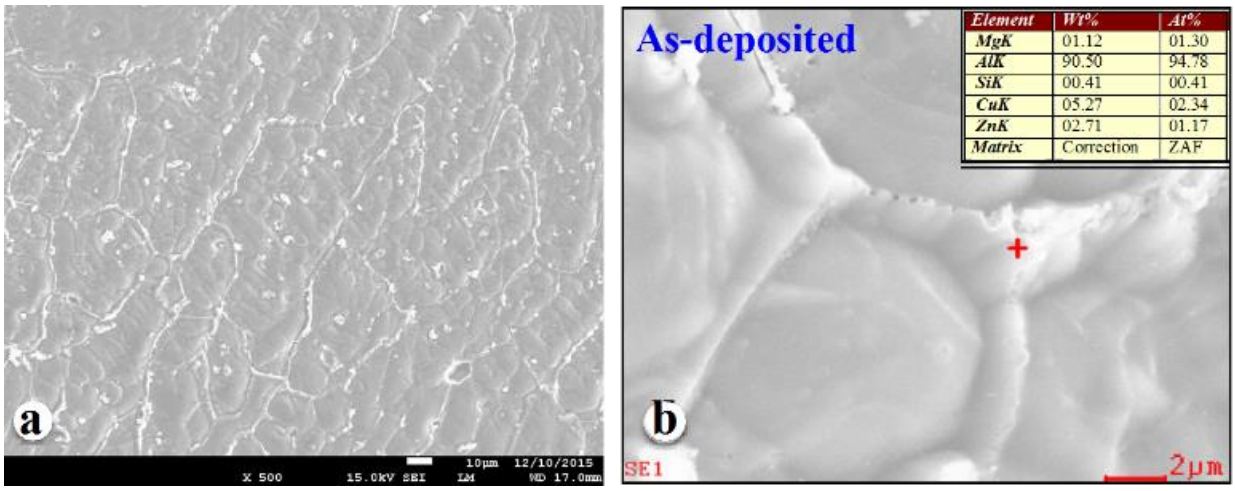

Figure 6.5: (a) As-deposited 7050 aluminum alloy and (b) EDS analysis of as-deposited alloy 7 deposits.

However, during subsequent deposition, the top part of each layer is re-melted and columnar dendrites grow epitaxially from the bottom part of deposit. As a result, only top part of the top layer exhibited equiaxed grains and rest of the deposit revealed columnar grains.

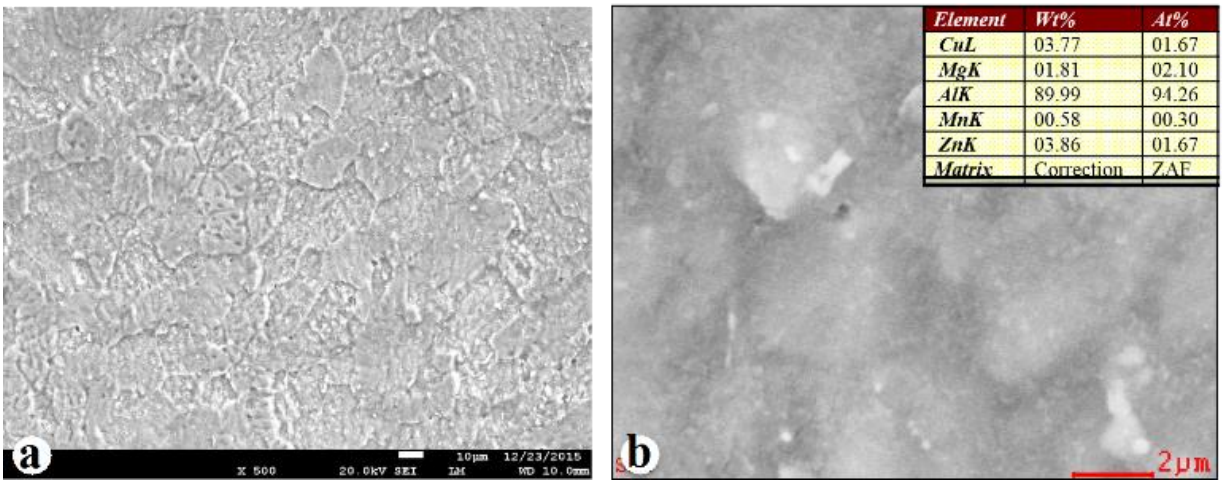

Figure 6.6: (a) HT 2 7050 aluminum alloy and (b) EDS area analysis of HT-2 7050 aluminum alloy.

SEM micrographs as shown in figure 6.5 (a) shows that the α-Al grain boundaries decorated with the intermetallic phases. EDS analysis revealed that these second phase particles are rich in Cu, Zn and Mg. They are segregated in the interdendritic region and coarser in nature, which makes the material brittle and results in low tensile strength. XRD investigation also confirms the Al_2CuMg phase present in as-deposited 7050 aluminum alloy as shown in figure 6.7. The coarser second phase particles goes in solid solution during the SHT and forms finer precipitates during two stage aging process as explained in heat treatment section. Figure 6.6 shows the coarser second phase particles have become finer as compared to as- deposited 7050 aluminum alloy. XRD analysis also shows that Al_2CuMg phase has been vanished after heat treatment, which can happen if Al_2CuMg precipitate is so finer that X-ray not able to detect or this phase was completely dissolved. This can be confirmed using TEM analysis, which we intended to do in future. XRD analysis as shown in figure 6.7 confirms strengthening phase $MgZn_2$ precipitates were definitely formed after aging process. . As heat of solution for Zn and Mg is negative, they form cluster together on quenching [27].

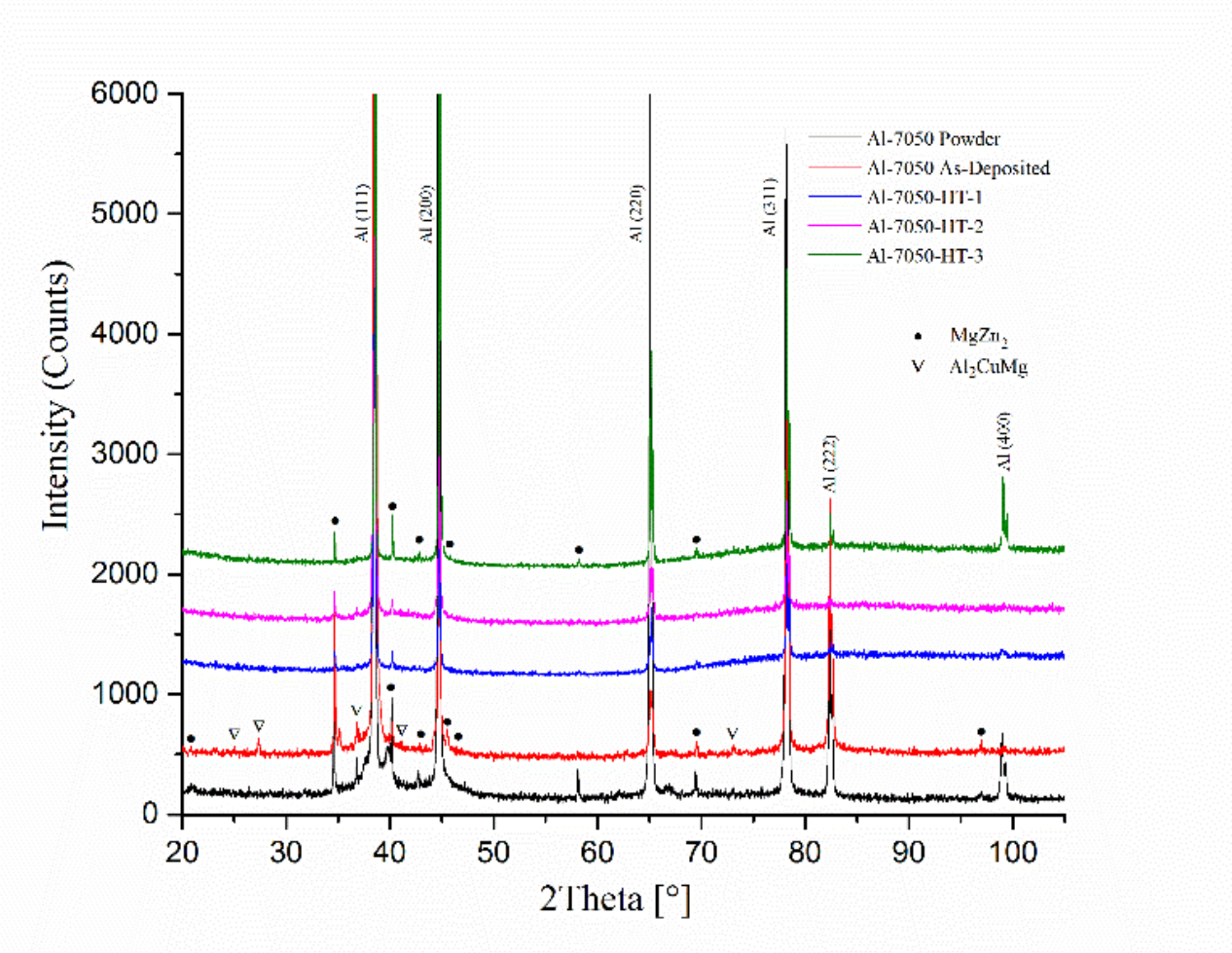

Figure 6.7: XRD plots of 7050 powder, as-deposited and heat treated 7050 aluminum samples.

SHT for different time was performed to observe the effect of heat treatment on phase formation as shown in figure 6.7. XRD analysis confirmed only two strengthening expected phases ($MgZn_2$, Al_2CuMg) formed after different SHT. The microhardness test revealed the hardness of the as-deposited sample was 100 HV (average value) that increased to 128 HV (average value) after heat treatment. Literature [18] suggests that hardness value should have restored to about 150 HV. High input laser vaporizes Zn and Mg as shown in table 6.2. Reduction in Mg and Zn would also decrease the formation of $MgZn_2$ strengthening phase. As 7050 aluminum alloy is precipitation hardening alloy and reduction in strengthening precipitate would mean lower hardness and lower strength values. It is evident in tensile test results of heat-treated samples that

strength not recovered to conventional value. Tensile test of as-deposited samples revealed the yield strength of 199.9 MPa as the average value. Heat treatment did not had any significant impact on the yield strength, as only increment of 30 MPa to as-deposited sample was observed.

Table 6.2: EDS composition by weight of 7050 aluminum alloy powder and as deposited.

	Mg	**Zn**	**Cu**	**Zr**	**Al**
Powder	2.25	6.18	4.23	0.13	91.44
As-Deposited	1.26	3.10	3.78	-	91.45

CHAPTER 7 LASER METAL DEPOSITION OF NI COATED AL 7050 ALLOY

Additive manufacturing of aluminum alloys always remained a challenge and specifically for 7xxx series aluminum alloys. Recently, Reschntnik et al. [19] and Hansong et al. [20] additively manufactured Al 7075 alloy using powder sintering and micro metal deposition technique respectively. Process induced cracks were found by Reschtnik et al. during AM of Al 7075 alloys using selective laser melting. Micro droplet deposition manufacturing (MMDM) technique involves melting of Al 7075 billets using induction furnace. The major challenge in laser additive manufacturing of Al 7050 alloy is the low boiling point of alloying elements such as Zn and Mg as compared to aluminum, which evaporates during laser deposition. This evaporation decreases the quantity of strengthening elements and creates defects such as porosity and voids in the deposit. Moreover, Al is a highly reflective material. Consequently, deposition of Al alloys is challenging compares to Ni-, Fe-, Co-, and Ti-base alloys. Precipitation mechanisms have been widely studied in spray forming, equal channel angular pressing, controlled diffusion solidification etc. [12, 26, 30, 31, 36-41]. Precipitation was also observed during laser metal deposition of Al 7050 alloy. However, there is limited literature available on precipitation kinetics during laser additive manufacturing of Al 7050.

7.1 Motivation for Ni coating

Aluminum and Copper alloys are not a good candidate for Laser Metal Deposition (LMD) process because of high reflectivity and lower absorption of photons as compared to LMD friendly materials such as Ni and Fe based alloys. So the Al 7050 powdered was Ni coated for better absorption of photons which resulted in good deposit quality. The deposition quality was visually inspected to see any voids, cracks or any major defects before microscopic analysis. The laser photons first interact with the Ni coating and remaining photon energy travels through the core

interacting with Mg and Zn particles. Hence, Ni coating avoids the direct interaction of photons with low boiling particles such as Mg and Zn. The direct absorption of photons will result in loss of Mg and Zn particles, which can create porosity and other defects. After conducting LMD of Al 7050 without any coating, EDS results reported by Singh et al. [59] showed about 44% decrement in Mg composition.

7.2 Result and discussion

Advanced Powder Solutions Inc. supplied the gas atomized nickel coated Al 7050 alloy powder. The range of powder particle size found to be from 5 to 50 μm and most powder particles found to be spherical. Figure 7.1(a) exhibits the morphology of Ni coating on the Al 7050 powder particles. Note that the Ni coating was made by physical vapor deposition. Figure 7.1(b) shows cross sectional view of Al 7050 powder in which coating is clearly visible around the periphery of Al 7050 particle. The Ni coating thickness was about 0.5 μm. It should be also pointed out that the morphology of the Ni coating is rather discontinues granular surface. The deposition was conducted on a 12.7 mm thick Al 6061 rolled plate. The first objective was to achieve defect free deposition of nickel coated Al 7050 alloy powder.

Table 7.1: Optimized laser deposition parameters.

Laser Power (watt)	**Powder Flow Rate (gm/min)**	**Scan Speed (mm/min)**	**Nozzle Gas (l/min)**	**Shaping Gas (l/min)**	**Powder Carrier Gas (l/min)**
1050	3.3	500	15	15	20

Deposition parameters (laser power, powder feed rate, and scanning speed) were optimized to achieve high-density deposition, as each parameter has significant effect on the build quality of deposit. Process parameter window found to be rather small as all parameters are dependent on each other and cannot be varied much.

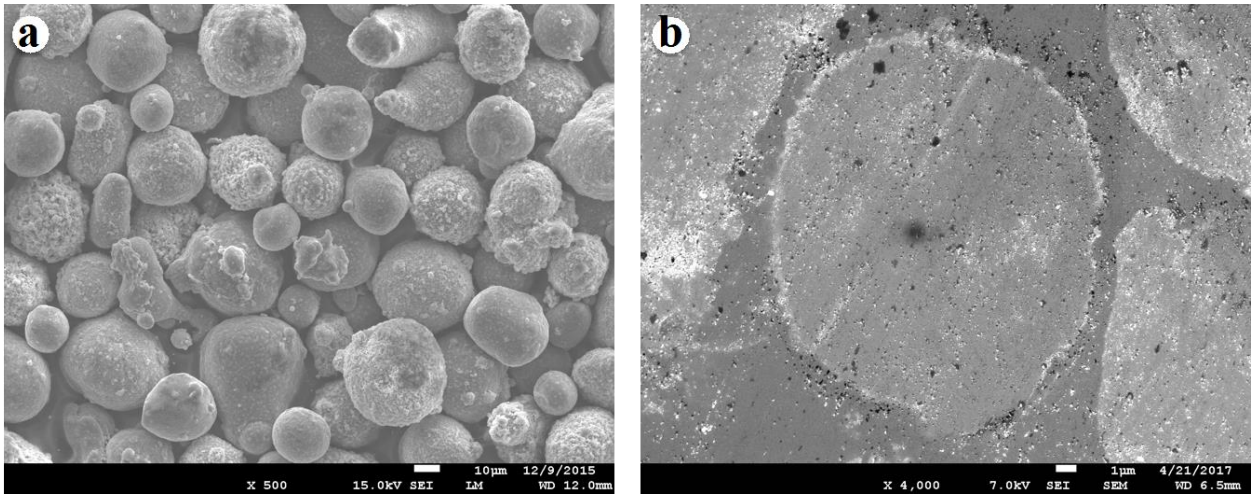

Figure 7.1: (a) Morphology of the as-received Al 7050 alloy powder, and (b) Cross sectional view of as-received Al 7050 powder particle showing coating around periphery.

Samples were deposited with optimized parameters as shown in figure 7.2 (a). For microstructural evolution and micro hardness study, coupons of 20 mm × 20 mm × 3.5 mm were made. In addition, a set of 100 mm × 20 mm × 3.5 mm block was made to prepare tensile test specimens. The hatched tool path pattern as shown in figure 7.2 (b) followed for both coupon and block sample with bead overlap of 1 mm and layer thickness of 0.5 mm. Optical micrograph as shown in figure 7.2 (c) of as-deposited nickel coated Al 7050 alloy revealed greater than 99.5 % dense deposition. No major defects like cracks, deboning at layer interface was observed.

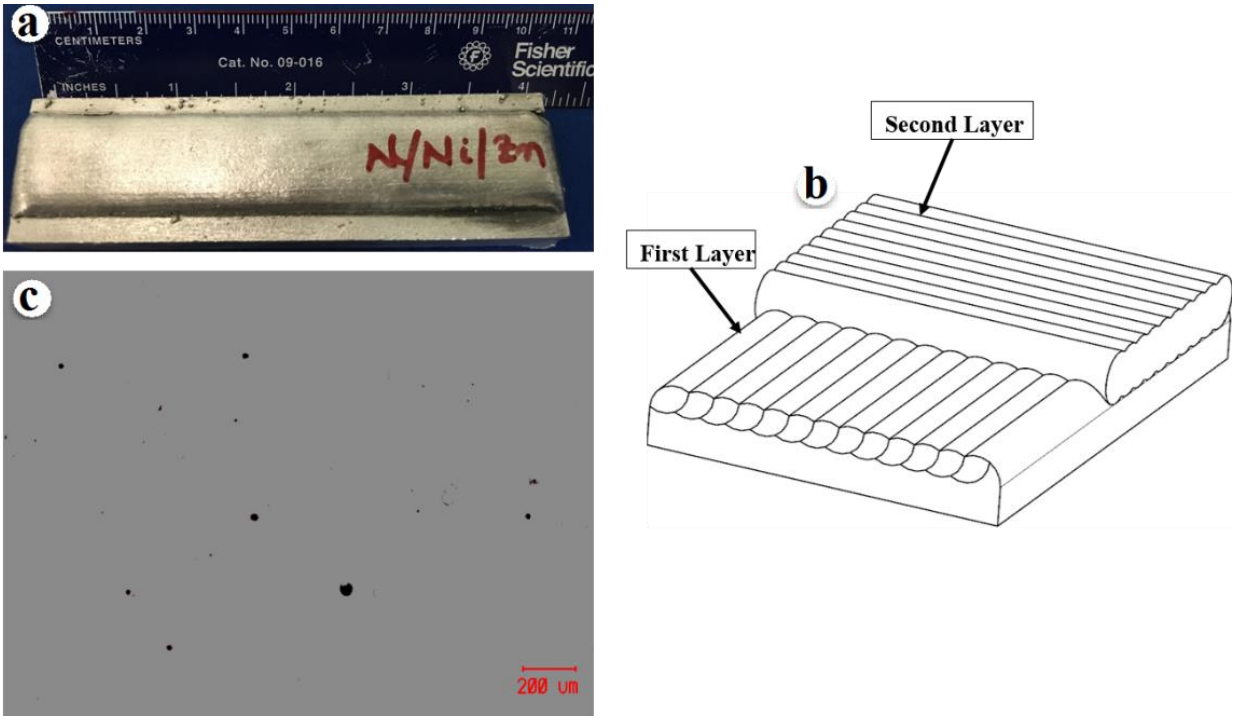

Figure 7.2: (a) Block deposition of Ni coated Al 7050 alloy, (b) Hatch deposition pattern, and (c) Optical micrograph of cross section showing little porosity.

Note that the 7xxx series aluminum alloys are mostly used in wrought form than in as-cast product. Hence, to alter the cast microstructure of the laser deposited samples to wrought microstructure, as-deposited samples were further plastically deformed by friction stir processing (FSP) technique. Friction stir processing (FSP) experiment was performed on the as-deposited sample of 150 mm × 100 mm × 3.5 mm as shown in figure 7.3. FSP is a severe plastic deformation process in which grains fully recrystallize and fine microstructure is produced. During FSP, a non-consumable rotating tool with a specially designed pin and shoulder, as shown in figure 7.3 (d), inserted into the sheet or plate and traversed at certain speed. Consequently, the material undergoes intense plastic deformation at the strain rates of 2–12 s^{-1} at elevated temperature, resulting fine and equiaxed recrystallized grains. Following FSP parameters were optimized and used to process the

as-deposited samples; spindle speed: 500 rpm, traverse speed: 25 mm/min, and tool tilt angle: 2.5 degrees.

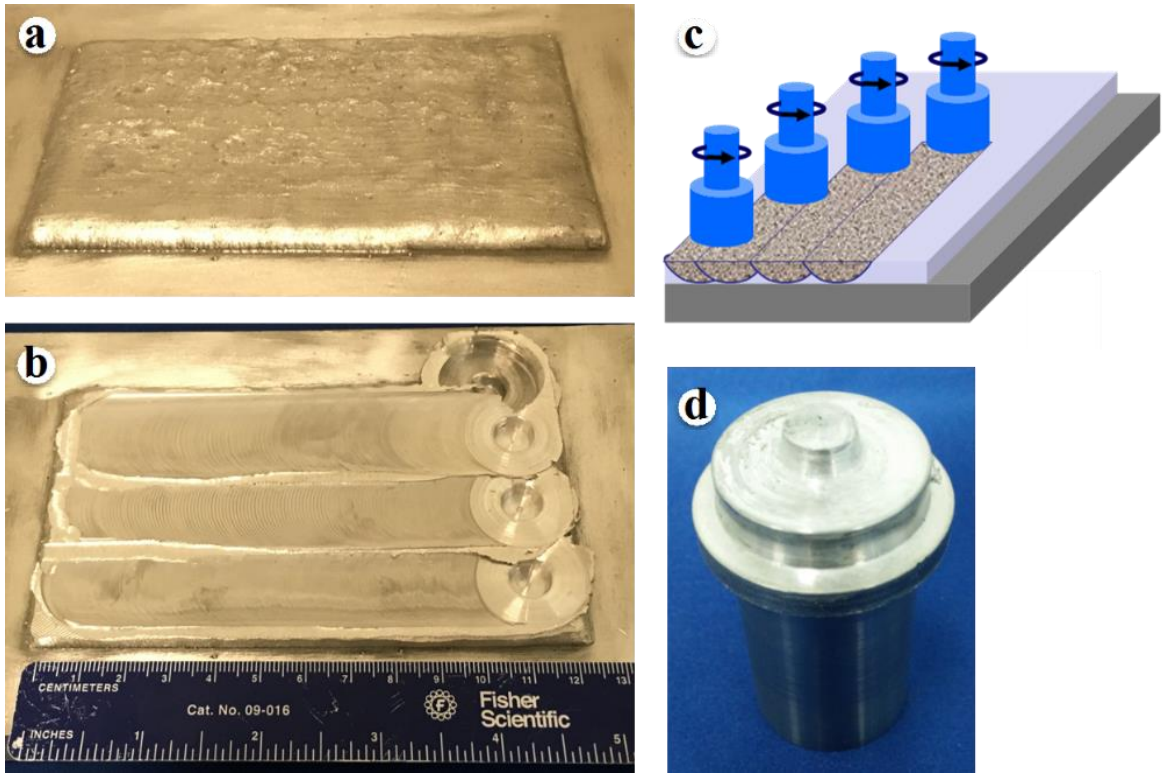

Figure 7.3: (a) As-deposited sample, (b) friction stir processed sample, (c) schematics of the friction stir processing (FSP) technique, and (d) FSP tool used in the FSP experiment.

Note that no major defects found during visual inspection. Image analysis of optical micrographs revealed that deposition was greater than 99.8% dense. The surface finish of deposit found to be very smooth and shiny as shown in figure 7.3 (a) because of the presence of Ni in the Al 7050 deposit but generally, laser metal deposition of conventional Al 7050 alloy does not have very smooth finish.

figure 7.4 (a) clearly shows the five layers out of total seven layers in which there is defined pattern of circular bead boundaries in first, third and fifth layers. This is due to the hatch tool path pattern followed during deposition as schematically shown in figure 7.2 (b); circular bead boundaries as shown in figure 7.4 (a) are the result of the overlapping beads to ensure high-density

deposition. The top most layer of the deposit is the thickest of all other deposited layers, which clearly noticed in figure 7.4 (b). High energy density is required to maintain a continuous melt pool because of high thermal conductive nature of aluminum. During deposition of subsequent layers, the top part of the underneath new layer partially re-melted. However, only the top layer never gets re-melted and stays thicker than rest of deposited layers as shown in figure 7.4 (b). There is very interesting repeating microstructure pattern was observed around the layer and bead boundaries. Figure 7.4 (e) exhibits the presence of columnar primary α-Al dendrites (gray phase) above the layer/bead boundaries. In addition, figure 7.4 (d) exhibits that the α-Al dendrites grew perpendicular to the bead boundary (solid/liquid interface). On the other hand, columnar dendrites gradually transformed to equiaxed α-Al dendrites around middle of each layers. In addition, inter-dendrite boundaries are decorated with bright phase particles. High magnification SEM image (figure 7.4(f)) exhibits the presence of alternate layer of bright phase and gray phase (α-Al). This alternate layer morphology demonstrates the presence of eutectic phase in the interdendritic regions. Image analysis revealed that the average eutectic spacing is 0.52 μm, dendrite arm spacing (DAS) of columnar dendrites is about 2.98 μm, and average equiaxed α-Al dendrites (cell) size is 4.41 μm around the middle of each layers. Note that high thermal gradient and low solidification velocity at the bottom of melt pool, just above the solid/liquid interface, results in columnar dendrites. In contrast, from middle to top section of each bead, an equiaxed microstructure developed due to high solidification velocity and low thermal gradient at the upper part of the melt pool. This is well known phenomenon in rapid solidification.

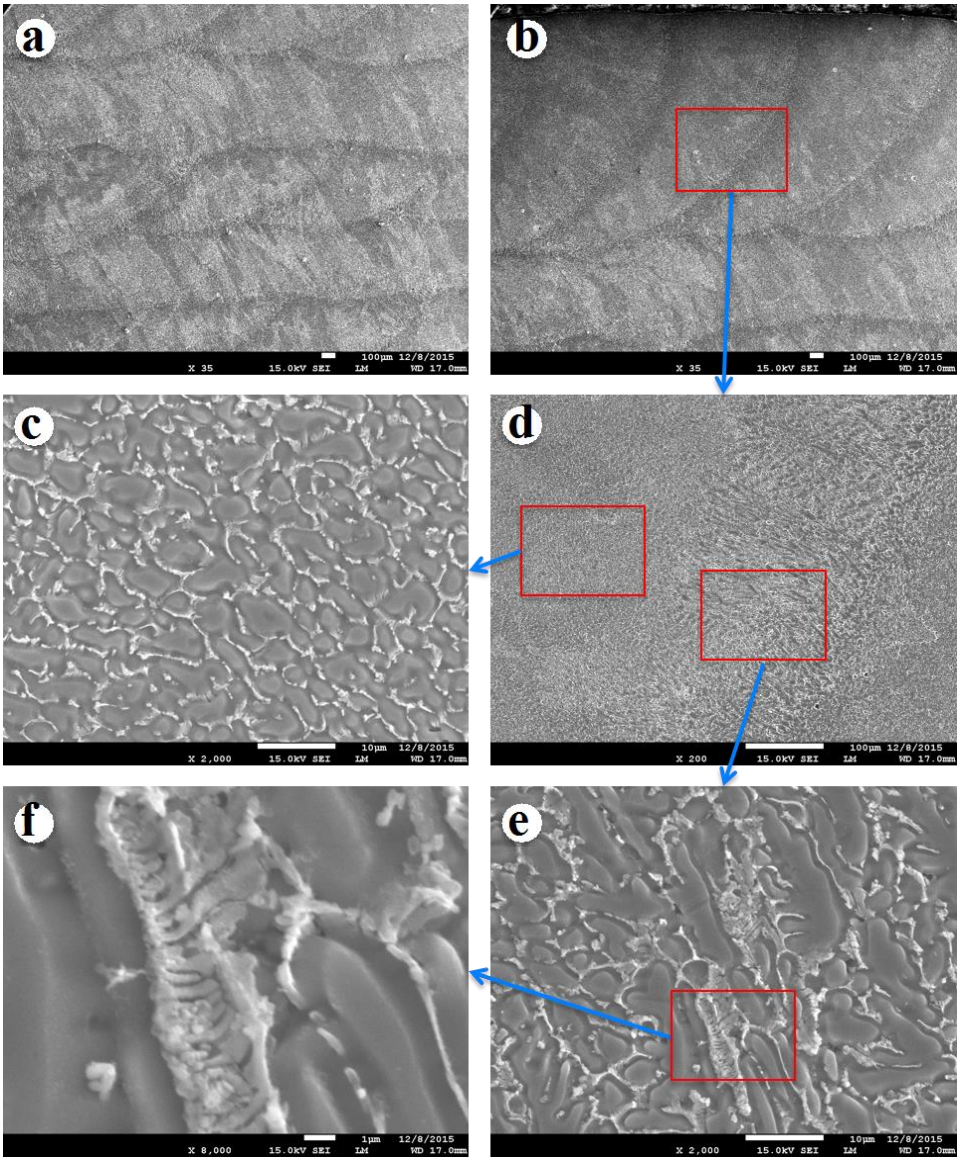

Figure 7.4: Optical micrographs of the as-deposited sample. (a) Overview showing five layers, (b) zoomed view of top two layers, (c) equiaxed α-Al dendrites around the middle of each layer, (d) zoomed view of bead boundary, (e) columnar α-Al dendrites just above the bead boundary, and (f) eutectic morphology of the interdendritic phase.

EDS investigation was carried out to study the composition of the second phase particle (bright phase) in the interdendritic eutectic phase. Figure 7.5 exhibits that the bright phase particles are relatively enriched with Ni (9.5 Wt.%) compared the primary α-Al dendrites. At this point, it

is not clear whether this bright phase is binary Al_3Ni intermetallics or Al-Ni-Zn ternary phase. Note that Zn content is approximately same in both bright phase (4.59 wt.%) and in α-Al dendrites (4.97 wt.%). Whereas, it is about 4.96 wt.% in the overall as-deposited sample. EDS analysis revealed that Ni is relatively segregated in the interdendritic region during rapid solidification.

Figure 7.4 (c, e, f) and figure 7.6 (a) exhibit that the inter-dendritic boundaries are decorated with bright phase particles. EDS analysis revealed that the Ni is relatively segregated in the inter-dendritic boundaries and most probably produced brittle intermetallic phases. Tensile test results revealed that as-deposited samples broken around yield point only. This poor tensile ductility of the as-deposited samples is most probably due to the presence of brittle intermetallic phase in inter-dendritic boundaries. To improve the tensile ductility of the laser deposited samples, post deposition heat treatment was carried out by solution treatment at 475 ^oC for 2 hours followed by two-stage aging at 135 ^oC for 5 hours and 163 ^oC for 24 hours. SEM investigation of heat-treated sample shown in figure 7.6 (b) revealed only partial dissolution (about 30%) of the interdendritic brittle phase in the aluminum matrix. The probable cause of partial dissolution of interdendritic particles is the presence of Al_3Ni phase, as detected in XRD analysis, in as-deposited Ni coated Al 7050 sample. The Al_3Ni phase is very stable phase and would not dissolved completely at low temperatures during conventional Al 7050 heat treatment process. Tensile test of the heat-treated samples also revealed no improvement of tensile ductility after heat treatment.

.

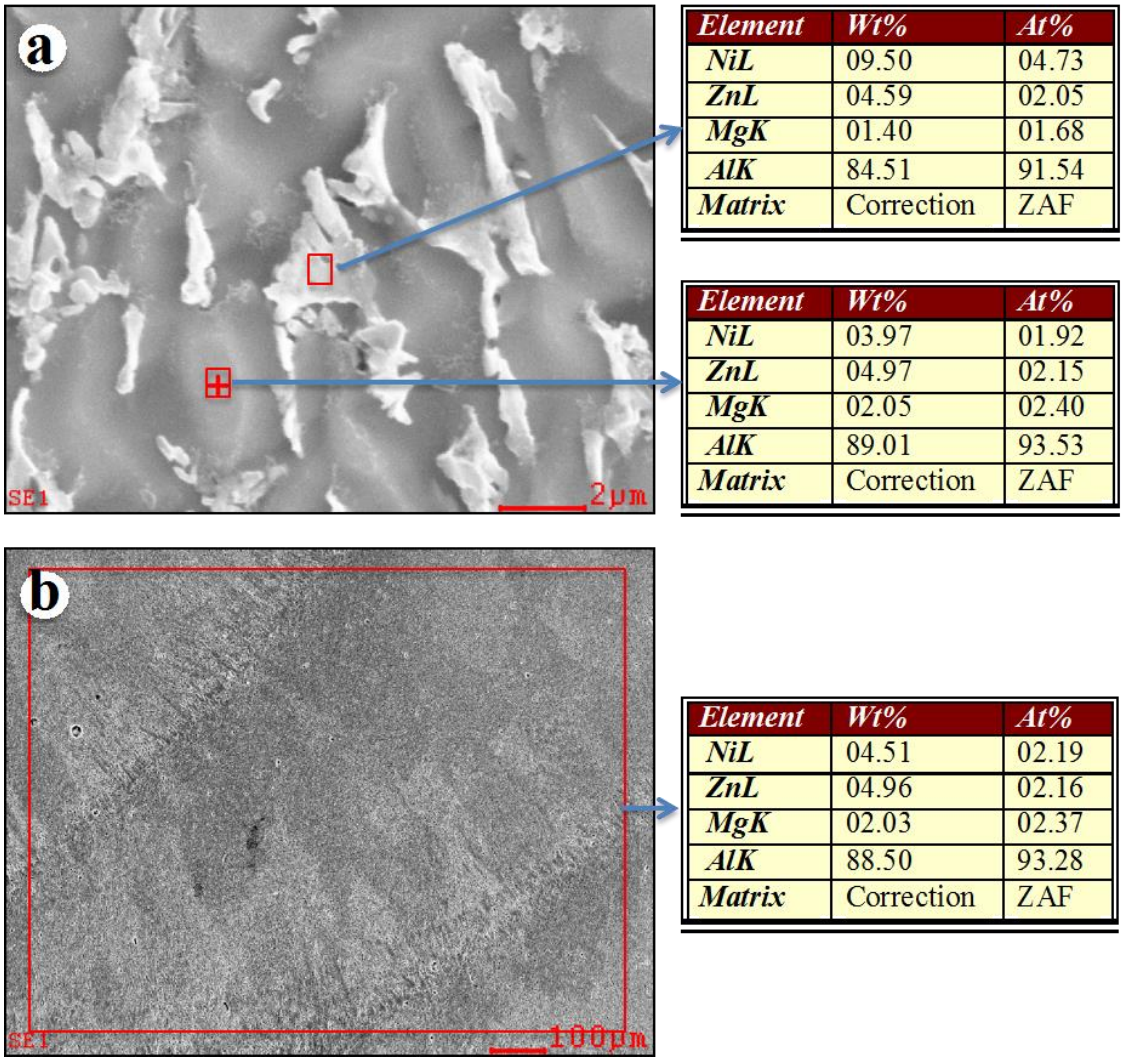

Element	Wt%	At%
NiL	09.50	04.73
ZnL	04.59	02.05
MgK	01.40	01.68
AlK	84.51	91.54
Matrix	Correction	ZAF

Element	Wt%	At%
NiL	03.97	01.92
ZnL	04.97	02.15
MgK	02.05	02.40
AlK	89.01	93.53
Matrix	Correction	ZAF

Element	Wt%	At%
NiL	04.51	02.19
ZnL	04.96	02.16
MgK	02.03	02.37
AlK	88.50	93.28
Matrix	Correction	ZAF

Figure 7.5: (a) EDS analysis of aluminum dendrites and interdendritic region, (b) area EDS analysis of as-deposited nickel coated Al 7050 alloy.

In order to improve the ductility, an as-deposited sample of 150 mm × 100 mm × 3.5 mm, as shown in figure 7.3, was friction stir processed to refine the detrimental inter-dendritic phase. Note that friction stir processing (FSP) is a severe plastic deformation process at elevated temperature. It is well know that aluminum alloys dynamically recrystallize during FSP. Since the Al 7050 alloy is mostly used in wrought form than as-cast, so as-deposited sample was friction stir processed to achieve wrought fine microstructure. Finer and uniformly distributed second phase particles were observed after FSP of as deposited sample as shown in figure 7.6 (c). Further heat

treatment of FSP sample was performed to dissolve the finer second phase particles further into the aluminum matrix to further enhance the mechanical properties. Note that finer second phase particles produced by FSP were partially dissolved during post FSP heat-treatment as shown in figure 7.6 (d).

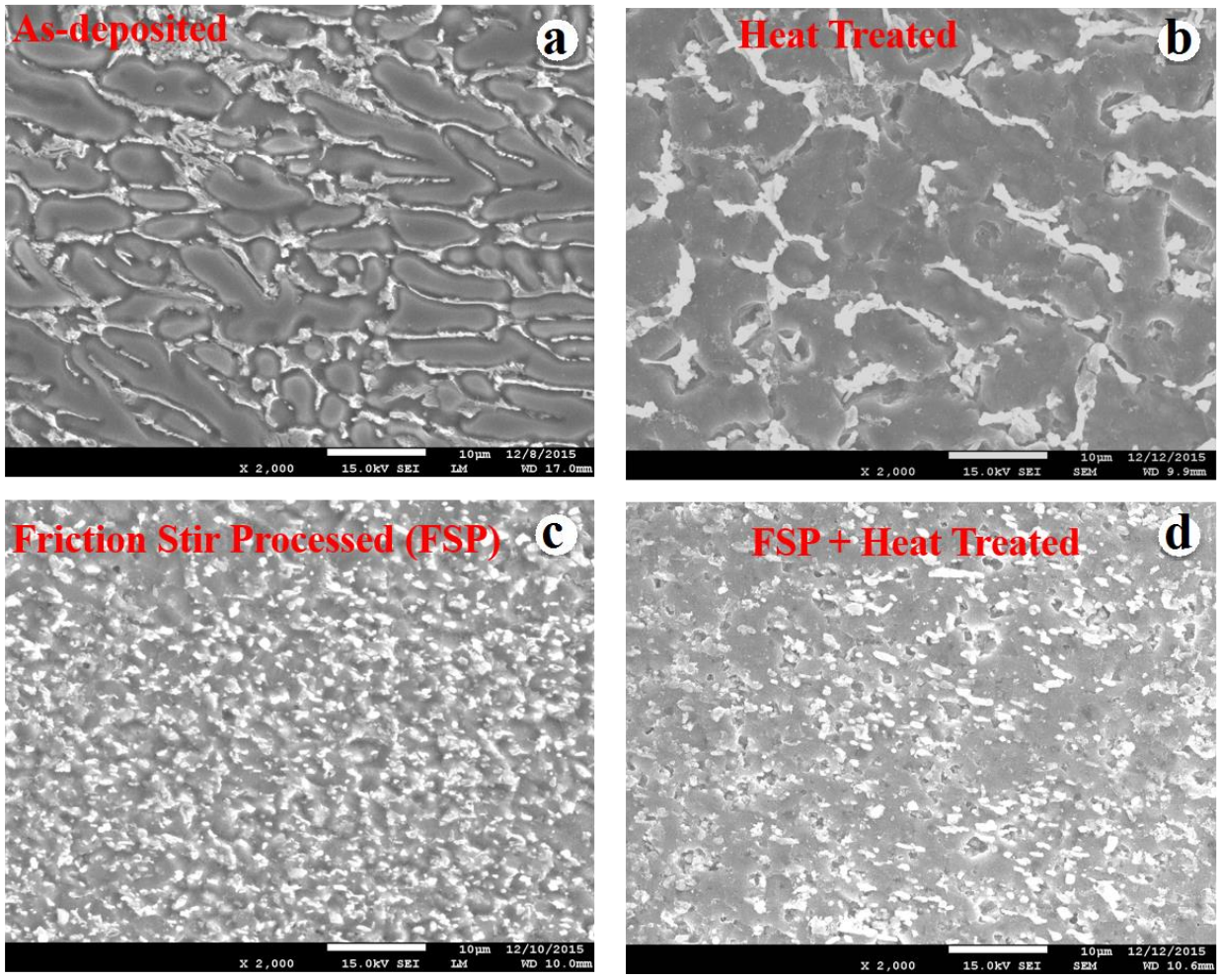

Figure 7.6: SEM micrographs of (a) as-deposited sample, (b) heat treated sample, (c) friction stir processed sample, and (d) post FSP heat-treated sample.

As described above laser deposited samples were severely deformed by friction stir processing technique to improve the mechanical response of the as-deposited samples. Figure 7.7 shows the stress-strain curves of friction stir processed (FSP) and heat-treated FSP samples. It

should be pointed out that as-deposited samples were very brittle with a tensile elongation of less than 0.5%. However, elongation was improved to about 6% after FSP. In addition, tensile elongation was further improved to about 6.5% due to post FSP heat-treatment.

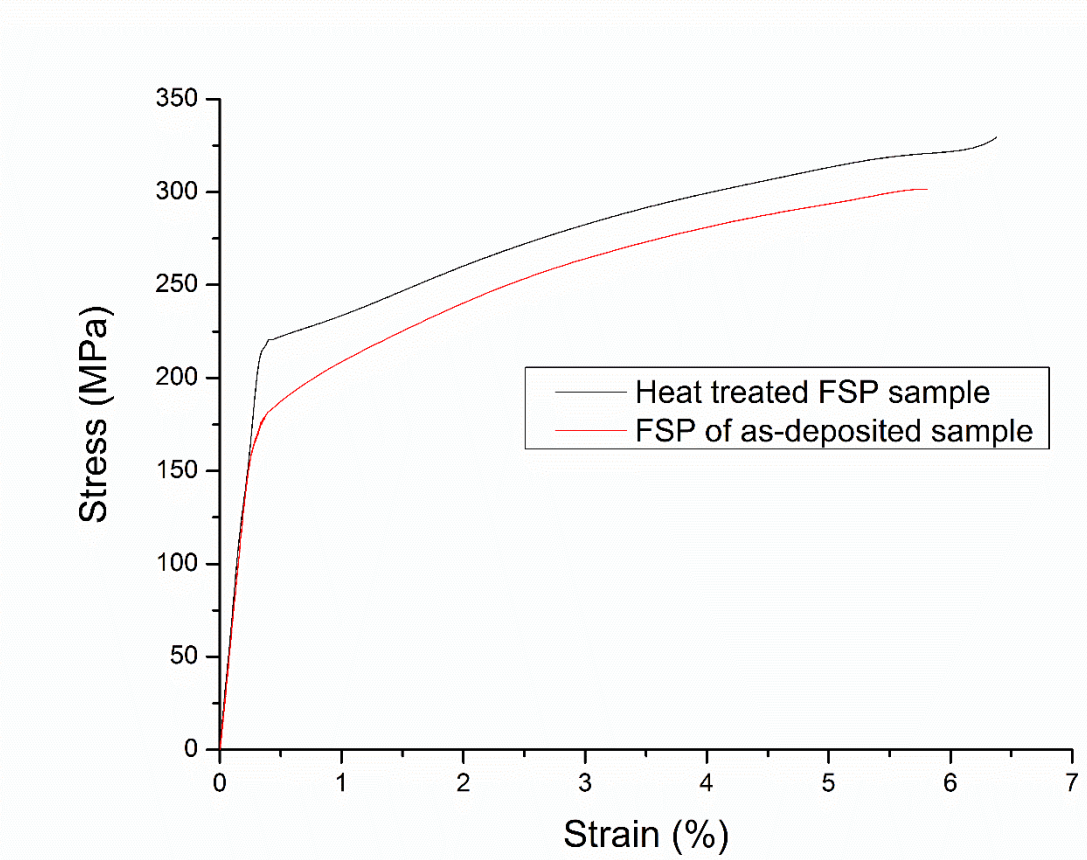

Figure 7.7: Stress-strain curves of friction stir processed (FSP) and heat-treated FSP Ni coated Al 7050 deposits.

Tensile test samples broke around yield point in both uncoated Al 7050 and Ni coated 7050 alloys. The yield strength was about 200 MPa in both uncoated and Ni coated 7050 alloys. Hence the Ni coating did not improve the ductility but the quality of deposit was enhanced substantially. The brittle coarse intermetallic particles were segregated around the interdendritic boundary reported by Singh et al. [59] might be the reason for brittle fracture in as-deposited Al 7050 alloy. The X-ray diffraction (XRD) investigation was carried out for better understanding the nature of

intermetallic phases in the deposit. The XRD scans (figure 7.8) exhibits the presence of α-aluminum dendrites along with $MgZn_2$, Al_2O_3, MgO, Al_3Ni, $MgCu_2$, $AlNi_2Zr_4$ etc. phases in the as-deposited, heat-treated, FSP and FSP heat treated samples. It should be noted that detailed TEM investigation is required for further confirmation of the presence of these phases in the deposit.

Microhardness measurements revealed the hardness of as-deposited sample is about 153 HV. After heat-treatment, the hardness decreased to 143 HV. However, the hardness of laser cladded Al 7050 sample found to be about 100 HV. Lower hardness is expected in the as-deposited sample because of cast microstructure of the laser deposited sample. Due to the rapid cooling during laser deposition, the main strengthening element such as Mg and Zn remain as solid solution in the α-Al matrix. As a result, a lower hardness is expected in the laser deposited Al 7050 alloy. However, in the present investigation the hardness of the nickel coated Al 7050 deposit found to be substantially high (153 HV) due to the presence of nickel in this modified alloy. It is anticipated that nickel formed Al_3Ni intermetallic phase in the inter-dendritic region that improved the hardness of as-deposited samples. It is also expected that post deposition heat treatment should improve the hardness due to the formation of strengthening $MgZn_2$ precipitates during two-stage aging. However, it was also found that inter-dendritic intermetallic phase partially dissolved during heat treatment that essentially reduced the hardness. Present results revealed that effect of softening due to the dissolution of inter-dendritic intermetallic is more predominant then the effect of hardening because of the precipitation of $MgZn_2$ particles during heat treatment. Note that the hardness of the as-deposited sample decreased to 120 HV after FSP operation. However, post FSP heat treatment further improved the hardness to 132 HV.

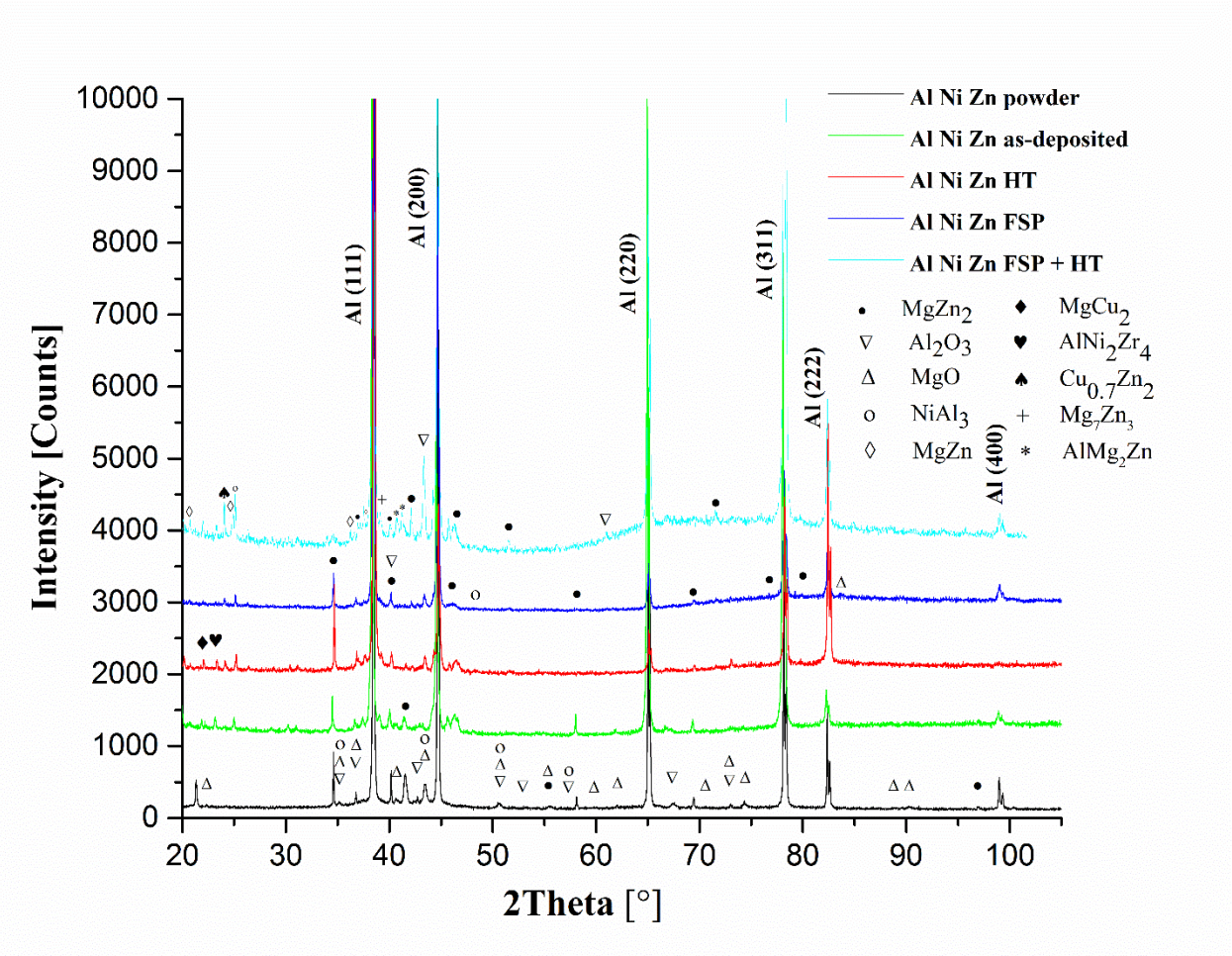

Figure 7.8: XRD plots of nickel coated Al 7050 alloy powder, as-deposited sample, heat treated sample, friction stir processed (FSP) deposit and post FSP heat-treated sample.

It is anticipated that the hardness decreased due to the refinement of coarse inter-dendritic intermetallic phase during FSP. Hardness was again improved after post FSP heat treatment because of formation of $MgZn_2$ precipitates. XRD results shows the peak intensity of $MgZn_2$ precipitates substantially increased after post FSP heat-treatment as shown in figure 7.8 that indicates the increased presence of strengthening precipitates. It should be noted that both hardness and strength (Yield and UTS) improved about 10% due to the post FSP heat-treatment.

Present results revealed that defect-free deposition of modified Al 7050 alloy can be successfully made using laser metal deposition starting with nickel-coated Al 7050 powder.

However, SEM investigation disclosed that Ni was partially segregated in the inter-dendritic boundaries and possibly formed Al_3Ni brittle intermetallic compound. Poor ductility of the as-deposited sample is anticipated due to the presence of Al_3Ni brittle intermetallic phase in the inter-dendritic boundaries. The microstructure of the as-deposited sample is not uniform due to the different local cooling rates at different part of the deposit. Columnar dendrites were observed above the bead/layer boundaries because of the high thermal gradient and low solidification velocity just above the solid/liquid interface. Columnar dendrites gradually transformed to equiaxed α-Al dendrites in the middle to upper part of each layer/bead due to the low thermal gradient and high solidification velocity at the upper part of the melt pool. Although defect free sample fabricated using optimized laser deposition parameters, however, mechanical properties especially tensile ductility found to be very poor (<0.5%) for any structural applications. Therefore, in order to improve the ductility, the as-deposited samples were severely deformed to alter the cast microstructure of the as-deposited sample to wrought microstructure. It is well known that the wrought product is more tough compared to cast product. In addition, the detrimental intermetallic coarse particle in the intermetallic region broke down to very fine particles and uniformly distributed in the aluminum matrix during FSP. This combined effect i.e. refinement of brittle intermetallic phase and transformation of cast-to-wrought microstructure improved the ductility of the as deposited sample to about 6%. Furthermore, post FSP heat treatment improved both strength and ductility of the FSP sample about 10%. This increase of strength is the consequences of formation of desired $MgZn_2$ precipitates. However, additional research is required to optimize chemical composition of the alloy powder to achieve the desired strength and ductility of the laser deposited samples comparable to the wrought 7xxx Al alloys.

CHAPTER 8 LASER METAL DEPOSITION OF MODIFIED AL 7050 ALLOY

The objective of making Al 7050 LMD friendly was achieved through the Ni coating of Al 7050 alloy as already explained in chapter 8. The Ni formed a stable phase with aluminum, which was not completely dissolved during the conventional heat treatment resulting in poor mechanical properties. The Mg and Zn were added with Al 7050 powder instead of Ni because Mg and Zn forms desired precipitates which can be dissolved using solution heat treatment. This Al 7050 alloy with added Mg and Zn is named as modified Al 7050 alloy.

8.1 Result and discussion

Advanced Powder Solutions Inc supplied the gas atomized powder Al 7050 with additional Zn and Mg. Table 8.1 lists the chemical composition of modified Al 7050 alloy powder. The range of particle size found to be 5 to 50 μm and most of the particles found to spherical. Figure 8.1 exhibits the morphology of the modified Al 7050 powder.

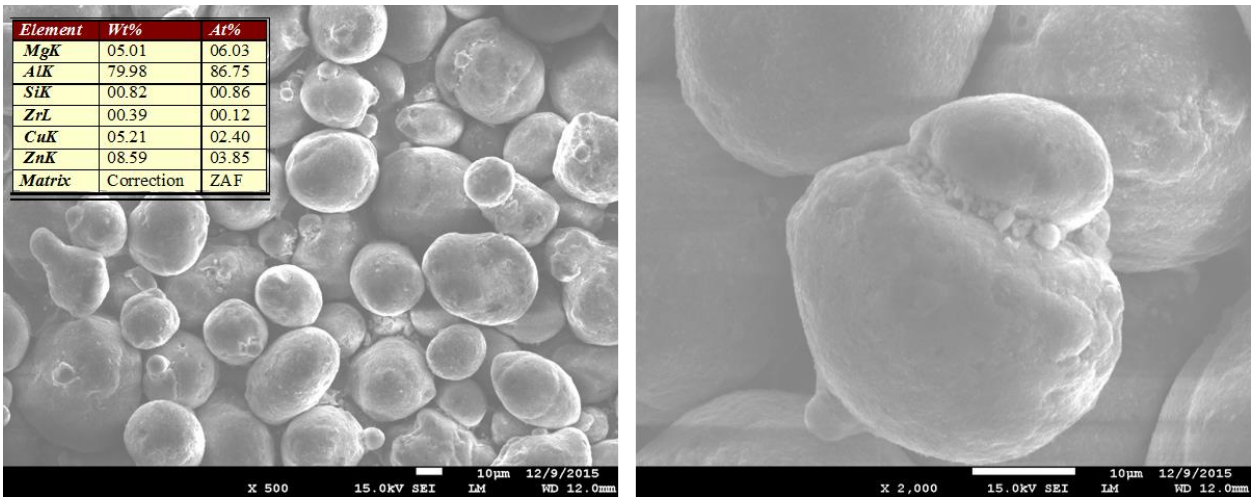

Figure 8.1: Powder morphology of modified Al 7050 alloy powder.

Table 8.1: Composition of modified Al 7050 alloy.

Mg	Zn	Cu	Zr	Al
5.01	8.59	5.21	0.39	Bal

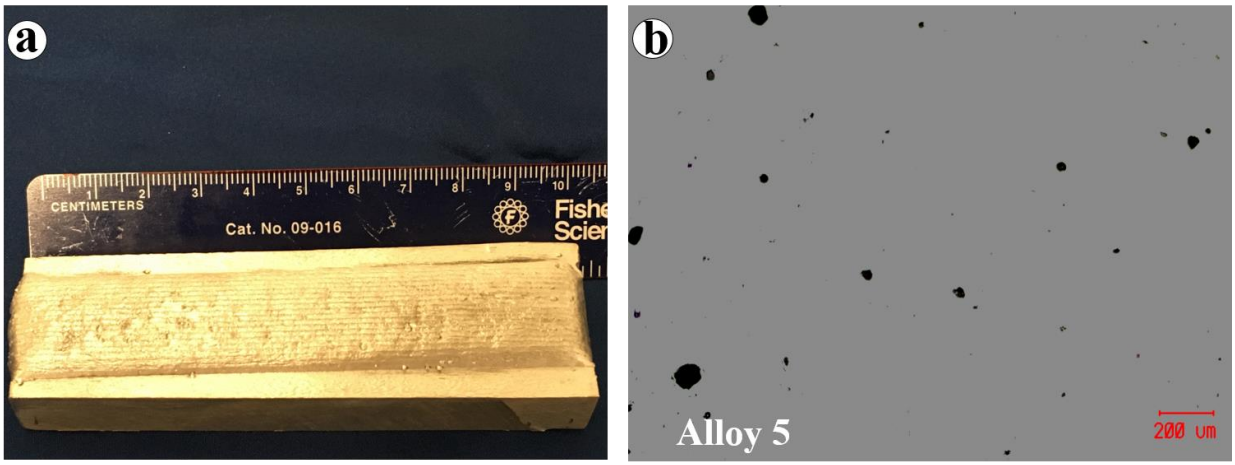

Figure 8.2: (a) Block deposit of modified Al 7050, and (b) Optical micrograph showing porosity in as-deposited modified Al 7050 deposit.

The deposition was conducted on rolled Al 6061 plate using optimized LMD parameters used to deposit pure Al 7050 alloy. Resulting block deposit is shown in figure 8.2. The surface finish of the block deposit was degraded as compared to Al 7050 block deposit. Optical micrograph exhibited the density greater than 97.5%, which is lower than the density of Al 7050 block deposit (>99.5%). No major defects like lack of fusion, crack etc. was observed during microscopy. Block deposit was made using hatch pattern as shown in Figure 7.2. SEM micrograph shown in figure 8.3 a exhibits the intermetallic phases in the interdendritic region. Heat treatment was conducted to dissolve segregated intermetallic phase in the interdendritic boundaries but it was found that some coarse precipitates were still present at the interdendritic region as shown in figure 8.3 b. Dark phase shown in the SEM micrographs are the primary α-Al dendrites and bright phase is the intermetallic phases.

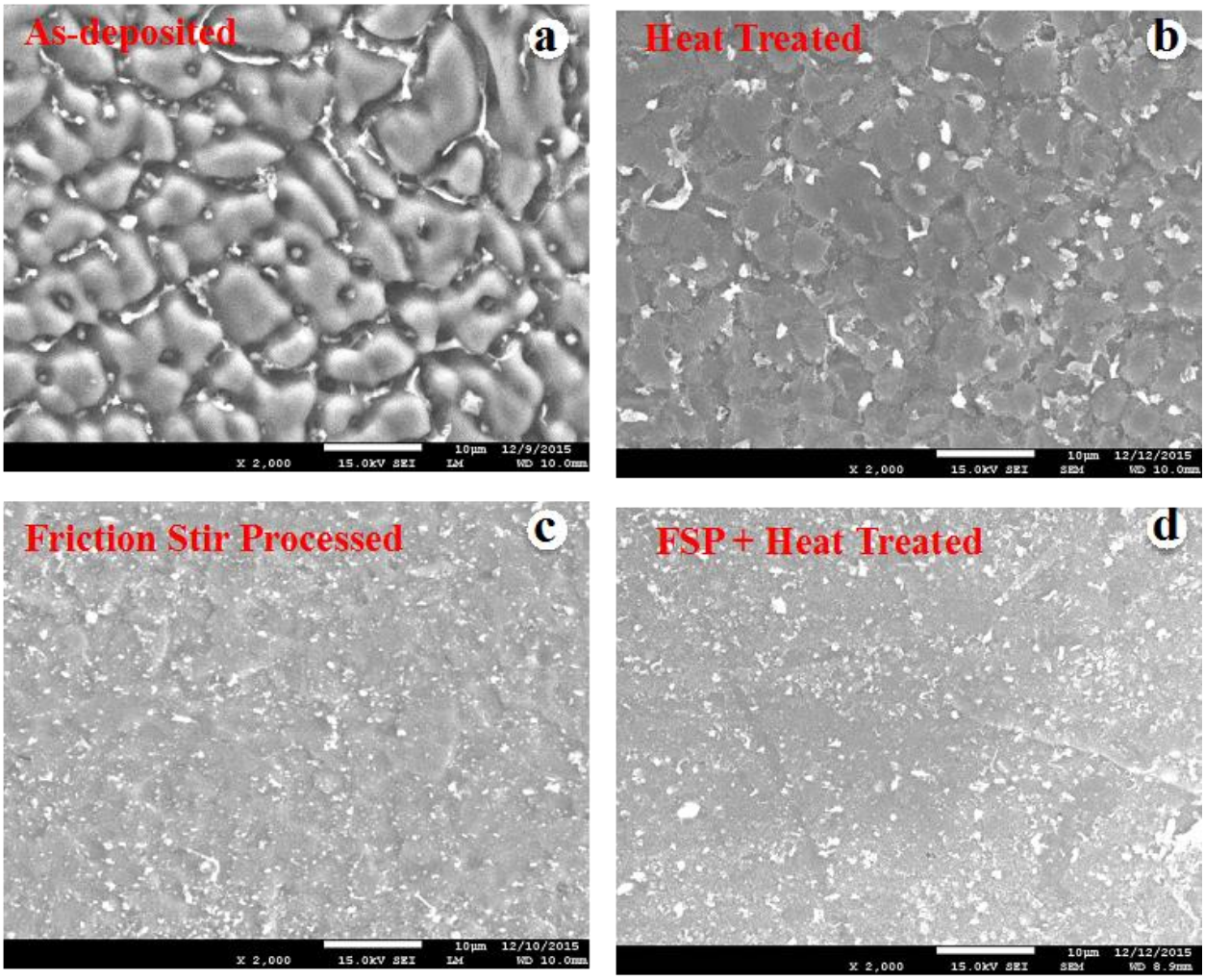

Figure 8.3: SEM micrographs of (a) As-deposited, (b) Heat-treated modified, (c) Friction stir processed, and (d) Post heat treated FSP modified Al 7050 alloy.

Further sample was friction stir processed to convert the cast microstructure to wrought microstructure. Friction stir processing of laser deposited sample resulted in finer and uniformly distributed second phase as shown in figure 8.3. Friction stir processing was conducted on a sample (150 mm × 100 mm × 3 mm) shown in figure 8.4(a). Optical microscopy exhibited density greater than 99.9 % as shown in figure 8.4(b).

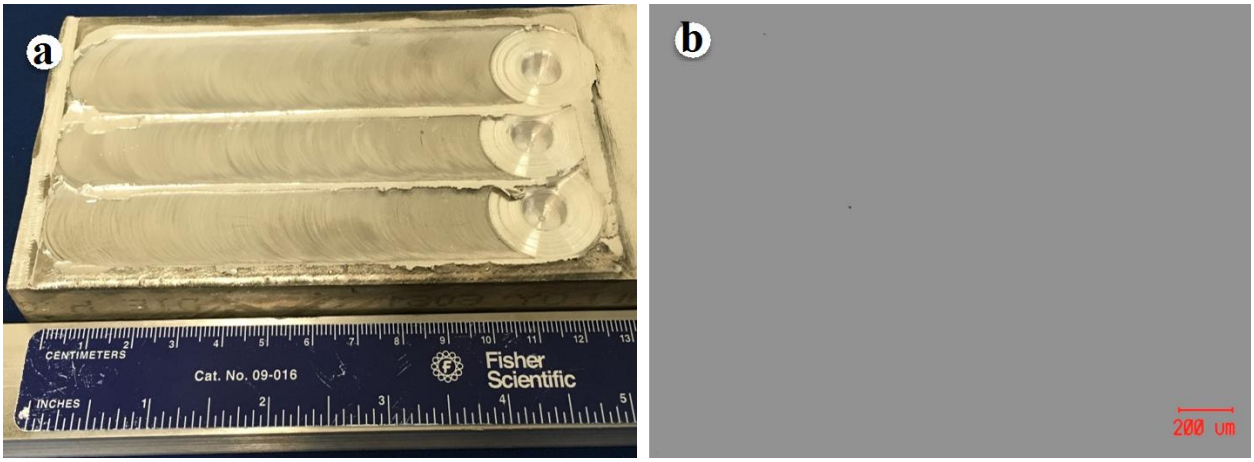

Figure 8.4: (a) Friction stir processed, and (b) optical micrograph for FSP modified Al 7050 sample.

In friction stir processing, the material undergo under intense plastic deformation at strain rate of 2-12 s^{-1} at elevated temperatures. Following FSP parameters were used to process the as-deposited sample: spindle speed: 500 rpm, tool tilt angle: 2.5 degree and traverse speed: 25 mm/min. SEM micrograph of friction stir processed sample exhibited the equiaxed microstructure and intermetallic phase was uniformly distributed throughout the sample as shown in figure 8.3(c). EDS analysis revealed the presence of segregation of Cu in the inter-dendritic region as shown in figure 8.5. EDS measurements revealed that the bright intermetallic phase is rich in Cu. Laser deposited sample was brittle due to coarse precipitates present in the interdendritic region. Tensile test was conducted on the post FSP laser deposited sample and post heat-treated FSP sample. The tensile stress results exhibited yield strength of 185 MPa which was increased to 225 MPa to after post heat-treatment of FSP sample. Tensile elongation of post FSP laser deposited sample was about 5.5% and almost remained constant after the heat treatment of FSP sample.

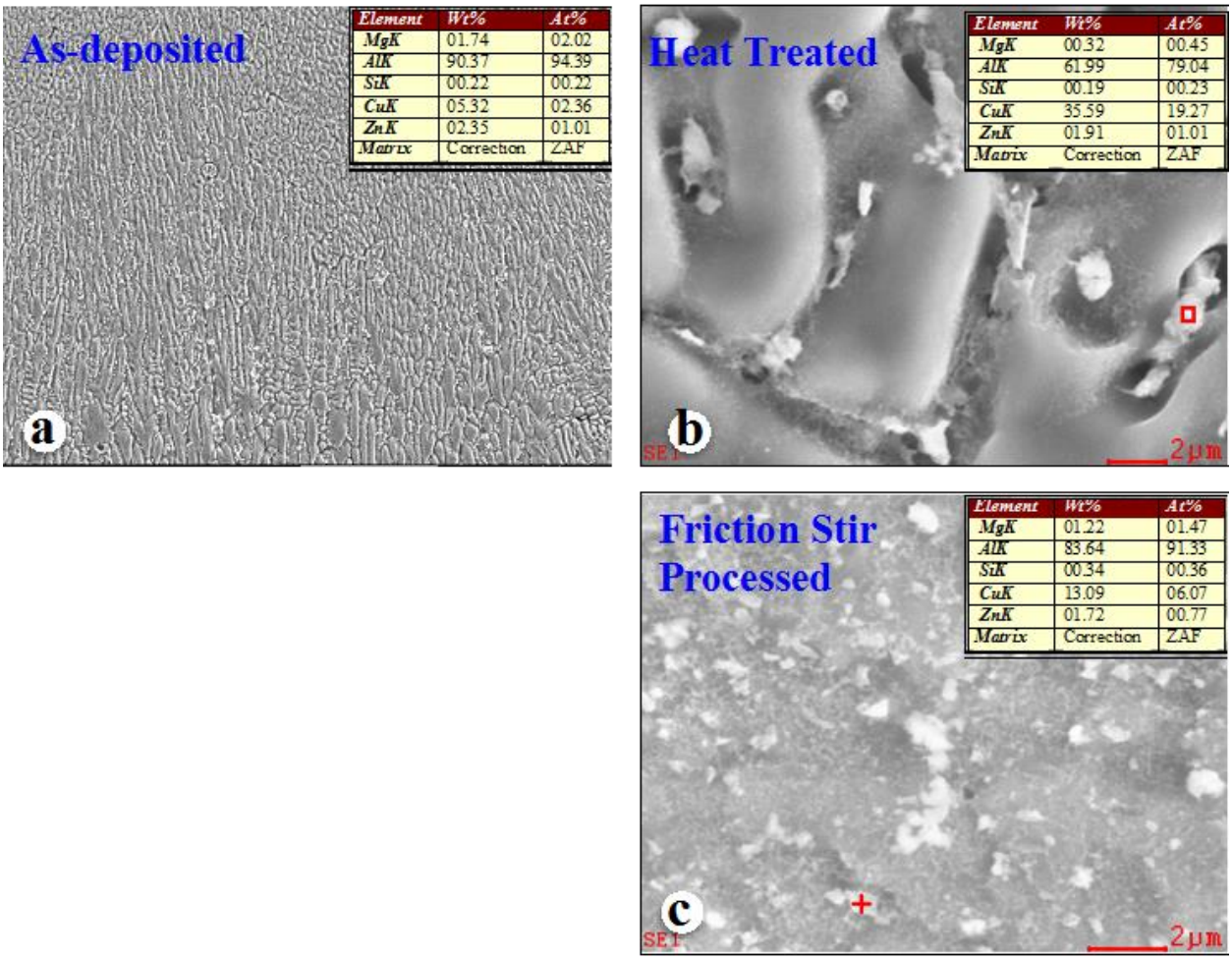

Figure 8.5: (a) Area EDS analysis of as-deposited, (b) EDS analysis of interdendritic region of post heat-treated , and (c) EDS analysis of FSP sample of modified Al 7050 alloy.

Microhardness of as-deposited modified Al 7050 was found to be 105 HV, which was increased by 5% after heat treatment. Since the Al 7050 is precipitation-hardening alloy, hence the less hardness value indicates towards the insufficient formation of strengthening precipitates. The major cause of less strengthening precipitates is the vaporization loss of low boiling elements such as Mg and Zn during the LMD process. Friction stir processing of sample resulted in even lower hardness value of 98 HV, which was regained to 105 after heat treatment of FSP sample. The amount of Mg and Zn addition was not enough to regain mechanical properties as compared to conventional wrought Al 7050 alloy mechanical properties.

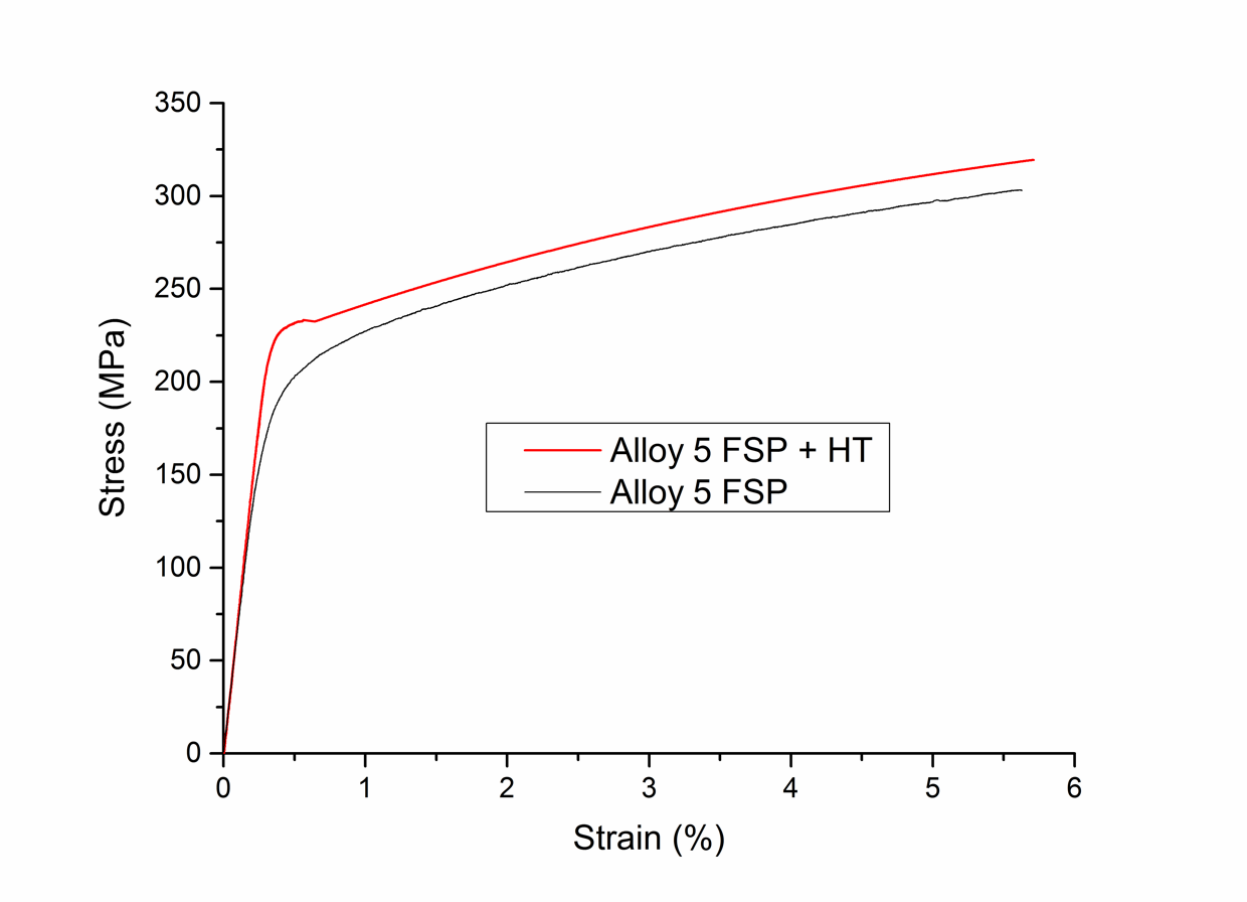

Figure 8.6: Stress-strain curves of friction stir processed (FSP) and post heat-treated FSP modified Al 7050 deposits.

Table 8.2: Microhardness values for modified Al 7050 alloy samples.

	Hardness Value
As-deposited	105 HV
Heat treated	111 HV
Friction stir processing	98 HV
FSP + Heat treated	105 HV

CHAPTER 9 LASER METAL DEPOSITION OF AL 7050 GRADIENT MATERIALS

Aluminum alloys are not suitable for LMD process because of inefficient absorption of photon energy as compared to Ni, Co, Fe based alloys and high thermal conductivity, though 4xxx series has been successfully additively manufactured [10, 14-17, 22, 58] without any major defects. LMD of high strength 7xxx series aluminum alloy remains a challenge till date. The low boiling elements vaporizes during the LMD of Al 7050 alloy resulting in low strength and results in high porosity [59]. Hence, there is dire need to find the optimized composition of LMD friendly 7xxx series aluminum alloy. Though conventionally available 4xxx series aluminum alloy powder is suitable for LMD process but alloy development has been ever ongoing process to enhance the micro-mechanical properties [60]. Effect of various alloying elements e.g. Mg, Zr, and Zn etc. on the resulting properties of deposited Al 7050 alloy has to be understood while processing via LMD [61-66] for developing LMD friendly Al 7xxx series alloys. Current alloy development process is one at a time practice, very time consuming and expensive. However, LMD process has a potential to produce a series of alloy in a single coupon and expedites the new alloy development process. In this present investigation, a gradient Al7050/Al50Mg50 specimen was fabricated by varying powder flow rates to develop a correlation between the Mg content in powder feed and deposited specimen at various composition level. Current study systematically demonstrates that instead of making separate samples, various compositions can be deposited into one single sample successfully. Current technique of making gradient samples can quickly predict the deposit quality in terms of density and major defects such as cracks, lack of fusion etc. resulting due to addition of alloying element. This study presents comprehensive microstructural development, microhardness distribution, and chemical composition in graded Al 7050/Al50Mg50 specimen. Based on these results, a correlation is developed to predict the amount of Mg vaporization during

LMD at different laser input power. The new alloy development would be much faster using current revolutionary technique than conventional way of making separate samples to study. In current study, two powder feeders were used though it can be extended to multiple powder feeders to study the effect of various alloying elements on resulting material properties.

9.1 Gradient materials deposition technique via laser metal deposition

Until now LMD technique has been applied for manufacturing and remanufacturing of components, however this study specifically applies LMD technology to deposit 10 different compositions of Al 7050/Al50Mg50 alloy in one coupon with dimension of 20 mm × 20 mm. To achieve the objective mentioned, two powder hoppers were used as shown in figure 9.1.

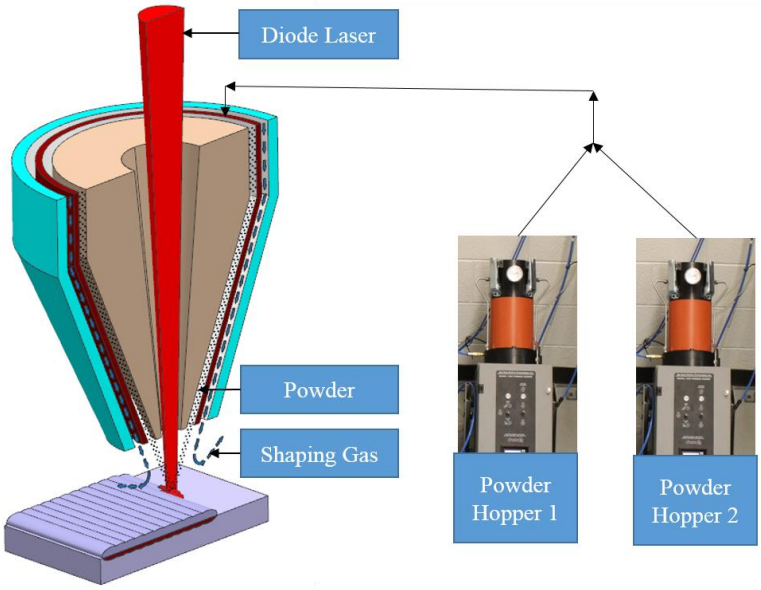

Figure 9.1: Schematic of LMD process showing nozzle and powder feeders.

Powder hopper 1 was filled with Al 7050 alloy powder. Prax Air supplied gas atomized Al 7050 powder. Figure 9.2) exhibits the morphology of Al 7050 powder. The powder particles were found to be mostly spherical in shape with some elongated powder particles and size range found to be around 10 µm to 50 µm. Powder hopper 2 was filled with a mixture of Al 7050 and Al50Mg50 (in 1:1 ratio) alloy powder. Figure 9.2 b exhibits the morphology of Al50Mg50 alloy powder. The

powder was found to be mostly spherical with some satellite powder particles. Magnesium-Elektron company supplied the gas atomized Al50Mg50 alloy powder with a particle size of 40-125 μm. Composition of the as-received Al 7050 and Al50Mg50 powder is listed in table 9.1.

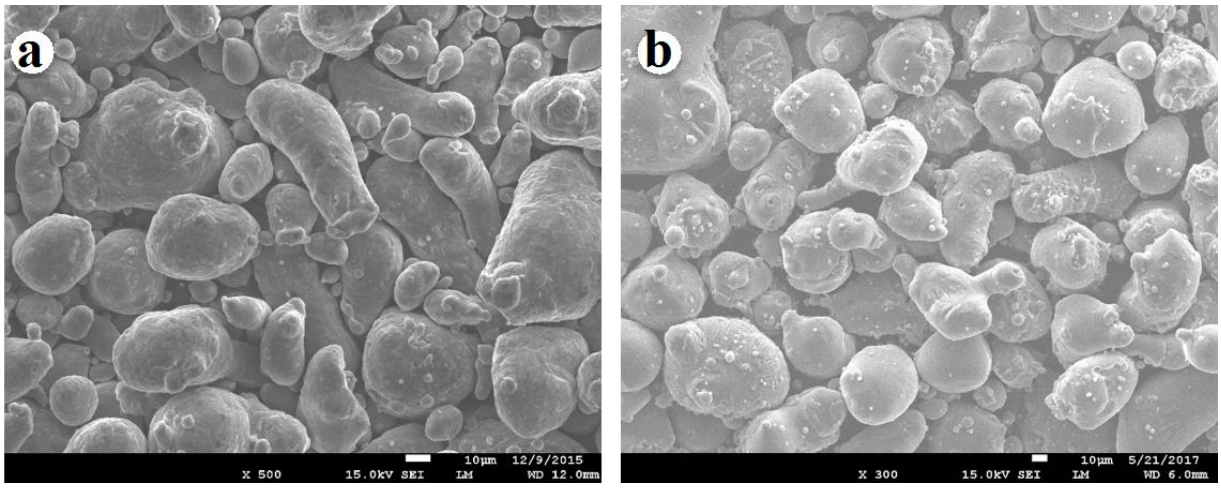

Figure 9.2: (a) Morphology of as- received Al 7050 alloy powder, and (b) Morphology of as-received Al50Mg50 alloy powder.

The defect free deposition of pure Al 7050 was achieved by optimizing the LMD parameters (laser power, powder feed rate, and scanning speed), as each LMD parameters has significant effect on the quality of deposition. The laser power had to be kept high for aluminum alloys as compared to other alloys such as Ni based alloys etc. to create a stable melt pool because of high thermal conductivity of aluminum alloys. The powder flow rate and scanning velocity was coupled in such a way that the standoff height of the nozzle remain constant at approximately 10 mm. The final optimized parameters for depositing pure Al 7050 alloy are shown in table 9.2. The same parameters were used during deposition of Al-7050/Al50Mg50 gradient sample. Powder hopper 1 was used to deposit Al 7050 deposit. To achieve the deposition of Al 7050 gradient sample, both powder hopper 1 and powder hopper 2 were coupled together using pipe connections as shown in figure 9.1. The powder flow rate of individual powder feeders was varied individually but the total powder flow rate (hopper 1 powder flow rate + hopper 2 powder flow rate) was kept constant at

optimized value of 3.5 gm/min as shown in table 9.2. The individual feed rate (gm/min) for powder feeders was varied (as shown in table 9.3) in such a way that Mg content in Al-7050/Al50Mg50 powder increased from layer 1 to layer 10, shown in figure 9.3 c. Hence, in a single coupon with ten layers of deposition, each layer contains unique Al 7xxx composition. Each layer of 20 x 20 mm coupon have different composition with different amounts of Al, Mg, Zn and Cu as shown in table 9.3.

Table 9.1: Composition of Al 7050 alloy powder and A50-Mg50 alloy powder by weight percent.

	Mg	**Zn**	**Cu**	**Zr**	**Al**
Al 7050	2.25	6.18	2.23	0.13	Bal
Al50-Mg50	50	-	-	-	50

The powder feed rate was varied by changing analog voltage signal, which in turn changed the rpm of powder feeder rate. Powder hopper 1 with Al 7050 and hopper 2 with a mixture of 50% Al 7050 and 50% Al50 Mg50 were calibrated against the voltage and powder feed rate. Powder hopper 2 was filled with mixture instead of pure Al50Mg50 because powder feeder with pure Al50Mg50 has to be operated at very low rpm, which is beyond the powder feeder range.

Table 9.2: Optimized LMD parameters for Al 7050 deposition.

Laser Power (Watt)	**Powder Flow Rate (gm/min)**	**Scan Speed (mm/min)**
1050	3.5	500

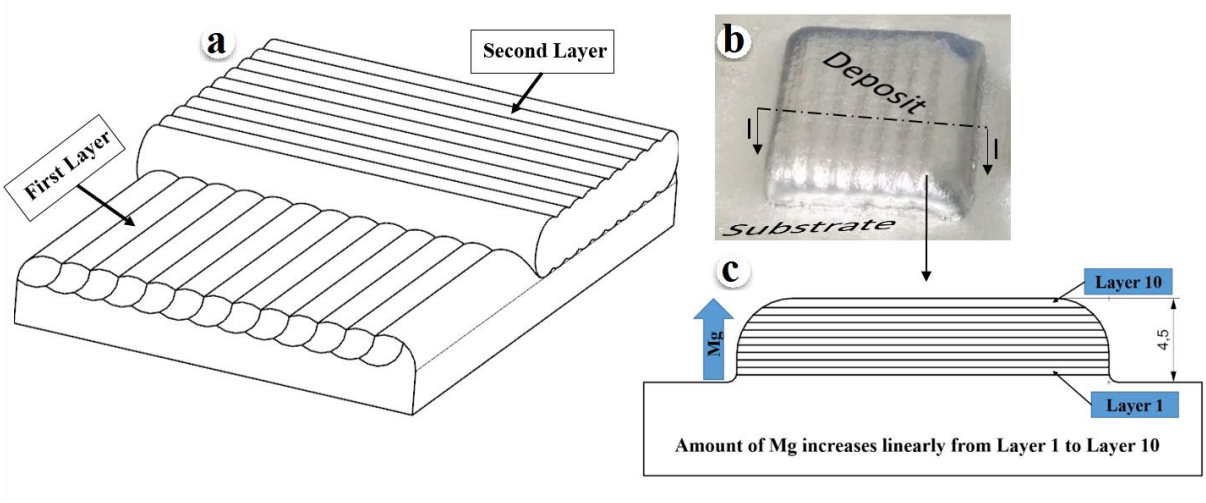

Figure 9.3: (a) Deposit scanning hatch pattern, (b) Al-7050/Al50Mg50 gradient block deposit, and (c) Schematic of cross sectional view of deposit showing increment in Mg composition from layer 1 to layer 10.

Table 9.3: Al-7050/Al50Mg50 powder composition (wt. %) for depositing gradient specimen.

Layer Number	Powder Hopper 1 Al 7050 (gm/min)	Powder Hopper 2 50% Al 7050+50% Al50 Mg50 (gm/min)	Mg (%)	Zn (%)	Cu (%)
1 (Bottom)	3.50	0.00	2.3	6.18	2.23
2	3.15	0.35	4.6	5.87	2.12
3	2.80	0.70	7.0	5.56	2.01
4	2.45	1.05	9.4	5.25	1.96
5	2.10	1.40	11.8	4.94	1.79
6	1.75	1.75	14.2	4.64	1.69
7	1.40	2.10	16.6	4.32	1.58
8	1.05	2.45	19.0	4.017	1.47
9	0.70	2.80	21.4	3.71	1.36
10(Top)	0.0	3.15	23.7	3.39	1.26

9.2 Results and discussion

The main objective of this study develop a correlation between the Mg content in powder feed and laser deposited Al-7050/Al50Mg50 gradient material at various composition level. In addition, the benefit of this study is that deposition of ten different compositions can be studied in a single sample, which saves time and resources. Before depositing the gradient sample, conventional Al 7050 was deposited on a substrate using optimized parameter to check for any voids, cracks or any major defects. These initial checks were conducted to ensure the optimization of LMD parameters for defect free deposition of Al 7050 gradient sample. Deposition parameters for gradient sample was kept similar to that of Al 7050 deposition parameters. Two powder feeders were used as already explained in experimental section to deposit every layer with different composition. Powder flow rate for these two powder feeders were varied in such a way that resulted in layers with linearly increased Mg content as shown in table 9.3.

After visual inspection, it was clear that Al 7050 sample was very flat and shiny (shown in figure 9.3 b). No major defects like crack or de-bonding was observed in Al-7050/Al50Mg50 gradient sample. Scanning speed and laser power was maintained at a constant value throughout the deposition. Figure 9.4 exhibits the microstructure transformation from layer 1 to layer 6. In the very first layer as shown in figure 9.4 a, interdendritic boundaries are decorated with intermetallic phases revealed by XRD analysis. XRD analysis revealed that these intermetallic phases present in interdendritic regions are mostly MgZn2, Al2CuMg, Al3Mg2, and AlMg2. The grey phase is the primary α-aluminum and bright phase is the intermetallic phases.

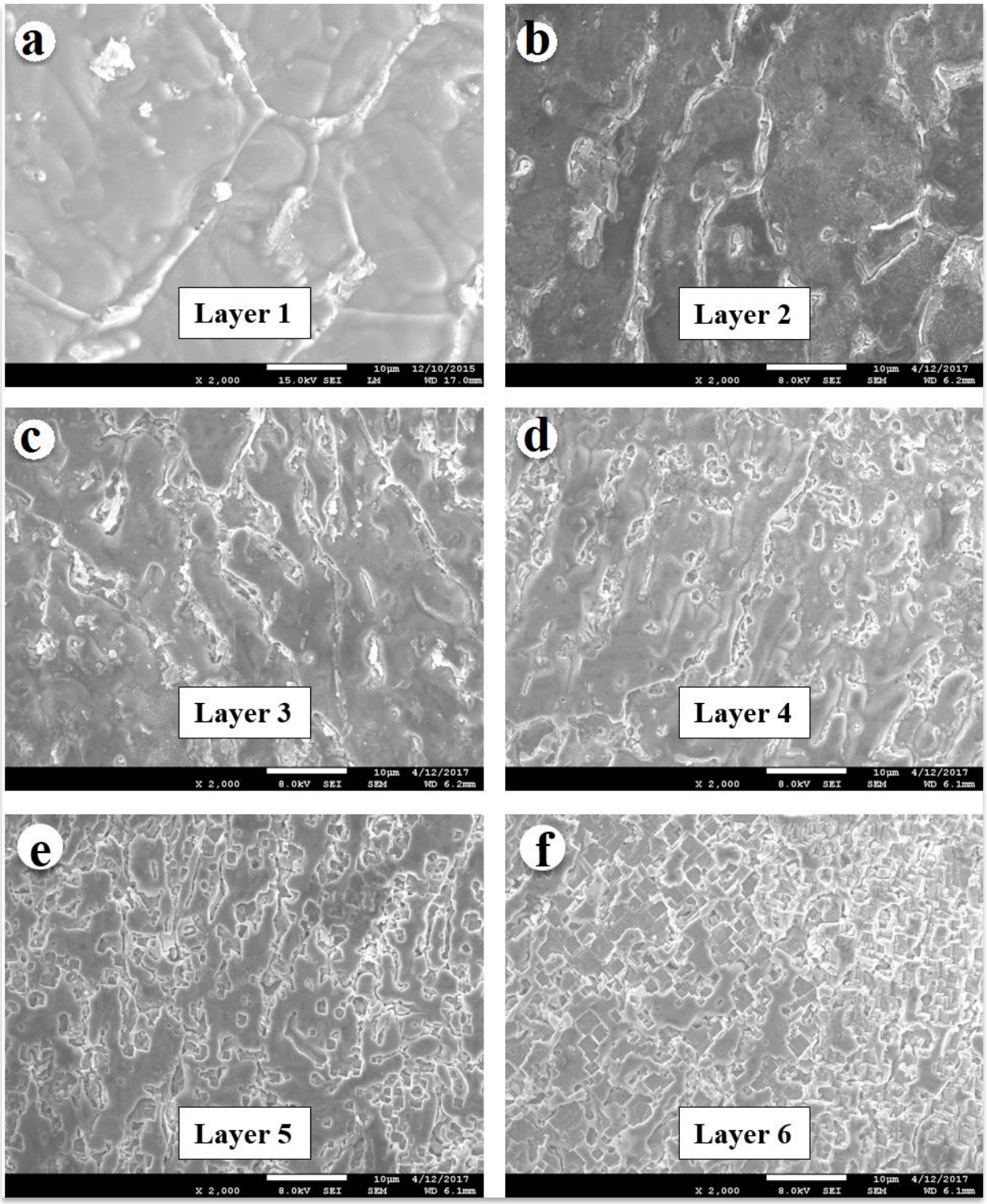

Figure 9.4: SEM micrographs of as-deposited Al 7050 gradient sample showing Layer 1 through Layer 6.

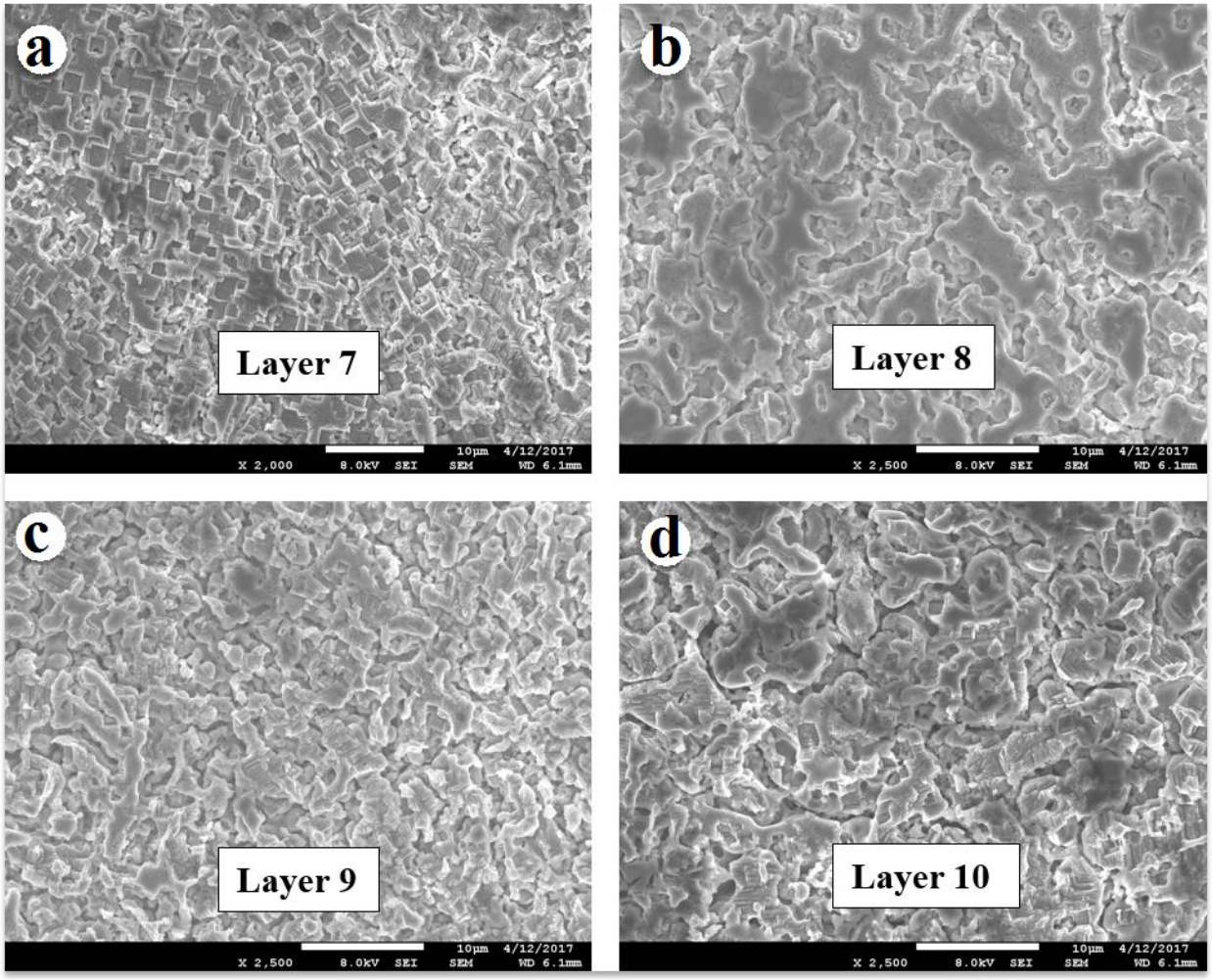

Figure 9.5: SEM micrographs of as-deposited Al 7050 gradient sample showing Layer 7 through Layer 10.

With Mg addition (about 2.3 wt. %) for depositing layer 2, the size of the α-Al dendrites was reduced though the interdendritic boundary was still decorated with intermetallic phases but interdendritic boundary was not completely continuous as it was in layer 1. In layer 3, as an effect of adding more Mg, primary α-Al dendrite size was further reduced and intermetallic phase along the interdendritic boundary found to be more discrete. Layer 4 exhibited similar type of microstructure as layer 3. Interdendritic boundary in layer 4 was more etched more as compared to previous layers, leaving a gap, which is evident from figure 9.4 d.

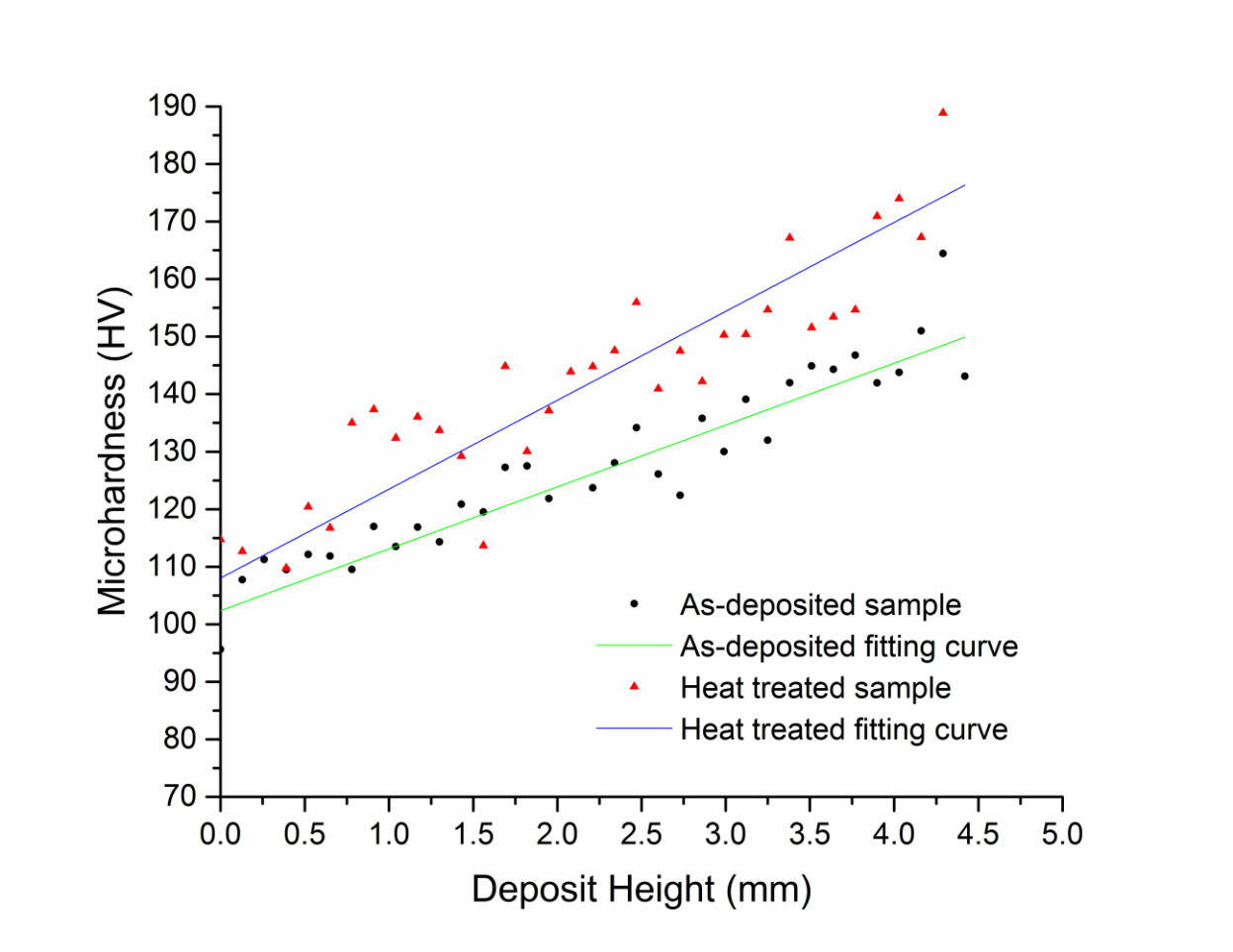

Figure 9.6: Microhardness distribution of as-deposited and heat treated Al-7050/Al50Mg50 gradient sample.

In layer 5 as shown in figure 9.4 e, it is very hard to determine the size of α-Al dendrites. Microstructure transformed from irregular (polygonal) shape in layer 5 to cuboid type structure in layer 6 as shown in figure 9.4 f. In previous layers, intermetallic phases were typically present along the interdendritic boundary but layer 6 onwards; it appears that intermetallic phases are distributed uniformly throughout the entire specimen. Figure 9.5 shows the micrograph for layer 7, which exhibited similar microstructure to layer 6. The size of cuboid shaped phases almost remained same as compared to layer 6. Severe etching was observed in layer 8 because of the

presence of high amount of Mg and etchant being quite reactive with Mg. Mg rich phase has been dissolved quite a bit because of severe etching. Layer 9 and Layer 10 followed same trend of dissolved Mg because of etching as these layers have even higher concentration of Mg. It is very difficult to predict the size of primary α-Al dendrites.

Microhardness testing was conducted on the as-deposited and heat treated Al-7050/Al50-Mg50 gradient sample at equal interval of 130 microns which implies that almost three readings were recorded per layer. The resulting microhardness values were plotted against the deposit height as shown in the figure 9.6. The microhardness of the as-deposited Al-7050/Al50Mg50 gradient sample increased almost linearly with increasing height of the deposit. Note that Mg content gradually increased with the increase in the height of the deposit. It was observed that the linear increment in the Mg content in powder feed resulted in linear increment in hardness of the deposited sample. The resulting increase in hardness is due to the rise in formation of MgZn2 and Al3Mg2 intermetallic phase. The minimum value recorded at bottommost layer was about 94 HV and maximum observed was about154 HV at topmost layer of as-deposited Al-7050/Al50Mg50 gradient sample. The heat treated sample showed the higher microhardness at same deposit height. Heat-treated Al 7050 gradient sample showed almost same trend of linear increment in microhardness except some outliers between the height of 1 and 1.5 mm. The minimum value observed in the heat-treated Al-7050/Al50Mg50 gradient sample was 110 HV at bottom most layer and maximum value of microhardness was 190 HV at top most layer. This increment in hardness value at same height after heat treatment was again due to formation of more MgZn2, Al3Mg2 and Al2CuMg intermetallic phases. The slopes of the fitted curves of as-deposited and heat-treated are not same as observed in figure 9.6. Different slopes indicate that at different height, the increment was not constant throughout the deposited height. The reason could be that though there is an

increase in Mg content, resulting in generation of higher amounts of intermetallic phases but simultaneously the percentage of Zn reduces due to mixing of Al 7050 and Al50Mg50.

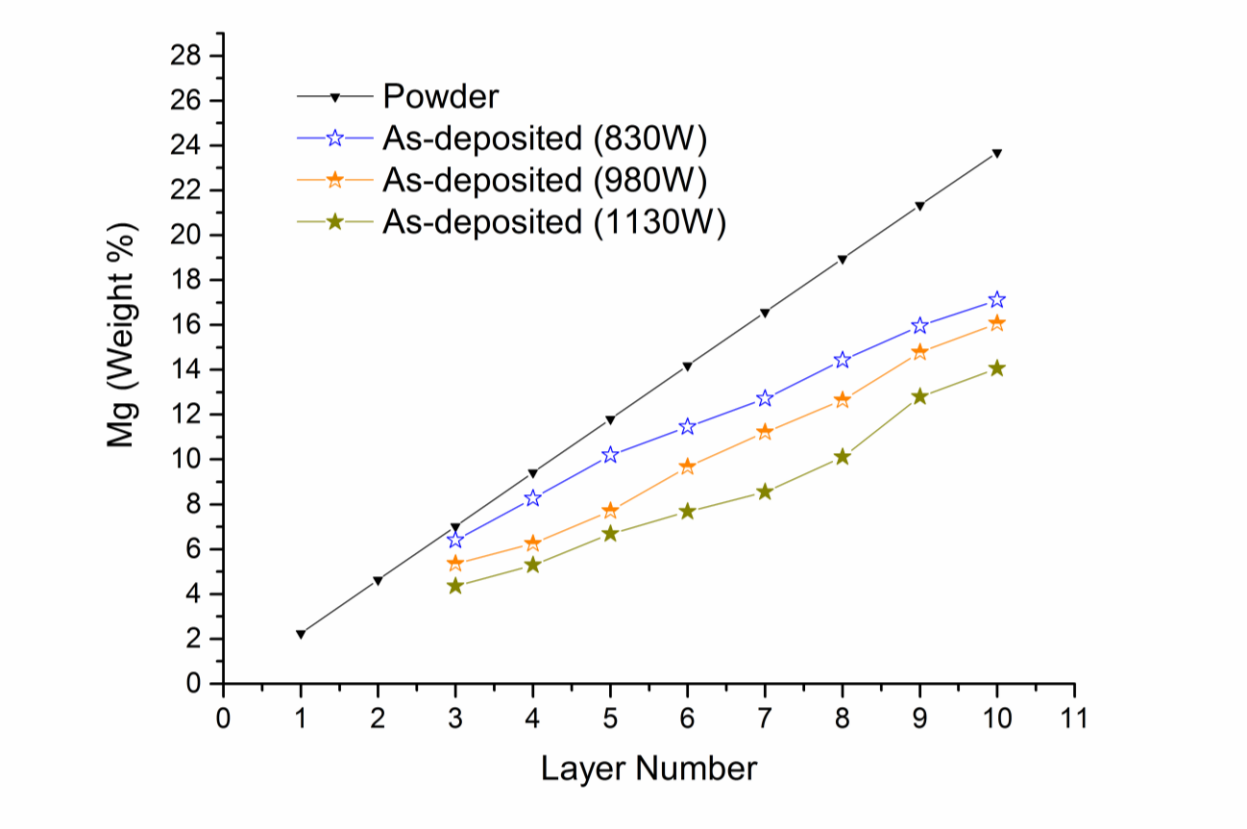

Figure 9.7: Plot showing percentage of Mg content in powder feed, and as-deposited sample fabricated with 830 W, 980 W and 1130 W input laser power, respectively.

The interesting fact that can be noticed from microhardness plot is that there is hardly any increase in the microhardness in layer 1 (between 0 mm and 0.4 mm) after heat treatment. On the contrary, in conventional 7xxx alloys, the microhardness value should reach about 150 HV after heat-treatment [18, 67]. Hence, there may not be enough formation of desired strengthening precipitates MgZn2 and Al2Cu during heat treatment.

EDS investigation was conducted to measure the amount of Mg and Zn in as-deposited gradient sample. It was found in EDS investigation that the low boiling point elements such as Mg

and Zn were evaporated during the LMD of Al 7050 alloy [59]. Hence, it was necessary to understand the vaporization behavior of low boiling point elements during LMD of Al 7050. In current study, the Al-7050/Al50Mg50 gradient sample had different amount of Mg and Zn in each deposited layer. Figure 9.7 Figure 7 shows the amount of Mg present in Al-7050/Al50Mg50 powder feed mixture and Mg content in the as-deposited sample produced with 830 W, 980 W and 1130 W for each layer, respectively. The Mg evaporated substantially during LMD of gradient material containing different amount of Mg in powder feed mixture. In addition, amount of Mg loss increases with increasing laser power. The vaporization of low boiling point elements such as Mg and Zn results in low volume fraction of desired strengthening precipitates which reduces the hardness of as-deposited and heat treated Al-7050/Al50Mg50 gradient sample. From figure 9.7, a correlation was developed between the Mg content (in wt. %) in powder feed and Mg (in wt. %) content in as-deposited sample at various laser power.

$$Cad = (-0.38 \times L^2 + 0.027262 \times L + 1) \times Cpwd - 0.032675 \times L^2 + 0.20701 \times L \quad (1)$$

Where Cad= Amount of Mg present (by wt. %) in as-deposited sample, Cpwd= Amount of Mg present in as-deposited sample, L=Input laser power (KW)

Equation 1 represents relationship between Mg content in starting powder and Mg content in deposited material. Note that this correlation is valid for sample deposited with a scanning speed of 500 mm/min.

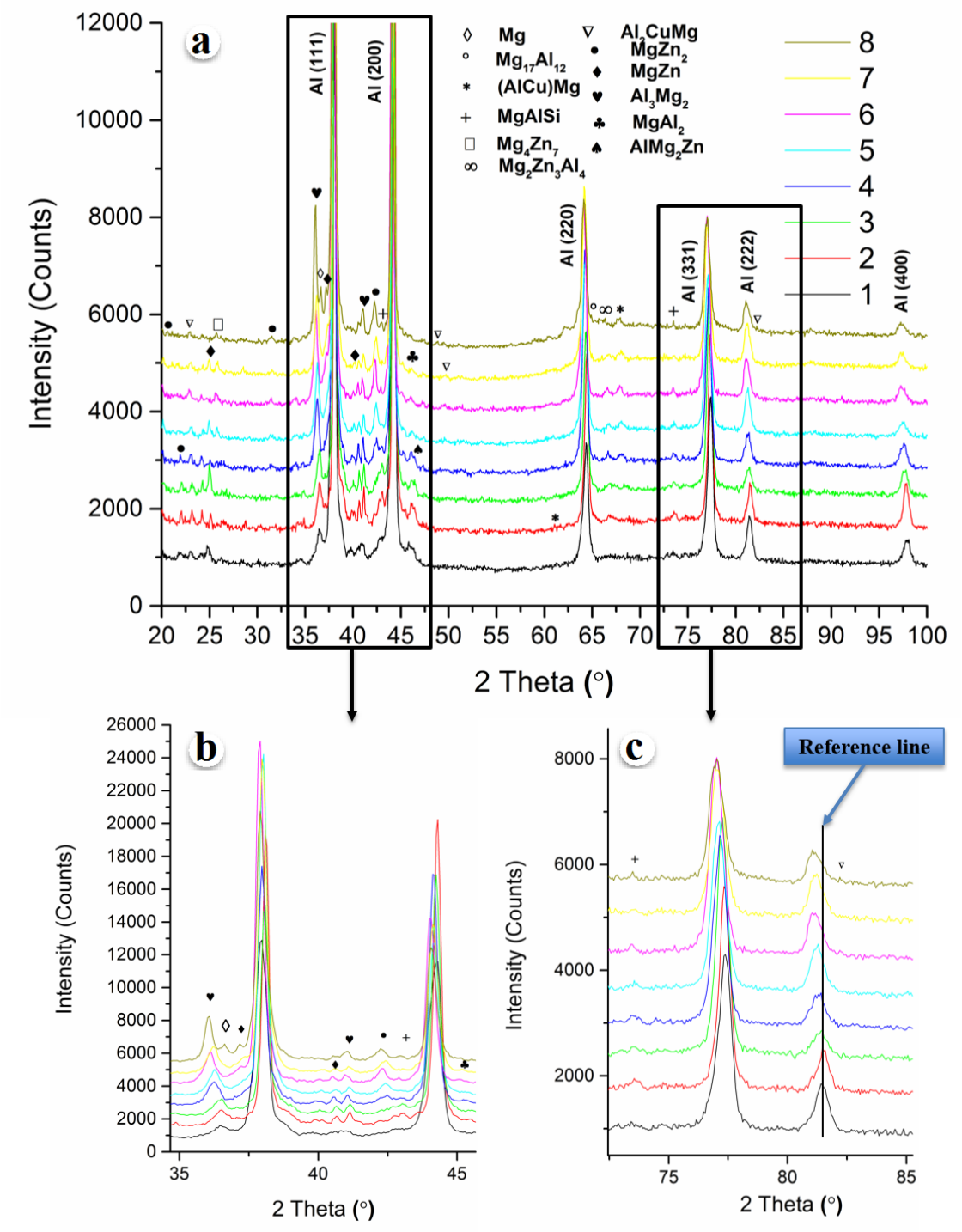

Figure 9.8: (a) XRD plot of 8 layers from top of as-deposited Al 7050 gradient sample, (b) magnified view of range between 32 and 45 degree, (c) magnified view of range between 72 and 85 degree.

XRD experiment was conducted to investigate the presence of various phases and their lattice constant in laser deposited gradient sample. XRD analysis was conducted on top eight layers of laser deposited material. Note that plot number 1 is corresponding to third layer and plot number eight corresponds to the tenth layer of deposit. Significant aluminum peak shift was noticed as shown in figure 9.8 b and figure 9.8 c. The aluminum peaks gradually shifted towards lower angle with the increase in amount of Mg content in deposited layers. This peaks shift suggests increase in lattice parameter with the addition of Mg, which in turn implies that more Mg was dissolved in Al matrix. Remaining Mg, which was not dissolved in the α-Al matrix formed the intermetallic compounds. Lattice parameter calculation revealed gradual increase of lattice parameter of α-Al from third layer to tenth layer. Lattice parameter of third layer and tenth layer found to be 407.94 pm and 410.99 pm, respectively. Whereas the lattice parameter of pure Al is about 404.95 pm which is substantially lower than super saturated α–Al in topmost layer [68]. Increase in Mg content is clearly indicated by multifold increase in intensity of Al3Mg2 peaks (around 36o) as shown in figure 9.8 b. In addition, rise in formation of other strengthening precipitates (MgZn2) from third to topmost layer is indicated by increase in MgZn2 peak intensity in XRD plot. The presence of other phases such as Mg17Al12, Al2CuMg, MgZn, Mg4Zn7, MgAl2, and AlMg2Zn were also detected in XRD analysis.

CHAPTER 10 SUMMARY

This research deals with the successful deposition of defect free 7050 and Al1.2Si aluminum alloys using LMD. This study addresses the challenges of building tall wall and cuboid shapes eutectic Al-Si and 7050 aluminum alloy components by direct laser metal deposition technique for automotive and aerospace applications. Current study revealed that direct laser metal deposition process can be applied successfully to manufacture bracket on cast shock tower hood. As compared to conventional way of making parts separately and spot welding on shock tower hood, current method saves time and expenses. It further gives freedom for sophisticated designs. In both cases of block and single wall deposition, tensile tests exhibited excellent combination of 225 MPa UTS and 9 % of elongation. Effect of reducing laser power in case of single wall deposit resulted in defect free deposition until 15 mm. Laser Power cannot be decreased after 800 watt as more reduction would create unstable melt pool, which would disrupt the further deposit growth and can cause major defects. Average microhardness of block deposition and single wall deposition was exhibited almost same hardness difference of about 3 HV from bottom to top of the deposits. Density of deposits was greater than 99.9 % in both cases. Bottom part of each layer exhibited columnar microstructure due to the high thermal gradient and low solidification velocity in both deposit. In contrast, top of each layer exhibited equiaxed dendritic structure due to low thermal gradient and high solidification velocity at the upper part of melt pool. This research also presents the effect of various laser deposition parameters like laser power, powder flow rate, and scanning speed on the microstructure and mechanical properties distribution from substrate to deposit.

Current investigation revealed that 7050 aluminum alloy can be successfully manufactured using LMD technique without any major defect. After deposition, composition changes from

original 7050 aluminum powder because of substantial evaporation of low boiling point elements such as Zn and Mg. The heat treatment did not have significant effect on the yield strength of 7050 aluminum alloy. Yield strength increased by 30 MPa after heat treatment. The microhardness of the as-deposited samples found to be 100 HV and 128 HV after heat treatment. Segregated second phase particles were dissolved and re-precipitated after heat treatment. Further investigation is required to have insight in poor ductility of heat treated and as-deposited samples.

Since the ductility and hardness was still a key issue after the successful deposition of Al 7050 alloy, modification was necessity to enhance the mechanical properties. The major challenge in laser additive manufacturing of Al 7050 alloy was the low boiling point of alloying elements such as Zn and Mg, which evaporates during laser deposition. This evaporation decreases the quantity of strengthening elements and creates defects such as porosity and voids in the deposit. Moreover, Al is a highly reflective material. Consequently, deposition of Al alloys is challenging compares to Ni-, Fe-, Co-, and Ti-base alloys. In the present investigation, Ni coated Al 7050 powder was additively manufactured using direct Laser Metal Deposition (LMD) to overcome the above stated challenges. The present investigation demonstrated that the Ni coated Al 7050 alloy components can be deposited using laser metal deposition technology. However, a major portion of added Ni was segregated in the inter-dendritic boundaries during laser deposition. As a result, the mechanical properties especially the tensile ductility of the as-deposited sample found to be very poor (<0.5%) due to the presence of brittle intermetallic phase in the inter-dendritic region. To improve the ductility, the as-deposited samples were severely deformed by friction stir processing to refine the detrimental intermetallic phase and distribute uniformly in the aluminum matrix. In addition, FSP also transformed the cast microstructure of the as-deposited sample to wrought microstructure. Consequently, the ductility of the laser deposited sample improved to

about 6% after FSP. Further research is required to design and develop new 7xxx Al alloy for additive manufacturing applications. Furthermore, post FSP heat treatment improved both strength and ductility of the FSP sample about 10%. This increase of strength is the consequences of formation of desired $MgZn_2$ precipitates.

After successful deposition of Al 7050 without coating and Ni coated Al 7050, it was clear that the loss of Mg and Zn plays a significant role of decrementing the mechanical properties. The composition after the deposition of Al 7050 sample was different from the Powder composition used for same deposition. Hence, if the Mg content was incremented in the Al 7050 powder then composition after deposition might yield conventional Al 7050 composition. A systematic study was conducted to analyze the effect of Mg addition in Al 7050 sample. The Mg quantity was gradually increased from bottom of sample to the top using two powder feeders as explained in Chapter 8 called as Al 7050 gradient sample. This study of making gradient sample also demonstrated that the various alloy compositions could be deposited into a single coupon using LMD when coupled with two or more powder feeders. The ten different compositions of Al 7050 alloy were successfully deposited in single coupon of 20 mm × 20 mm called as Al 7050 gradient sample using two powder feeders. Mg and Zn rich phase was segregate along the interdendritic boundary continuously in layer 1 and continued to become discrete with addition of Mg until layer 10. Primary α Al dendrites size decreased from layer 1 to almost not measurable in layer 10 due to the dissolution of Mg while etching. The microhardness of as-deposited Al 7050 gradient sample was 94 HV at layer 1 and gradually increasing to about 154 at the top of sample. The microhardness of heat-treated Al 7050 gradient sample was 110 HV at the layer 1 and gradually increased to about 190 HV at the top of the sample where the Mg is highest in weight percent. With the linear increment in Mg addition, microhardness of as-deposited and heat-treated Al 7050 sample found

to be almost linear in nature. The low microhardness of layer 1 (conventional Al 7050 composition) was due to vaporization of low boiling point elements such as Mg and Zn. The empirical correlation was developed between the Mg content by weight percent present in the Al 7050 feed powder and Mg content by weight percent present in the laser deposited material. Al 7050 gradient sample study showed that the vaporization of elements have major impact on the quality of deposit, mechanical properties and microstructural evolution.

10.1 Recommendations for future work

After the successful deposition of 7050 aluminum alloy, it was found that the mechanical properties were poor as compared to the conventional wrought Al 7050 alloy. Hence, more efforts are required to look into possibilities for enhancement of properties of as-deposited 7050 aluminum alloy.

1. Investigate the effect of Cu and Zr coating of Al 7050 alloys. It was observed that Ni coating was able to preserve but simultaneously resulted in the formation of intermetallic, which could not dissolved after heat treatment.
2. Study the effect of Zn additions simultaneously with the additions of Mg would be helpful in understanding the nature of precipitation mechanism.
3. Effect of the hot isostatic pressing and high-pressure equal channel angular extrusion along with torsion on as-deposited samples mechanical properties.
4. Study the additional mechanical properties such as fatigue strength and fracture toughness of laser deposited Al alloys.

REFERENCES

1. Ian Gibson, D.R.a.B.S., *Additive Manufacturing Technologies 3D Printing, Rapid Prototyping, and Direct Digital Manufacturing*. 2010, New York.
2. Shoji Maruo, O.N., and Satoshi kawta, *Three-dimensional microfabrication with two-photon-absorbed photopolymerization.pdf*. Optics Letters, 1996. **22**.
3. Sidambe, A., *Biocompatibility of Advanced Manufactured Titanium Implants—A Review.* Materials, 2014. **7**(12): p. 8168-8188.
4. University, L.; Available from: http://www.lboro.ac.uk/research/amrg/about/the7categoriesofadditivemanufacturing/binderjetting/.
5. W.D.P inc.; Available from: http://www.wanhao3dprinter.com/FAQ/ShowArticle.asp?ArticleID=62.
6. Conner, B.P., G.P. Manogharan, A.N. Martof, L.M. Rodomsky, C.M. Rodomsky, D.C. Jordan, and J.W. Limperos, *Making sense of 3-D printing: Creating a map of additive manufacturing products and services.* Additive Manufacturing, 2014. **1-4**: p. 64-76.
7. Totten, G.E. and D.S. MacKenzie, *Handbook of Aluminum: Vol. 1: Physical Metallurgy and Processes*. 2003: CRC Press.
8. A*luminium-alloys and its application*. The Aluminum Association,Inc., 1998; Available from: http://www.calm-aluminium.com.au/documents/aluminium-alloys.pdf.
9. Kaufman, J.G., E.L. Rooy, and A.F. Society, *Aluminum Alloy Castings: Properties, Processes, and Applications*. 2004: ASM International.

10. Dinda, G.P., A.K. Dasgupta, and J. Mazumder, *Evolution of microstructure in laser deposited Al–11.28%Si alloy.* Surface and Coatings Technology, 2012. **206**(8-9): p. 2152-2160.

11. Warmuzek, M., *Aluminum-silicon Casting Alloys: An Atlas of Microfractographs*. 2004: ASM International.

12. Ghiaasiaan, R., X. Zeng, and S. Shankar, *Controlled Diffusion Solidification (CDS) of Al-Zn-Mg-Cu (7050): Microstructure, heat treatment and mechanical properties.* Materials Science and Engineering: A, 2014. **594**: p. 260-277.

13. Bai, Q.L., Y. Li, H.X. Li, Q. Du, J.S. Zhang, and L.Z. Zhuang, *Roles of Alloy Composition and Grain Refinement on Hot Tearing Susceptibility of 7××× Aluminum Alloys.* Metallurgical and Materials Transactions A, 2016. **47**(8): p. 4080-4091.

14. Chou, R., J. Milligan, M. Paliwal, and M. Brochu, *Additive Manufacturing of Al-12Si Alloy Via Pulsed Selective Laser Melting.* Jom, 2015. **67**(3): p. 590-596.

15. Nahmany, M., I. Rosenthal, I. Benishti, N. Frage, and A. Stern, *Electron beam welding of AlSi10Mg workpieces produced by selected laser melting additive manufacturing technology*. Additive Manufacturing, 2015. **8**: p. 63-70.

16. Olatunde Olakanmi, E., K.W. Dalgarno, and R.F. Cochrane, *Laser sintering of blended Al‐Si powders.* Rapid Prototyping Journal, 2012. **18**(2): p. 109-119.

17. Wang, X.J., L.C. Zhang, M.H. Fang, and T.B. Sercombe, *The effect of atmosphere on the structure and properties of a selective laser melted Al–12Si alloy*. Materials Science and Engineering: A, 2014. **597**: p. 370-375.

18. Cottam, R., Q. Liu, Y.C. Wong, J. Wang, and M. Brandt, *Laser cladding of high strength aluminium alloy 7075 powder on a 7075 substrate for repair of damaged components*.

19. Reschetnik, W., J.P. Brüggemann, M.E. Aydinöz, O. Grydin, K.P. Hoyer, G. Kullmer, and H.A. Richard, *Fatigue crack growth behavior and mechanical properties of additively processed EN AW-7075 aluminium alloy.* Procedia Structural Integrity, 2016. **2**: p. 3040-3048.

20. Zuo, H., H. Li, L. Qi, and S. Zhong, *Influence of Interfacial Bonding between Metal Droplets on Tensile Properties of 7075 Aluminum Billets by Additive Manufacturing Technique.* Journal of Materials Science & Technology, 2016. **32**(5): p. 485-488.

21. Simchi, A., *Direct laser sintering of metal powders: Mechanism, kinetics and microstructural features.* Materials Science and Engineering: A, 2006. **428**(1-2): p. 148-158.

22. Thijs, L., K. Kempen, J.-P. Kruth, and J. Van Humbeeck, *Fine-structured aluminium products with controllable texture by selective laser melting of pre-alloyed AlSi10Mg powder.* Acta Materialia, 2013. **61**(5): p. 1809-1819.

23. Wang, P., H.C. Li, K.G. Prashanth, J. Eckert, and S. Scudino, *Selective laser melting of Al-Zn-Mg-Cu: Heat treatment, microstructure and mechanical properties.* Journal of Alloys and Compounds, 2017. **707**: p. 287-290.

24. Haboudou, A., P. Peyre, A.B. Vannes, and G. Peix, *Reduction of porosity content generated during Nd:YAG laser welding of A356 and AA5083 aluminium alloys.* Materials Science and Engineering: A, 2003. **363**(1–2): p. 40-52.

25. Chao, Y.-p., L.-h. Qi, Y. Xiao, J. Luo, and J.-m. Zhou, *Manufacturing of micro thin-walled metal parts by micro-droplet deposition.* Journal of Materials Processing Technology, 2012. **212**(2): p. 484-491.

26. Dixit, M., R.S. Mishra, and K.K. Sankaran, *Structure–property correlations in Al 7050 and Al 7055 high-strength aluminum alloys.* Materials Science and Engineering: A, 2008. **478**(1-2): p. 163-172.

27. Healey, J.T., *Guinier-Preston Zone Evolution in 7075 Aluminum*, in *Department Of Material Science*. 1976, University of Florida

28. Han, N.M., X.M. Zhang, S.D. Liu, D.G. He, and R. Zhang, *Effect of solution treatment on the strength and fracture toughness of aluminum alloy 7050.* Journal of Alloys and Compounds, 2011. **509**(10): p. 4138-4145.

29. Liu, Y., X. Luo, and Z. Li, *Microstructure evolution during semi-solid powder rolling and post-treatment of 7050 aluminum alloy strips.* Journal of Materials Processing Technology, 2014. **214**(2): p. 165-174.

30. Sha, G. and A. Cerezo, *Early-stage precipitation in Al–Zn–Mg–Cu alloy (7050).* Acta Materialia, 2004. **52**(15): p. 4503-4516.

31. Zheng, L.J., H.X. Li, M.F. Hashmi, C.Q. Chen, Y. Zhang, and M.G. Zeng, *Evolution of microstructure and strengthening of 7050 Al alloy by ECAP combined with heat-treatment.* Journal of Materials Processing Technology, 2006. **171**(1): p. 100-107.

32. R.G> Song, Q.Z. Zhang, *Heat treatment technique optimization for 7175 aluminum alloy by an artificial neural network and a genetic algorithm.pdf.* Journal of Material Processing technology, 2001(2001): p. 84-88.

33. Mishra, R.S. and M.W. Mahoney, *Friction Stir Welding and Processing*. 2007: ASM International.

34. Rhodes, C., *Fine-grain evolution in friction-stir processed 7050 aluminum.* Scripta Materialia, 2003. **48**(10): p. 1451-1455.

35. Davis, J.R., *Understanding basics Aluminum and Aluminum Alloys Davis.* 2001.

36. Carvalho, A.L.M. and H.J.C. Voorwald, *The surface treatment influence on the fatigue crack propagation of Al 7050-T7451 alloy.* Materials Science and Engineering: A, 2009. **505**(1-2): p. 31-40.

37. Chen, J., L. Zou, Q. Li, and Y. Chen, *Microstructure evolution of 7050 Al alloy during age-forming.* Materials Characterization, 2015. **102**: p. 114-121.

38. Hou, W., W. Ji, Z. Zhang, J. Xie, and X. Cheng, *The effect of homogenization temperature on the corrosion resistance of extruded 7050 Al-alloy bars.* Journal of Materials Processing Technology, 2014. **214**(3): p. 635-640.

39. Huo, W., L. Hou, Y. Lang, H. Cui, L. Zhuang, and J. Zhang, *Improved thermo-mechanical processing for effective grain refinement of high-strength AA 7050 Al alloy.* Materials Science and Engineering: A, 2015. **626**: p. 86-93.

40. Li, M.H., Y.Q. Yang, Z.Q. Feng, G.H. Feng, B. Huang, Y.X. Chen, M. Han, and J.G. Ru, *Influence of equal-channel angular pressing on aging precipitation in 7050 Al alloy.* Intermetallics, 2014. **55**: p. 49-55.

41. Mazzer, E.M., C.R.M. Afonso, C. Bolfarini, and C.S. Kiminami, *Microstructure study of Al 7050 alloy reprocessed by spray forming and hot-extrusion and aged at 121 °C.* Intermetallics, 2013. **43**: p. 182-187.

42. Dinda, G.P., A.K. Dasgupta, and J. Mazumder, *Laser aided direct metal deposition of Inconel 625 superalloy: Microstructural evolution and thermal stability.* Materials Science and Engineering A, 2009. **509**(1-2): p. 98-104.

43. Dinda, G.P., L. Song, and J. Mazumder, *Fabrication of Ti-6Al-4V scaffolds by direct metal deposition.* Metallurgical and Materials Transactions A: Physical Metallurgy and Materials Science, 2008. **39**(12): p. 2914-2922.

44. Mazumder, J., J. Choi, K. Nagarathnam, J. Koch, and D. Hetzner, *The direct metal deposition of H13 tool steel for 3-D components.* JOM, 1997. **49**(5): p. 55-60.

45. Mazumder, J., D. Dutta, N. Kikuchi, and A. Ghosh, *Closed loop direct metal deposition: Art to Part.* Optics and Lasers in Engineering, 2000. **34**(4-6): p. 397-414.

46. Zhuang, W., Q. Liu, R. Djugum, P.K. Sharp, and A. Paradowska, *Deep surface rolling for fatigue life enhancement of laser clad aircraft aluminium alloy.* Applied Surface Science, 2014. **320**: p. 558-562.

47. Mathew, R., P.R. Stoddart, D. Nolan, and Y. Durandet, *Microstructural refinement of aluminium-zinc-silicon coated steels.* Surface and Coatings Technology, 2016.

48. Keicher, D.M., W.D. Miller, J.E. Smugeresky, and J.A. Romero, *Laser engineered net shaping (LENS (TM)): Beyond rapid prototyping to direct fabrication.* Hard Coatings: Based on Borides, Carbides & Nitrides: Synthesis, Characterization & Applications, 1998: p. 369-377.

49. Mah, R., *Directed light fabrication.* Advanced Materials & Processes, 1997. **151**(3): p. 31-33.

50. Deng, Y.-L., L. Wan, Y. Zhang, and X.-M. Zhang, *Evolution of microstructures and textures of 7050 Al alloy hot-rolled plate during staged solution heat-treatments.* Journal of Alloys and Compounds, 2010. **498**(1): p. 88-94.

51. Hailing, T., B. Rui, Z. Jianyu, Z. Xiaoling, and F. Binjun, *Influence of Low Load Truncation Level on Crack Growth for Al 2324-T39 and Al 7050-T7451*. Chinese Journal of Aeronautics, 2009. **22**(4): p. 401-406.

52. Liu, S.H., X.J. Liu, B. Liu, L.M. Liu, W.Z. Jin, and X.J. Hu, *Effect of some alloying elements on boiling point of magnesium.* Materials Science and Technology, 2013. **21**(6): p. 735-738.

53. Rossino, L.S., F.C. Castro, W.W. Bose Filho, and J.A. Araújo, *Issues on the mean stress effect in fretting fatigue of a 7050-T7451 Al alloy posed by new experimental data.* International Journal of Fatigue, 2009. **31**(11-12): p. 2041-2048.

54. Sha, G. and A. Cerezo, *Kinetic Monte Carlo simulation of clustering in an Al–Zn–Mg–Cu alloy (7050).* Acta Materialia, 2005. **53**(4): p. 907-917.

55. Wu, Y., B. Feng, Y. Xin, R. Hong, H. Yu, and Q. Liu, *Microstructure and mechanical behavior of a Mg AZ31/Al 7050 laminate composite fabricated by extrusion.* Materials Science and Engineering: A, 2015. **640**: p. 454-459.

56. Prashanth, K.G., S. Scudino, and J. Eckert, *Defining the tensile properties of Al-12Si parts produced by selective laser melting.* Acta Materialia, 2017. **126**: p. 25-35.

57. Kang, N., P. Coddet, L. Dembinski, H. Liao, and C. Coddet, *Microstructure and strength analysis of eutectic Al-Si alloy in-situ manufactured using selective laser melting from elemental powder mixture.* Journal of Alloys and Compounds, 2017. **691**: p. 316-322.

58. Dinda, G.P., A.K. Dasgupta, S. Bhattacharya, H. Natu, B. Dutta, and J. Mazumder, *Microstructural Characterization of Laser-Deposited Al 4047 Alloy.* Metallurgical and Materials Transactions A, 2012. **44**(5): p. 2233-2242.

59. Singh, A., A. Ramakrishnan, and G. Dinda, *Direct Laser Metal Deposition of Al 7050 Alloy*. 2017. **1**.

60. Palm, F., R. Leuschner, T. Schubert, and B. Kieback. *PM Aluminiumn and Magnesium 2: Scalmalloy®= A Unique High Strength AlMgSc Type Material Concept Processed by Innovative Technologies for Aerospace Applications*. in *European Congress and Exhibition on Powder Metallurgy. European PM Conference Proceedings*. 2010. The European Powder Metallurgy Association.

61. Engler, O., C.D. Marioara, T. Hentschel, and H.-J. Brinkman, *Influence of copper additions on materials properties and corrosion behaviour of Al–Mg alloy sheet.* Journal of Alloys and Compounds, 2017. **710**: p. 650-662.

62. Spierings, A.B., K. Dawson, T. Heeling, P.J. Uggowitzer, R. Schäublin, F. Palm, and K. Wegener, *Microstructural features of Sc- and Zr-modified Al-Mg alloys processed by selective laser melting.* Materials & Design, 2017. **115**: p. 52-63.

63. Shi, Y., P. Rometsch, K. Yang, F. Palm, and X. Wu, *Characterisation of a novel Sc and Zr modified Al–Mg alloy fabricated by selective laser melting.* Materials Letters, 2017. **196**: p. 347-350.

64. Hirai, K., H. Somekawa, Y. Takigawa, and K. Higashi, *Effects of Ca and Sr addition on mechanical properties of a cast AZ91 magnesium alloy at room and elevated temperature.* Materials Science and Engineering: A, 2005. **403**(1-2): p. 276-280.

65. Hsieh, J.-H. and C.-G. Chao, *Effect of magnesium on mechanical properties of Al2O3/AlZnMgCu metal matrix composites formed by squeeze casting.* Materials Science and Engineering: A, 1996. **214**(1-2): p. 133-138.

66. Remøe, M.S., K. Marthinsen, I. Westermann, K. Pedersen, J. Røyset, and C. Marioara, *The effect of alloying elements on the ductility of Al-Mg-Si alloys.* Materials Science and Engineering: A, 2017. **693**: p. 60-72.

67. Kumar, P.V., G.M. Reddy, and K.S. Rao, *Microstructure, mechanical and corrosion behavior of high strength AA7075 aluminium alloy friction stir welds – Effect of post weld heat treatment.* Defence Technology, 2015. **11**(4): p. 362-369.

68. Hatch, J.E., A. Association, and A.S. Metals, *Aluminum: Properties and Physical Metallurgy*. 1984: American Society for Metals.

ABSTRACT

ADDITIVE MANUFACTURING OF AL 4047 AND AL 7050 ALLOYS USING DIRECT LASER METAL DEPOSITION PROCESS

by

AMRINDER SINGH

August 2017

Advisor: Dr. Guru P. Dinda

Major: Mechanical Engineering

Degree: Doctor of Philosophy

Additive manufacturing (AM) of metals is finding numerous applications in automotive, biomedical, and aerospace industries. In 21st century, aluminum is second to steel in industrial applications because of its high strength to weight ratio, superior corrosion resistance, and high electrical conductivity. The primary objective of this research is to investigate the effect of laser deposition parameters on the resulting microstructural evolution and mechanical properties to deposit defect free Al 4047 and Al 7050 alloys. This research deals with the practical challenges of building single wall and block deposit of Al 4047 and Al 7050 alloys via direct laser metal deposition process. Microstructural investigation using optical and scanning electron microscopy revealed 99.8% density of as-deposited Al 4047 and Al 7050 alloys. Tensile test sample extracted from Al 4047 deposit showed an impressive elongation of 9% with an ultimate tensile strength of 225 MPa. Laser metal deposition of Al 7050 is a challenging task because of high reflectivity, high thermal conductivity and due to the presence of various low melting and boiling point alloying elements such as Zn and Mg. EDS investigation revealed the substantial evaporation of Mg and Zn during laser metal deposition of Al 7050 alloy. To cope with the issue of vaporization of low

boiling point elements, laser metal deposition of Al 7050 alloy powder coated with nickel was conducted using optimized parameters. Microstructural investigation using optical and electron microscopy revealed that the deposits was free from relevant defects such as porosity or lack of fusion. However, the added nickel was partially segregated in the inter-dendritic boundaries and formed brittle Al_3Ni intermetallic. Consequently, Ni coated Al 7050 alloy deposit showed almost no tensile ductility. Laser deposited samples were friction stir processed to refine and uniformly distribute Al_3Ni particles in the α-Al matrix. Friction stir processed (FSP) samples showed a good combination of yield strength (178 MPa), UTS (302 MPa), and tensile elongation (6%). Post FSP heat treatment additionally improved both strength and elongation about 10%. Microstructural investigation exhibited a systematic change of columnar to equiaxed dendrites from bottom to top of each deposited layer in all Al alloys studied in this investigation. A correlation was developed between Mg content in powder feed and deposited sample at various input laser power. To achieve the correlation, a gradient material was deposited with gradual addition of Mg with the increase in height of deposit. Final compositions were measured using EDS to establish correlation between Mg content in powder feed and laser deposited material. Formation of strengthening precipitates primarily Al_3Mg_2 and $MgZn_2$ were escalated with the gradual addition of Mg from bottom to the top layer of Al 7050 gradient sample. This technique is very useful to develop new alloy by studying various compositions in one sample saving time and effort.

AUTOBIOGRAPHICAL STATEMENT

AMRINDER SINGH

EDUCATION

- M.S., Mechanical Engineering, Wayne State University, Detroit, Michigan, 2008.
- B.Tech, Guru Nanak Dev Engineering College, Punjab Technical University, Ludhiana, India, 2007.